USGS Award Number 07HQGR0053

Calibration of Liquefaction Potential Index for Assessment and Mapping of Liquefaction Hazards

Final Report to the
United States Geological Survey

By

C. Hsein Juang, Ph.D., P.E.
Department of Civil Engineering
Clemson University
110 Lowry Hall
Clemson, South Carolina 29634-0911 USA
Telephone: (864) 656-3322
Fax: (864) 656-2670
E-mail: hsein@clemson.edu

January 2009

Statement

This report presents the results of research supported by the United States Geological Survey (USGS), Department of Interior under USGS award number 07HQGR0053. The views and conclusions contained in this report are those of the author and should not be interpreted as necessarily representing the official policies, either expressed or implied, of the United States Government. The views and conclusions presented can not be taken as recommendations for managing specific engineering projects.

USGS Award Number 07HQGR0053

Calibration of Liquefaction Potential Index for Assessment and Mapping of Liquefaction Hazards

EXECUTIVE SUMMARY

This report documents the results of the research project conducted during the period of January 1, 2007 through December 31, 2008. The report consists of three parts. Part I describes the work on the development of a new empirical model for assessing soil liquefaction potential using piezocone penetration test (CPTU). One unique feature of this method is the inclusion of excess porewater pressure ratio (B_q) in the formulation of soil behavior type index (I_c); the latter is then used for evaluating liquefaction resistance. This CPTU-based simplified method is shown to be more applicable to a wider range of soils, including geomaterials that were previously considered "too clay-rich to liquefy."

Part II documents the results of an extensive calibration of the Liquefaction Potential Index (LPI) with a focus on the newly developed CPTU-based model. The results show that the threshold criteria developed by Iwasaki and his co-workers for interpreting the calculated LPI are not universally applicable. To the contrary, the LPI must be re-calibrated when any component model of the LPI framework is replaced with a new model. The calibration of the LPI in this study enables the use of CPTU-based model for predicting the potential for surface manifestation of liquefaction using the entire CPTU sounding profiles.

Part III documents the results of an effort to extend the use of LPI that is computed for a given site subjected to a given shaking level (represented by a pair of peak ground surface acceleration a_{max} and moment magnitude M_w). First, a simplified model based on LPI was

created for computing the conditional probability of surface manifestation of liquefaction (P_G) subjected to a given pair of a_{max} and M_w. Then, this conditional probability model is extended into a complete framework for assessing the probability of surface manifestation of liquefaction in a given exposure time at a given site subjected to all possible ground motions at all seismic hazard levels. This new framework is formulated and demonstrated with an example site in 10 different seismic regions in the United States.

ACKNOWLEDGMENTS

This research was supported by the U.S. Geological Survey (USGS), Department of the Interior under USGS award number 07HQGR0053, with C. Hsein Juang as Principal Investigator. The views and conclusions contained in this report are those of the writer and should not be interpreted as necessarily representing the official policies, expressed or implied, of the U.S. Government.

The writer also wishes to thank Mike Jefferies and Rodolfo Sancio of Golder Associates for their insights and helpful discussions on CPT measurements and effects of porewater pressure ratio. Paul Mayne of Georgia Tech is thanked for his contribution to the development of the CPTU-based simplified method, and Jin-Hung Hwang of National Central University and Chia-Nan Liu of National Chi-Nan University are thanked for their contributions to the LPI-based model development. Chien-Hsun Chen, Chih-Chieh Lu, and Jerry Z. Luo, research assistants at Clemson University, are thanked for their work on data analysis and model development presented in this report.

TABLE OF CONTENTS

Page

TITLE PAGE i

STATEMENT ii

EXECUTIVE SUMMARY iii

ACKNOWLEDGEMENTS v

TABLE OF CONTENTS vi

PART I

CPTU-based model for evaluating soil liquefaction potential 1

Tables 28

Figures 29

PART II

Calibration of Liquefaction Potential Index 46

Tables 67

Figures 70

PART III

Assessing Probability of Surface Manifestation of Liquefaction 88

Tables 104

Figures 108

APPENDIXES 122

REFERENCES 126

Part I:
CPTU simplified stress-based model for evaluating soil liquefaction potential*

ABSTRACT

Part I of the Report presents a new method based on piezocone penetration test (CPTu) for evaluating soil liquefaction potential, which covers a wider range of soil types than previous approaches. In the new approach, the adjusted cyclic stress ratio is calculated with a recent formula created by Idriss and Boulanger, and the cyclic resistance ratio is determined as a function of both adjusted cone tip resistance (q_{t1N}) and soil behavior type index (I_c). The new method is established through artificial neural network learning of documented cases. One unique feature of this method is the inclusion of excess porewater pressure ratio (B_q) in the formulation of I_c as per Jefferies and Davies. The new method is shown to be more applicable to a *wider range* of soils, including geomaterials that were previously considered "too clay-rich to liquefy." The ability of this method to delineate liquefied cases from non-liquefied cases is clearly depicted with 3-D and 2-D graphs. Case studies of selected ground failure sites in Adapazari using the proposed method yield results that agree well with field observations in the 1999 Kocaeli earthquake.

---

*The contents of this part (Part I) of the report have been published as a Technical Paper in Soils and Foundations. The article citation is as follows: Juang, C. H., et al. (2008b), "CPTU simplified stress-based model for evaluating soil liquefaction potential," *Soils and Foundations*, Vol. 48, No. 6, 2008, pp. 755-770.

INTRODUCTION

The simplified procedures for evaluating the liquefaction potential of a soil was created by Seed and Idriss (1971) in which the seismic loading required to initiate liquefaction was expressed as a cyclic stress ratio (CSR) and the soil resistance against liquefaction was measured by the energy-corrected blow count (N_{60}) from the standard penetration test (SPT). Using this general framework, many subsequent simplified models were later developed based on different *in situ* tests such as the cone penetration test (CPT), flat dilatometer test (DMT), Becker penetration test (BPT), and shear wave velocity (V_s) measurements. An excellent summary of the latest consensus versions of the SPT-, CPT-, and V_s-based models was documented by Youd et al. (2001). This study focuses on the evaluation of liquefaction potential using CPT, in particular, the piezocone penetration test (CPTu) that obtains three readings with depth: cone tip resistance (q_t), sleeve friction (f_s), and penetration porewater pressures at the shoulder position (u_2).

Many investigators have contributed to the development of the CPT-based simplified models for liquefaction evaluation (e.g., Robertson and Campanella 1985, Seed and de Alba 1986, Mitchell and Tseng 1990, Stark and Olson 1995, Suzuki et al. 1995, Olsen 1997, Robertson and Wride 1998, Juang et al. 2003, and Moss et al. 2006). Among these CPT-based models or methods, that developed by Robertson and Wride (1998) and updated in Zhang et al. (2002) is arguably the most widely used. This method is a *deterministic* model, meaning that the soil and seismic parameters are treated as if they were not subject to random variations. Thusly, the assessment of liquefaction potential can be carried out with a calculated factor of safety (F_S), which is generally defined as the ratio of cyclic resistance ratio (CRR) over cyclic stress ratio

(CSR). In a deterministic solution, the results are interpreted in a "yes-or-no" manner; the occurrence of liquefaction is "predicted' if $F_S < 1$ whereas no liquefaction is predicted if $F_S > 1$.

CPT-based methods for liquefaction evaluation are attractive because of two important test characteristics: capability of continuous profiling and superior measurement repeatability over other *in situ* tests such as SPT (Shuttle and Cunning 2007). The capability of continuous profiling is of particular advantage if the results of liquefaction potential evaluation at depths are to be integrated over the entire soil column into Liquefaction Potential Index (LPI), an index that is often used to characterize the potential for occurrence of damaging liquefaction in a geologic unit (Iwasaki et al. 1982, Toprak and Holzer 2003, Li et al. 2006). During SPT and conventional shear wave methods (i.e., crosshole and downhole), common test intervals are at 1 to 1.5 m intervals, thereby perhaps missing weak layers in the profile.

Yet, in normal CPT practice, soil samples are not taken and examined, which can be a significant disadvantage compared to SPT. Furthermore, for the so-called "clay-rich" soils, defined by Robertson and Wride (1998) as those with soil behavior type index (I_c) greater than 2.6, the liquefaction potential must be confirmed by different means (such as the Chinese Criteria or those proposed by Bray and Sancio 2006), although these soils are usually considered "non-liquefiable." Because samples are not retrieved during CPT, the criteria such as those by Bray and Sancio (2006) are not readily applicable without additional data from nearby SPTs. This poses a challenge for the evaluation of liquefaction potential of silty and clayey soils using CPT and for the integration of the CPT-based evaluation into the framework of LPI.

The existing simplified methods, such as Seed et al. (1985), Robertson and Wride (1998) and Youd et al. (2001), were originally developed for clean sands. For the evaluation of sands with significant fines content (*FC*), the concept of "equivalent clean sand" was employed,

suggesting that liquefaction resistance would increase as the *FC* increases. This concept is reflected in the three boundary curves corresponding to three ranges of fines content ($FC \leq 5\%$, $5\% < FC \leq 35\%$, and $FC > 35\%$) recommended by Seed et al. (1985), which has been well accepted by the profession. However, liquefaction of soils with high fines content (as high as 90%) in the past earthquakes has been observed (Kishida 1969, Tohno and Yasuda 1981, Bray et al. 2004). Laboratory cyclic simple shear tests, cyclic ring-shear tests, and cyclic triaxial tests of these soils (for example, Ishihara 1993, Perlea et al. 1999, Guo and Prakash 1999, Gratchev et al. 2006) suggest that the soil plasticity, and not necessarily the fines content alone, plays a major role in the liquefaction resistance behavior, i.e., the liquefaction resistance increases as the plasticity index increases. On the other hand, for sands with significant non-plastic fines content, the effect of fines content on the liquefaction resistance is less conclusive based on laboratory cyclic test results (for example, Carraro, et al. 2003; Thevanayagam et al. 2000).

Since the Robertson and Wride (1998) method is widely used, one concern has been raised regarding the validity of using their simplified form of soil behavior type index I_c (where porewater pressures are omitted) as a proxy to the effect of fines on liquefaction resistance (Idriss and Boulanger 2004, 2006). To ease this concern, Moss et al. (2006) suggested use of friction ratio ($R_f = f_s/q_t$) in lieu of I_c to account for the effect of fines, whereas Li et al. (2007) and Shuttle and Cunning (2007) suggested using a version of I_c that includes excess pore pressure ratio in the formulation. The excess porewater pressure ratio B_q, defined in Appendix I along with other CPTu parameters, correlates well with the behavior of fine-grained soils and has been incorporated into soil classification charts (Robertson 1990, Jefferies and Davies 1993). Thus, inclusion of B_q in the formulation of I_c appears suitable for extending the existing CPT-based evaluation from sands and silty sands to soils that are described as "too clay-rich to liquefy." A

CPT-based method that can evaluate the liquefaction resistance of soils over a *wide range* of I_c values would enable a more meaningful modeling of liquefaction effects within the framework of LPI.

In this study, the effects of CPT measured porewater pressures on soil liquefaction resistance are investigated through a study of case histories by considering the soil behavior type index I_c as defined by Jefferies and Davies (1993). In essence, knowledge is "extracted" from collected case histories using an artificial neural network (ANN), a well-established technique that can learn from examples (Rumelhart et al. 1986). This knowledge is then used to develop a new simplified model based on piezocone penetration testing (CPTu). The developed CPTu-based model is assessed and demonstrated with recent liquefaction case histories. Finally, it should be emphasized that the proposed CPTu model is not entirely new; it is built on the foundation of the previous work by many investigators.

LEARNING FROM CASE HISTORIES - ARTIFICIAL NEURAL NETWORK

Artificial Neural Network Approach for Liquefaction Evaluation

Training an artificial neural network (ANN) to approximate a highly nonlinear relationship for predicting the occurrence of liquefaction/no-liquefaction has been reported by various researchers (Goh 1994, Agrawal et al. 1995, Goh 1996, Juang et al. 1999a). In these previous studies, ANNs were trained using databases of case histories in which field observation, in the binary form of "yes" or "no," was available. If the ANN has "learned" adequately from case histories, it may then be used for "forecasting" whether liquefaction could occur under a given scenario. Thus, the trained ANN may be used as a tool for assessing liquefaction potential of a soil in a given seismic loading. Recently, Juang et al. (2000a, 2003) took this approach a

step further. They developed a procedure with which the *limit state* for liquefaction triggering, commonly expressed as a boundary curve, can be established based on the trained ANN. It should be noted that the limit state for liquefaction triggering is essentially a model of CRR at a given CSR. Other ANN-based models developed for CRR have also been suggested (e.g., Kim and Kim, 2006).

Selection of Input and Output Variables

To learn effectively from a data set of case histories, choices must be made regarding the types of information to include from each case. Previous studies (e.g. Goh 1994, Juang et al. 1999a) provide adequate guidance here. Each case history is an "instance" (data point) where the input consists of soil and earthquake data and the output consists of a field observation. The field observation is generally represented by only one variable, liquefaction indication (LI), in which LI = 1 for cases with surface manifestations of liquefaction (e.g. sand boiling, ground settlement, and lateral spreading) and LI = 0 for cases without surface manifestations of liquefaction. The following paragraphs detail the selection process for the input variables.

Selecting CSR as an input variable is the obvious choice because, in any cyclic stress-based method that follows the simplified procedure of Seed and Idriss (1971), CSR is used to characterize the earthquake load for assessing liquefaction potential. Throughout this report, the variable CSR is the adjusted cyclic stress ratio as defined by Idriss and Boulanger (2004; 2006). It is expressed as:

$$\mathrm{CSR} = 0.65\left(\frac{\sigma_v}{\sigma'_v}\right)\left(\frac{a_{max}}{g}\right)(r_d)\left(\frac{1}{MSF}\right)\left(\frac{1}{K_\sigma}\right) \tag{1-1}$$

where σ_v and σ'_v are the total stress and the effective stress, respectively, of the soil of concern at a given depth, *g* is the acceleration of gravity, which is the unit for peak ground surface acceleration a_{max}, r_d is the depth-dependent shear stress reduction factor, MSF is the magnitude scaling factor, and K_σ is the overburden correction factor for cyclic stress ratio. Both σ_v and σ'_v are in same units, and r_d, MSF, and K_σ are dimensionless. It should be noted that this definition of CSR (Equation 1-1) is already adjusted to the conditions of moment magnitude $M_w = 7.5$ and $\sigma'_v = 100$ kPa. This adjustment is essential to process case histories that were collected from different earthquakes of various magnitudes and to unify the influence of confining pressures. The intermediate parameters, r_d, K_σ, and MSF as defined by Idriss and Boulanger (2006) are employed herein. The formulations of these parameters are listed in Appendix II.

It should be noted that various forms of CSR are available in the literature and differ primarily in the formulation of their intermediate variables, r_d, K_σ, and MSF. Please reference Youd et al. (2001) and Idriss and Boulanger (2006) for detailed discussions of these intermediate variables. However, a previous study by Juang et al. (2006), and a sensitivity analysis performed in this study showed that CSR values, determined with the formulation by Idriss and Boulanger (2006), agreed well with those obtained using the formulation recommended by Youd et al. (2001).

In addition to the data of earthquake loading as represented by CSR, the data of liquefaction resistance are needed to completely characterize a case history. Selecting the most suitable input variables to characterize liquefaction resistance of soils based on CPTu measurements is not a trivial task. In a CPTu, profiles of cone tip resistance q_t, sleeve friction f_s, and porewater pressure u_2 are recorded. Various derived dimensionless parameters are used to characterize the soils encountered in the CPTu measurement, including friction ratio R_f,

normalized cone tip resistance Q_t, excess pore pressure ratio B_q, and normalized friction ratio F (Robertson 1990; Jefferies and Davies 1993). Additional derived parameters such as stress-adjusted cone tip resistance q_{t1N} and soil behavior index I_c (note: as is discussed later, different formulations of I_c are found in the literature; for example, Jefferies and Davies 1993, Robertson and Wride 1998) have also been used. These CPTu parameters are defined in Appendix I.

Using knowledge from previous studies (Juang et al. 2000a; Juang et al. 2003; Juang et al. 2006), and the results of practically exhaustive analyses using ANNs with tens of different combinations of parameters in this study, two derived parameters, q_{t1N} and I_c, are judged most suitable for use as input variables for the intended ANN model.

The adjusted cone tip resistance q_{t1N} is determined as follows (Idriss and Boulanger 2004; 2006):

$$q_{t1N} = C_N \, q_t / \sigma_{atm} \tag{1-2a}$$

$$C_N = \left[\frac{\sigma_{atm}}{\sigma'_v} \right]^{\alpha} \leq 1.7 \tag{1-2b}$$

$$\alpha = 1.338 - 0.249 (q_{t1N})^{0.264} \tag{1-2c}$$

where σ_{atm} is the atmosphere pressure (1 atm = 1.013 bars = 101.3 kPa).

Use of Equation 1-2 requires a simple iterative procedure, as C_N and q_{t1N} are inter-dependent on the exponent α. Equation 1-2 was proposed by Idriss and Boulanger (2004; 2006) in conjunction with their CPT-based method for evaluation of liquefaction resistance of *sands*. This equation was derived using the concept of "state" parameter and an empirical relationship with relative density (Boulanger and Idriss, 2004). However, in this report, the parameter q_{t1N} is

used to capture the resistance behavior of clean sands and the effect of fines type and content is included by the soil behavior type index I_c. The choice of q_{t1N} as defined in Equation 1-2, in contrast to other normalization models such as Olsen (1997) and Robertson and Wride (1998), is based on the fact that it produced the best results in the ANN learning of case histories.

The parameter I_c used in this report is defined as follows (after Jefferies and Davies 1993, Jefferies and Been 2006, with a very slight modification as noted below):

$$I_c = \sqrt{\left[3 - \log_{10}\left\{Q_t\left(1 - B_q\right) + 1\right\}\right]^2 + \left[1.5 + 1.3\left(\log_{10}F\right)\right]^2} \tag{1-3}$$

It should be noted that in the original 1993 formulation, the bracket $\left\{Q_t\left(1 - B_q\right) + 1\right\}$ was expressed as $\left\{Q_t\left(1 - B_q\right)\right\}$. The value "1" is added here to prevent the bracket from becoming negative should B_q be greater than 1 (in such cases, Q_t is very small and $\left\{Q_t\left(1 - B_q\right)\right\}$ is less than 1). Moreover, according to Shuttle and Cunning (2007), the dimensionless term $\left\{Q_t\left(1 - B_q\right) + 1\right\}$ is "fundamental for the evaluation of undrained response during CPTu sounding," which allows for greater differentiation between silty clays and clayey silts.

It should also be noted that the more well-known soil behavior type index used in the Robertson and Wride (1998) method is actually a simplification of the original 1993 form for sandy soils. The inclusion of B_q in the formulation of I_c in this study is essential to allow the evaluation of liquefaction resistance to accommodate a wider range of soils. To avoid confusion, the soil behavior index determined with the Robertson and Wride's formulation is denoted in this study as $I_{c,RW}$. The formulation of this index $I_{c,RW}$ is listed in Appendix I.

In summary, three input variables (CSR, q_{t1N}, and I_c as per Equations 1-1, 1-2, and 1-3, respectively) and one output variable (LI) are employed to characterize a case history. After processing all case histories into a data set of instances, a three-layer, feed-forward artificial neural network is trained to approximate the following function: $LI = f(q_{t1N}, I_c, CSR)$.

Database for Development of Artificial Neural Network

A database of case histories, consisting of 190 liquefied cases and 123 non-liquefied cases, was compiled from five key and well-documented sources (Moss et al. 2006, Ku et al. 2004, Lai et al. 2004, Bray et al. 2004, and PEER 2007). These cases were derived from the 1964 Niigata, Japan earthquake (M_w = 7.5), the 1976 Tangshan, China earthquake (M_w = 8.0), the 1977 Vrancea, Romania earthquake (M_w = 7.2), the 1979 Imperial Valley, California earthquake (M_w = 6.5), the 1980 Mexicali, Mexico earthquake (M_w = 6.2), the 1983 Borah Peak, Idaho earthquake (M_w = 6.9), the 1987 Edgecumbe, New Zealand earthquake (M_w = 6.6), the 1987 Elmore Ranch, California earthquake (M_w = 6.2), the 1987 Superstition Hills, California earthquake (M_w = 6.6), the 1989 Loma Prieta, California earthquake (M_w = 7.0), the 1995 Hyogoken-Nanbu, Japan earthquake (M_w = 7.2), the 1999 Chi-Chi, Taiwan earthquake (M_w = 7.6), and the 1999 Kocaeli, Turkey earthquake (M_w = 7.4). The binary criterion of liquefaction/no-liquefaction was primarily based on surface manifestation of liquefaction, such as sand boils, ground settlement, and lateral spreading (or lack thereof), and in some cases (such as those reported by Bray et al. 2004), critical layers were identified by field observations supplemented with detailed dynamic finite element analyses or confirmed by multiple existing liquefaction evaluation methods.

Figure 1-1 shows the soils in these cases in the soil behavior type classification chart. Table 1-1 shows the soil behavior types and their ranges of I_c values defined by Jefferies and

Davies (1993) and employed in this study. Table 1-2 shows the ranges of the values of various parameters in these cases. Together, Figure 1-1 and Tables 1-1 and 1-2 characterize the database used in this study. This database is available from the first writer upon request.

It should be noted that the CPT data reported in the database of Moss et al. (2006) did not include B_q. An examination of all other CPTu data revealed that for those cases with $I_{c,RW} < 2.2$ and friction ratio $R_f < 1.5\%$, the values of B_q are very small ($-0.06 < B_q < 0.02$). Assuming $B_q = 0$ for these cases will cause a maximum error in the computed I_c of less than 2%. Thus, the database from Moss et al. (2006) was screened with the criteria of $I_{c,RW} < 2.2$ and $R_f < 1.5\%$, and 116 cases were selected. These cases are assumed to have $B_q = 0$ and are included in the new database for the present study. The rest of the data in this new database were derived from the 1999 Chi-Chi, Taiwan Earthquake and the 1999 Kocaeli, Turkey Earthquake where B_q was directly included.

Training and Testing of Artificial Neural Network

In ANN terminology, a three-layer, feed-forward neural network consists of an *input* layer, an *output* layer and a *hidden* layer. For each case in the database, the input layer consists of three *neurons* (representing q_{t1N}, I_c, and CSR, respectively) and the output layer consists of one neuron (representing LI). The goal of ANN learning from case histories is to map the input layer to the output layer by determining the connection weights and biases through an error reduction process (Juang et al. 1999a). This is expressed as:

$$\mathrm{LI} = f_T\left\{\mathrm{B}_O + \sum_{k=1}^{n}\left[\mathrm{W}_k \cdot f_T\left(\mathrm{B}_{Hk} + \sum_{i=1}^{m}\mathrm{W}_{ik}\mathrm{P}_i\right)\right]\right\} \tag{1-4}$$

where B_0 is bias at the output layer (only one neuron in this layer), W_k is weight of the connection between neuron k of the hidden layer and the single output layer neuron, B_{Hk} is bias at neuron k of the hidden layer (k = 1, n), W_{ik} is weight of the connection between input variable i (i = 1, m) and neuron k of the hidden layer, P_i is input parameter i, and $f_T(\theta)$ is a transfer function defined as: $f_T(\theta) = 1 / (1+ e^{-\theta})$ where θ is a dummy variable.

The number of input variables, m, is equal to 3 in this ANN. Thus, $P_1 = q_{t1N}$, $P_2 = I_c$, and P_3 = CSR. The number of hidden neurons is determined through a trial-and-error process; in the present study, the number of neurons is chosen to be 7 based on numerous experiments with the goal of securing high success rate (defined later) and repeatability in training and testing.

As in the conventional approach, two-thirds of the instances (cases) in the database are used as the training data set and the rest are used as the testing data set. In principle, ANN is trained with *only* the training data set, and the trained ANN is then examined for how well it generalizes the input-output relationship using a testing data set that was *not* employed in the training. Numerous trials have also been performed with different combinations of training and testing data to ensure *repeatability* of the trained ANN. The repeatability is important as the desired network must be stable and yield consistent results. In the present study, the Levenberg-Marquardt (LM) algorithm is adopted for its efficiency in training networks. The LM algorithm, illustrated in Figure 1-2, yields an update of weights and biases (denoted here as x_{k+1}) as follows:

$$x_{k+1} = x_k - [J^T J + \mu I]^{-1} J^T e \tag{1-5}$$

where x_k and x_{k+1} are the previous and the updated vectors of weights and biases, respectively; J is the Jacobian matrix that contains the first derivatives of the network errors with respect to the weights and biases; μ is a scalar that is decreased after each successful step (in reduction of the performance function), I is the identity matrix, and e is a vector of network errors. Further details about the implementation of the LM algorithm can be found in Hagan and Menhaj (1994) and the neural network toolbox of MATLAB (MathWork, Inc. 2002, Demuth and Beale 2002).

Because the output of the ANN is an indication of liquefaction, the success rate of the trained network in "predicting" whether or not liquefaction occurred in each of the cases in the database can be used to characterize the performance of the developed ANN. In the present study, multiple ANNs are found to yield satisfactory success rates (≈ 90%). Although any of these ANNs may be used for "predicting" whether liquefaction will occur for a given soil under a given seismic loading, additional criterion is put in place in this study to select the most desirable ANN. This criterion is based on how well boundary surface or limit state surface generated by the developed ANN can delineate liquefied cases from non-liquefied cases. This point will be discussed later in detail.

BOUNDARY SURFACE SEARCHED WITH AID OF NEURAL NETWORK

The search procedure that utilizes ANN for locating data points on the unknown *boundary surface*, referred to herein as the limit state surface, was developed by Juang et al. (2000a). The concept behind this procedure is very simple. For each case in the database, if liquefaction is observed (output LI = 1), the search for a point on the boundary surface involves a gradual reduction of CSR or a gradual increase in q_{t1N}. Each search, if successful, results in a

three-dimensional data point (CSR, q_{t1N}, I_c) that is located on the unknown boundary surface. The CSR of this "searched" data point is referred to herein as the *critical* CSR, and by definition, the critical CSR on the limit state surface is the CRR for the given soil conditions represented by q_{t1N} and I_c. Thus, a limit state function CRR = $f(q_{t1N}, I_c)$ can be established once a large number of data points have been "found" through the search. In this study, 91 data points were successfully generated.

As noted previously, the success rate of the developed ANN in "predicting" the occurrence/no-occurrence of liquefaction in the case histories examined is one indication of the performance of this ANN. However, the success rate examines *only* the performance of the developed ANN with data employed. To see how well the trained ANN has *generalized* the input-output relationship, an additional check is desirable. The data points on the unknown boundary surface generated from the trained ANN may be used to assess the adequacy of neural network generalization. This can be carried out in two steps. Least-square regression is first performed on the generated data to establish an empirical model, CRR = f (q_{t1N}, I_c), of the boundary surface. The boundary surface is then examined to see how well liquefied and non-liquefied cases can be delineated by this surface. A satisfactory ANN must have a satisfactory success rate and the generated boundary surface must be able to delineate liquefied cases from non-liquefied cases.

A series of least-squares regression analyses were conducted on the 91 boundary-surface data points that were "found" in the search process using the developed ANN model. The following least-squares expression was obtained (in reference to Figure 1-3):

$$\mathrm{CRR} = 0.05 + \exp\left[\mathrm{A} + \mathrm{B} \times (q_{t1N}/100)^{\mathrm{C}}\right] \tag{1-6}$$

where

$$A = I_c \cdot (q_{t1N}/100) - 10.455$$

$$B = 0.669 \cdot I_c^3 - 5.55 \cdot I_c + 12.993$$

$$C = 0.284 - 0.0214 \cdot I_c^2$$

and where q_{t1N} is per Equation 1-2 and I_c is per Equation 1-3. These definitions must be strictly followed whenever Equation 1-6 is employed for evaluating CRR, and the resulting CRR must be compared to CSR defined in Equation 1-1 for assessing liquefaction potential, as Equations 1-1, 1-2, 1-3 and 1-6 were calibrated as a whole in the ANN learning and interpolation.

In short, the proposed CPTu-based method involves evaluation of CSR by Equation 1-1 and CRR by Equations 1-2, 1-3, and 1-6. The liquefaction potential is then assessed with factor of safety (F_S) defined as F_S = CRR/CSR.

The developed boundary surface (CRR model expressed in Equation 1-6) is then examined to see whether it can delineate liquefied cases from non-liquefied cases. Figure 1-4 shows three dimensional (3-D) graphs of case history data points in different angles in space, with and without the boundary surface. While not shown herein, the 3-D graph can be rotated in a Matlab window from 0° to 360° and thus unlimited number of "views" of the boundary surface can be shown to observe the performance of this ANN-generated boundary surface. Based on these views, the same conclusion can be reached: the ANN-generated boundary surface can delineate liquefied cases from non-liquefied cases in the 3-D space.

The capability of the developed CPTu-based model to delineate liquefied cases from non-liquefied cases has been demonstrated with the 3-D graphs shown in Figure 1-4. The accuracy of this model is also revealed in the success rates in "predicting" both liquefied and non-liquefied

cases, listed in Table 1-3. Much higher success rates in predicting liquefied cases than non-liquefied cases, shown in this table, implies that the developed model is conservatively biased, which is desirable for engineering applications using a deterministic approach. The degree of this conservative bias will be examined later.

CAPABILITY AND ACCURACY OF PROPOSED CPTu-BASED METHOD

It is desirable to compare the new CPTu-based method with the existing methods. Because the existing boundary curves (CRR models) are all presented in 2-D graphs, it is necessary to present the developed model accordingly. Figure 1-5 depicts the CRR model at selected I_c levels, where the boundary surface becomes a boundary curve. Also shown in this figure are case history data points within the corresponding ranges of I_c. Because each boundary curve is derived from Equation 1-6 by setting I_c at the midpoint of the corresponding range of I_c, the examination of the "performance" of boundary curves with these data points is seen *only* as an approximation. Nevertheless, the results presented in Figure 1-5 clearly show the capability and accuracy of the developed CRR model. It is noted that as I_c increases beyond 2.4, in which q_{t1N} is generally small, the ability of the CRR-q_{t1N} boundary curve to delineate liquefied cases from non-liquefied cases reduces drastically. Thus, for soils with high I_c, which generally have low q_{t1N} values ($q_{t1N} < 40$), the traditional 2-D graphs of CRR (or CSR) versus q_{t1N} offer little information. On the other hand, for these soils, a plot of CRR (or CSR) versus I_c, presented later, can help delineate liquefied cases from non-liquefied cases. This suggests that for soils with high I_c and low q_{t1N}, the variable I_c has a much greater influence on liquefaction resistance than the variable q_{t1N}.

Figure 1-6 shows a set of "family" CRR-q_{t1N} boundary curves that correspond to different soil types implied by I_c. Each of the boundary curves represents the intersection of a given plane I_c = constant (say, I_c = 1.51) and the boundary surface (Equation 1-6) in the 3-D space. One interesting observation is that *for a given* q_{t1N}, the liquefaction resistance is the lowest at $I_c \approx$ 1.51, which is approximate at the *midpoint* of the range of I_c for "sands" (where the lower end of the range is I_c = 1.25 for gravelly sand, and the higher end is I_c = 1.8 for silty sand; see Table 1-2). The soils with lower I_c, such as "gravelly sands" ($I_c \leq 1.25$), is found to have higher liquefaction resistance than those soils with $I_c \approx 1.51$ (clean sands). In other words, for soils with the same q_{t1N}, the liquefaction resistance increases as I_c decreases from 1.51 to 1.25. It is easily understood as the soils in this range (I_c = 1.25 to 1.51) contain practically no fines, and the liquefaction resistance increases with the increase in the particle size and strength. On the other hand, for soils with the same q_{t1N}, the liquefaction resistance increases as I_c increases from 1.51 to 1.8 (Figure 1-6), which is also easily understood as the soils in this range [from I_c = 1.51 (clean sand) to 1.8 (silty sand)] tend to have greater liquefaction resistance due to the effect of the fines. Thus, the CPTu model developed in this study is different from the Robertson and Wride method (1998); the latter artificially set a lower bound at $I_{c,RW}$ = 1.64 (clean sand) for liquefaction resistance evaluation. In other words, the Robertson and Wride (1998) method implicitly assumed that soils with $I_{c,RW} < 1.64$ would have the same liquefaction resistance as those with $I_{c,RW}$ = 1.64.

Similar to the 2-D graphs of CRR versus q_{t1N} presented previously, a separate set of 2-D graphs depicting the relations between CRR and I_c at various q_{t1N} levels can also be derived from Equation 1-6. Figure 1-7 shows these 2-D graphs with case histories, which demonstrate again that the developed CRR model can delineate liquefied cases from non-liquefied cases. It should

be noted that the boundary curves shown in Figure 1-7 represent an interpretation of "behavior" of the data by the trained ANN model. These boundary curves were not visually drawn based on the 2-D data points. The data points were supper-imposed onto each chart merely for verifying whether the boundary curve can delineate liquefied cases from non-liquefied cases. It is noted that for the chart with $q_{t1N} > 100$, at the lower right part of Figure 1-7, the boundary curve is presented in dashed curve, indicating that it has not been verified with sufficient data points.

Furthermore, the ability to delineate liquefied cases from non-liquefied cases at lower q_{t1N} levels (say, less than 40) with these CRR-I_c boundary curves is particularly important as it complements the inability of the CRR-q_{t1N} boundary curve to delineate liquefied cases from non-liquefied cases at these lower q_{t1N} levels. Again, this indicates that for soils with high I_c and low q_{t1N}, the variable I_c has a much greater influence on liquefaction resistance than the variable q_{t1N}. On the other hand, these graphs also show that for soils with higher q_{t1N} (and generally lower I_c), variable q_{t1N} has a much greater influence on liquefaction resistance than variable I_c.

Figure 1-8 presents a set of "family" CRR-I_c boundary curves that correspond to various q_{t1N} levels. This figure clearly shows that for a given q_{t1N}, the liquefaction resistance is the lowest at $I_c \approx 1.51$.

Finally, it is of interest to show all case histories with different soils in the same 2-D graph of CRR (or CSR) versus q_{t1N}, at least from a historic perspective. This necessitates the development of the so-called "clean sand equivalence" of cone tip resistance for any given soil. Robertson and Wride (1988) developed a correction factor K_c that can be applied to the normalized cone tip resistance q_{c1N} to yield the "clean sand equivalence," $q_{c1N,cs}$. Their idea was to transform an empirical model, CRR = $f(q_{c1N}, I_{c,RW})$, into a new model, CRR = $f(q_{c1N,cs})$, subject to the constraint that both models yield the same liquefaction resistance. In the procedure

recommended by Robertson and Wride (1988), the correction factor K_c is a function *only* of $I_{c,RW}$. However, as discussed previously, at different levels of q_{t1N}, the influence of I_c differs, and the correction factor K_c then becomes a function of both soil type (represented by I_c) and normalized cone tip resistance (q_{t1N}). Thus, development of an empirical model for K_c will be of little practical value, since such empirical equations would be as complicated as Equation 1-6 and involving the same two input variables as required in Equation 1-6. Nevertheless, numerical solutions for an equivalent q_{t1N} value at a reference level of $I_c = 1.51$ (where the liquefaction resistance is the lowest for a given q_{t1N}) can be obtained for all cases ($I_c \neq 1.51$) by satisfying the constraint: $f(q'_{t1N}, 1.51) = f(q_{t1N}, I_c)$ where q'_{t1N} is the equivalent q_{t1N} value at $I_c = 1.51$, and f is the function for CRR expressed in Equation 1-6. Figure 1-9 shows all *transformed* data points along with the "base" boundary curve, which is obtained by plotting Equation 1-6 at $I_c = 1.51$. The developed empirical model (Equation 1-6), presented as a boundary curve in this 2-D graph, is again shown to be able to delineate liquefied cases from non-liquefied cases.

For comparison, two other $I_{c,RW}$-based CRR models are shown in Figure 1-9. It is important to emphasize that this comparison of the three boundary curves is *only approximate*, as the definition of the "base" boundary curves by Robertson and Wride (1998) and Juang et al. (2006) is not exactly the same as that adopted in this study. In addition, the CRR model developed in this study is based on CPTu, whereas the other two models are based on CPT. Nevertheless, the results show that the base boundary curve of the new model, in which the effect of B_q is negligible, is very comparable to those of the existing models. In fact, the base boundary curve of the new CPTu-based model is almost identical to that of Juang et al. (2006). This result is significant because the two models were developed with different formulations and databases.

Figure 1-10 further compares the base boundary curve with two additional models proposed by Moss et al. (2006) and Idriss and Boulanger (2006). Note that for the probabilistic model of Moss et al. (2006), an equivalent deterministic boundary curve is obtained by adopting a 15% probability as suggested by the authors. The results show that these base boundary curves are quite comparable, even though the Idriss and Boulanger curve appears conservative. At lower q_{t1N} (< 80), the proposed model is consistent with the Idriss and Boulanger curve. As q_{t1N} increases to the level of $q_{t1N} \approx 100$, the proposed model catches up with the Robertson and Wride curve; as q_{t1N} continues to increase to the level of $q_{t1N} \approx 125$, the proposed model catches up with the Moss et al. curve. Cautions must be exercised, however, in drawing conclusions based on Figure 1-10. *Firstly*, the above comparison is based on the 2-D view of the models (for the proposed model, it is the intersection of the boundary surface with the plane $I_c = 1.51$ in the 3-D space; and for other models, the base curves are assumed "equivalent" to the condition of $I_c = 1.51$). Because the proposed model is a boundary surface in the 3-D space, which is fundamentally different from the 2-D boundary curves, any such comparison in a 2-D graph should be viewed with caution, particularly in light of the results from Figures 1-5 and 1-7. *Secondly*, although the base boundary curves are similar, these CPT-based models can yield contradictory conclusions on liquefaction resistance for silty or clayey soils because the effect of fines is treated differently.

EFFECT OF EXCESS PORE PRESSURE RATIO IN THE PROPOSED MODEL

The effect of CPTu-measured porewater pressures can be ascertained with the proposed CPTu method. Figure 1-11 shows the influence of ignoring the parameter B_q in the formulation

of I_c on the calculated CRR. For a soil with a significant B_q, assuming $B_q = 0$ in Equation 1-3 results in a different I_c value, denoted as $I_{c,B_q=0}$, which in turn results in a different CRR. The resulting difference (in percentage) in CRR is depicted in Figure 1-11. If the true B_q is positive, ignoring B_q leads to an underestimation of CRR; conversely, if the true B_q is negative, ignoring B_q results in an overestimation. The percentage change in CRR (in reference to the CRR calculated from Equation 1-6 with correct I_c) may be estimated with the following equation obtained by curve-fitting ($r^2 = 0.994$, RMSE = 1.8):

$$\text{\% change in CRR} = aB_q^4 + bB_q^3 + cB_q^2 + dB_q + 0.205 \tag{1-7}$$

where

$$a = 632.45\, I_{c,B_q=0}^2 - 3430.99\, I_{c,B_q=0} + 4554.91$$

$$b = -1640.85\, I_{c,B_q=0}^2 + 8558.12\, I_{c,B_q=0} - 10970.40$$

$$c = 1223.26\, I_{c,B_q=0}^2 - 5934.08\, I_{c,B_q=0} + 7139.90$$

$$d = -158.56\, I_{c,B_q=0}^2 + 445.25 I_{c,B_q=0} - 248.53$$

For all data points shown in Figure 1-11, the percentage change in CRR strongly correlates with the magnitude of B_q, as reflected in the extremely high r^2. Figure 1-12 shows the effect of B_q in different angles. As reflected in Equation 1-7, the change in CRR is a function of B_q and $I_{c,B_q=0}$. As shown in Figure 1-12, when $I_{c,B_q=0} < 2.0$ (approximately), the soil is probably in a drained condition during penetration, no significant excess pore pressure is observed and the percentage change in CRR as a result of ignoring B_q is generally small (i.e., < 2%). As $I_{c,B_q=0}$ increases beyond 2.0, there is a significant increase in B_q, indicating a possible change from the

drained condition to the undrained condition. Thus, for soils with $I_{c,B_q=0} > 2.0$, ignoring B_q in the formulation of I_c (Equation 1-3) can lead to a significant error in the CRR calculated with Equation 1-6. The aforementioned discussions address the effect of B_q (or the consequence of ignoring B_q) on CRR in the proposed CPTu-based model. It should be noted, however, that the effect of B_q on CRR in other existing CPT-based models may not be as pronounced. First, the existing CPT-based models are mainly developed for sandy soils, and for sands, $B_q \approx 0$. Second, the effect of B_q may have been compensated *to some degree* by a combined use of CPT parameters such as q_c, R_f, and $I_{c,RW}$. Nevertheless, this effect of B_q (through I_c) on CRR is very significant particularly for silt mixtures.

PROBABILITY AND FACTOR OF SAFETY CONSIDERATIONS

The proposed CPTu-based method is able to delineate liquefied cases from non-liquefied cases (Figures 1-4, 1-5, 1-7, and 1-9 and Table 1-3). However, the success rate for liquefied cases (100%) is much greater than that for non-liquefied cases (74%), suggesting that the proposed model has a conservative bias. Thus, it is desirable to determine how conservative the proposed model is. A procedure to characterize a deterministic model in terms of probability based on a database of case histories has been developed by Juang et al. (1999b; 2002). This procedure involves an analysis of the distributions of F_S values for both liquefied and non-liquefied cases, respectively, followed by use of Bayes' theorem to create a mapping function that yields probability of liquefaction for a given F_S. Using this procedure, the following mapping function is developed in this study (RMSE ≈ 0.02):

$$P_L = \frac{1}{1 + e^{-3.64+5.37F_S}} \tag{1-8}$$

It should be emphasized that the probability of liquefaction P_L determined with Equation 1-8 is *conditioned* on a given F_S that is calculated with the proposed method (with CSR by Equation 1-1 and CRR by Equation 1-6). The meaning of F_S determined with different models can greatly differ from each other since different degrees of conservatism may have been implemented in these models. For the proposed method, a factor of safety of $F_S = 1$ yields a conditional probability of liquefaction of 0.15 according to Equation 1-8. This result confirms that the proposed method has a conservative bias. Previous studies (Cetin et al. 2004, Moss et al. 2006, Juang et al. 2006) have suggested an acceptable level of liquefaction probability of $P_L = 0.15$ for design of ordinary structures. Thus, when applying the proposed model in a deterministic analysis, a factor of safety of $F_S > 1.0$ is considered adequate for use in designing ordinary structures. In other words, no additional factor of safety is necessary when evaluating liquefaction potential at a site for ordinary structures using the proposed model. Should a more stringent level of tolerable risk ($P_L < 0.15$) be required, the minimum required F_S can be adjusted accordingly.

Finally, it should be noted that the conditional probability of liquefaction determined with Equation 1-8 is a *nominal* probability, meaning that good standards of engineering practice are followed in both data acquisition and analysis, and possible uncertainties are adequately compensated in the derived data.

LIQUEFACTION POTENTIAL OF SILT MIXTURE – CASES STUDY

One unique feature of the proposed CPTu-based method is its capability to assess liquefaction potential of "silt mixtures" (i.e., clayey silt to silty clay) using the modified I_c that considers porewater pressure ratio (B_q). To this end, it is of interest to demonstrate this capability by back-analysis of well documented case histories from the August 17, 1999 Kocaeli earthquake that involved soils considered to be "too clay-rich to liquefy."

An extensive site investigation program, including 135 CPT profiles and 46 exploratory SPT borings with energy measurements, was conducted in Adapazari, Turkey after the Kocaeli earthquake (Bray et al. 2004). All available CPTu sounding profiles were analyzed in this study and similar results were obtained. Two sets of CPTu sounding profiles along with results of the analysis are presented as examples.

Figure 1-13 shows the profiles from CPTu sounding number C4 which was conducted at the site of Building C2 (Bray et al. 2004). Included in this figure are q_t, R_f, u_2 (or P_w), $I_{c,RW}$, I_c, and soil classification as per an adjacent soil test boring. The critical layer marked in this figure is one that was judged to have liquefied in the 1999 earthquake by Bray et al. (2004) based on field observations and analysis of *in situ* test data. The layer marked with "$F_S < 1$" is the layer that was considered liquefiable by Bray et al. (2004) based on their analysis. It should be noted that the critical layer was later confirmed by detailed numerical analysis (Bray et al. 2006).

Using the CPTu data shown in Figure 1-13 and the seismic parameters of $M_w = 7.4$ and $a_{max} = 0.40g$, liquefaction potential in terms of factor of safety is calculated with both the proposed model and the RW/Zhang method, which is the shorthand of the Robertson and Wride (1998) method as updated in Zhang et al. (2002). Figure 1-14 shows the results of this analysis.

In the critical layer where $I_{c,RW} > 2.6$, direct application of the RW/Zhang method (or the Robertson and Wride method), would yield "no liquefaction" (it should be noted that in case of $I_{c,RW} > 2.6$, Robertson and Wride actually suggested use of other criteria to confirm this assertion), whereas the application of the proposed method would yield F_S much less than 1, indicating "liquefaction." In this case, the results obtained by the proposed model agree with field observation. Overall, improved results are obtained directly using the proposed CPTu method without resort to further analyses.

Figures 1-15 and 1-16 show similar results obtained for the case at CPT-B4. The proposed method is again able to produce results that agree well with field observations. In the critical layer, the proposed method yields F_S much less than 1, whereas the Robertson and Wride method suggests that the soils are "too clay-rich to liquefy."

As a final comparison, Figure 1-17 shows the factor of safety (F_S) computed with the RW/Zhang method (i.e., the Robertson and Wride method as updated in Zhang et al. 2002) and those computed with the proposed CPTu model. The data used in this analysis are those shown in Figure 1-1. It is noted that for graphing purpose, the F_S values are set to 3 if the computed values are greater than 3. When the RW/Zhang method is employed, if a soil is judged to be too clay-rich to liquefy ($I_{c,RW} > 2.64$), its F_S value is artificially set to 3. As shown in Figure 1-17, for most cases, the F_S values computed with the two methods are quite comparable. For some liquefied cases, shown in zones A and B in Figure 1-17, the RW/Zhang method yields $F_S > 1$ (zone A) or $F_S >> 1$ (zone B; cases that were judged to be too clay-rich to liquefy by the $I_{c,RW} > 2.64$ criterion of the RW/Zhang method), while the proposed CPTu model yields $F_S < 1$, suggesting that the proposed CPTu model yields more reasonable results in these cases. However, a few non-liquefied cases in zone B would have been incorrectly identified ($F_S < 1$)

using the proposed model. Overall, the proposed CPTu model is seen as an improvement over the existing CPT-based methods.

SUMMARY AND CONCLUSIONS

A CPTu-based method for evaluating liquefaction potential of soils is presented which incorporates excess porewater pressure ratio (B_q) in the formulation of soil behavior type index (I_c), as defined by Jefferies and Davies (1993) and Jefferies and Been (2006). The developed CRR model must be used with the CSR model developed by Idriss and Boulanger (2006), as the latter is an integral part of the calibration process in developing the proposed CRR model. The model described here is more applicable to a *wider range* of geomaterials, including soils that were once considered "too clay-rich to liquefy" using the existing method. Thus, the results of the analysis using the proposed CPTu-based method will enable a more meaningful modeling of liquefaction effect within the framework of the Liquefaction Potential Index (LPI).

The proposed CRR model is a function of two derived variables, q_{t1N} and I_c (as per Equations 1-2 and 1-3, respectively). Thus, the characteristics of the model can easily be depicted in 3-D graphs, in which its ability to delineate liquefied cases from non-liquefied cases is clearly shown. When data points of case histories are properly grouped, 2-D graphs can also delineate liquefied cases from non-liquefied cases. Examination of these 2-D graphs reveals that for soils with higher q_{t1N} (and thus lower I_c) the variable q_{t1N} has a much greater influence on liquefaction resistance than does the variable I_c. However, for soils with high I_c and low q_{t1N}, the variable I_c has a much greater influence on liquefaction resistance than the variable q_{t1N}. Thus, the traditional approach of using 2-D graphs of CSR versus q_{t1N} to examine the performance of a

simplified CRR model has limitations. Therefore, the advantage of the proposed model in delineating liquefied cases from non-liquefied cases using 3-D graphs is clearly demonstrated.

The effect of the excess pore pressure ratio B_q is examined in this study. Neglecting B_q in the determination of I_c can lead to either an underestimation or overestimation of CRR, depending upon whether B_q is a positive or negative value. The trends of the effect of B_q on the calculated CRR are clearly observed. For "silt mixture" (clayey silt to silty clay) where the liquefaction resistance was previously ill-defined, a strong effect of B_q on the calculated CRR is clearly demonstrated.

The results of the analysis of cases from critical layers at selected ground failure sites in Adapazari using the proposed CPTu-based method agreed well with field observations in the 1999 Kocaeli earthquake. The results showed that those liquefied cases previously identified as "too clay rich to liquefy" based on the existing CPT-based methods can be correctly "predicted" using the proposed model.

The proposed CPTu model is shown to be comparable to the existing CPT-based methods such as the Robertson and Wride method in most of the cases examined. In some liquefied cases, particularly those that were judged to be too clay-rich to liquefied by the $I_{c,RW}$ >2.64 criterion, the proposed CPTu model is shown to be able to improve upon the Robertson and Wride method. Finally, it should be emphasized that the proposed CPTu model is not entirely new; it is built on the foundation of the previous work by many investigators.

Table 1-1. Soil behavior types by the index I_c (after Jefferies and Davies 1993)

Range of I_c (Equation 1-3)	Zone (or type)	Soil classification
$I_c < 1.25$	7	Gravelly sands
$1.25 \leq I_c < 1.80$	6	Sands: clean sand to silty sand
$1.80 \leq I_c < 2.40$	5	Sand mixture: silty sand to sandy silt
$2.40 \leq I_c < 2.76$	4	Silt mixture: clayey silt to silty clay
$2.76 \leq I_c < 3.22$	3	Clays
$I_c \geq 3.22$	2	Organic soils & peats

Table 1-2. Ranges of values of various parameters in case histories

	Depth (m)	q_t (MPa)	f_s (kPa)	u_2 (kPa)	R_f (%)	F (%)	σ_v (kPa)	σ'_v (kPa)	q_{t1N}	B_q	I_c	a_{max} (g)	M_w	CSR
Max	20.0	23.9	456	421	5.9	6.9	370	263	217	0.3	3.2	0.70	8.0	0.83
Min	1.3	0.4	3	-104	0.1	0.1	22	17	7	-0.2	0.9	0.09	5.9	0.05

Table 1-3. Success rates of the ANN-generated CRR model by category

Range of I_c	No. of cases	Success rate
$I_c < 1.25$	25	96%
$1.25 \leq I_c < 1.80$	126	86%
$1.80 \leq I_c < 2.40$	96	96%
$I_c > 2.40$	66	86%
All cases	313	90%
Liquefied group	190	100%
Non-liquefied group	123	74%

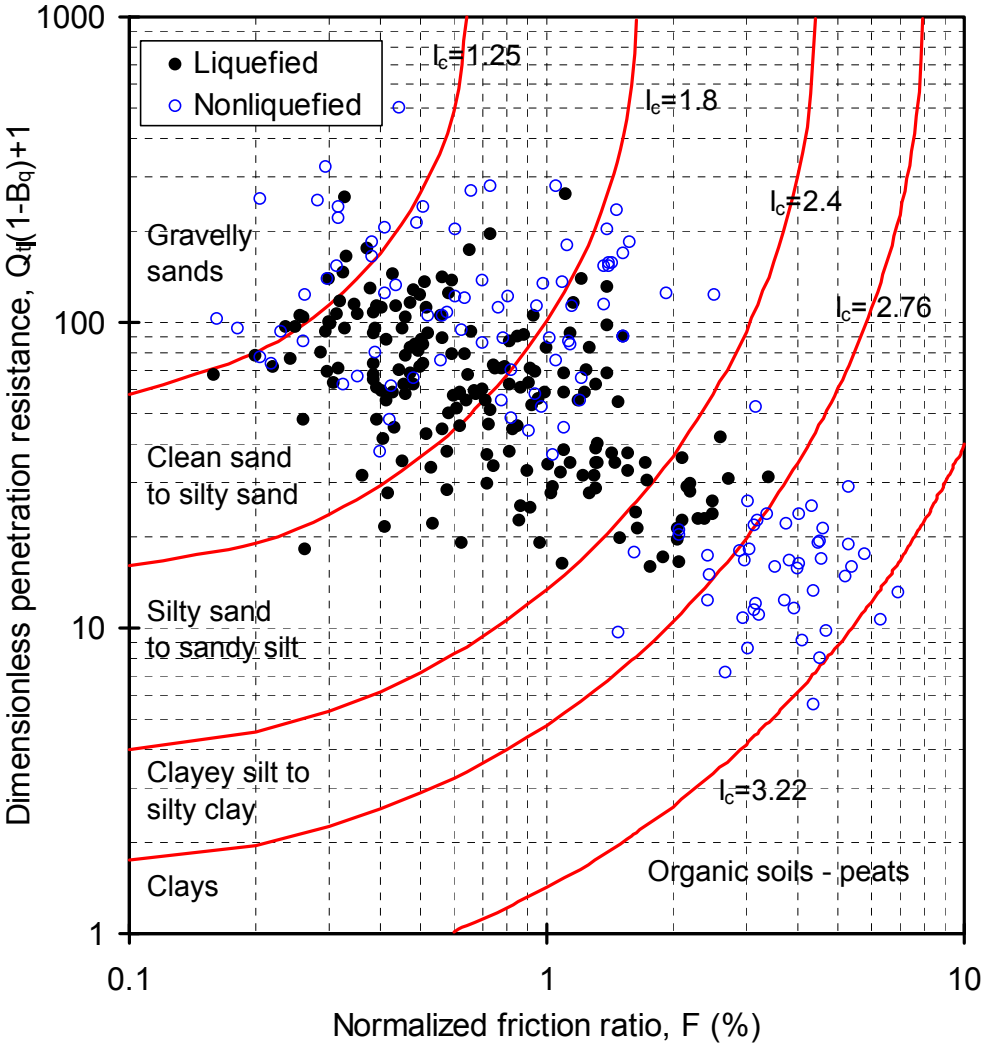

Figure 1-1. Case histories in the database plotted on the CPT soil behavioral classification chart

- Calculate initial network performance (NP_0)
- i = 0

While ($\mu_i \leq \mu_{max}$)

- $X_{i+1} = X_i - [J^T J + \mu I]^{-1} J^T e$

  Where J is Jacobian matrix; μ is scalar; I is identity matrix; e is error vector

- Calculate network performance (NP_i)

If ($NP_{i+1} > NP_i$) then

- $\mu_{i+1} = \mu_i \cdot F_\mu$

  Where F_μ is increasing factor of μ

Else

- $\mu_{i+1} = \mu_i \cdot DF_\mu$

  Where DF_μ is decreasing factor of μ

- Break (Terminate execution of while loop)

End

- i = i + 1

End

Figure 1-2. Levenberg-Marquardt algorithm for neural network training

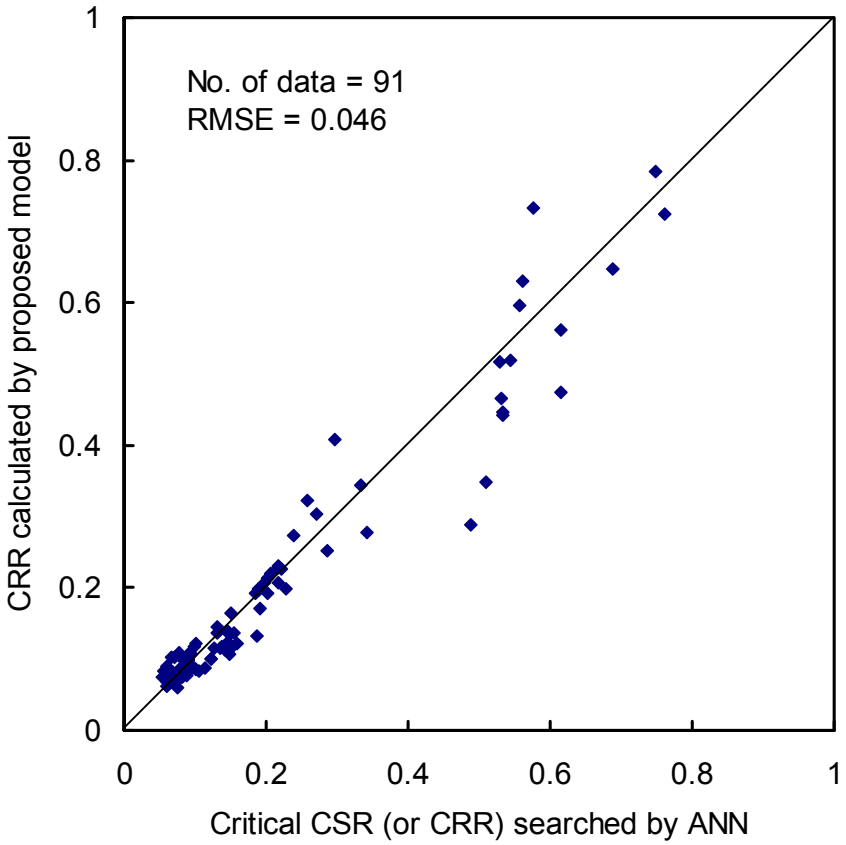

Figure 1-3. Scatter of the CRR predictions using the proposed model

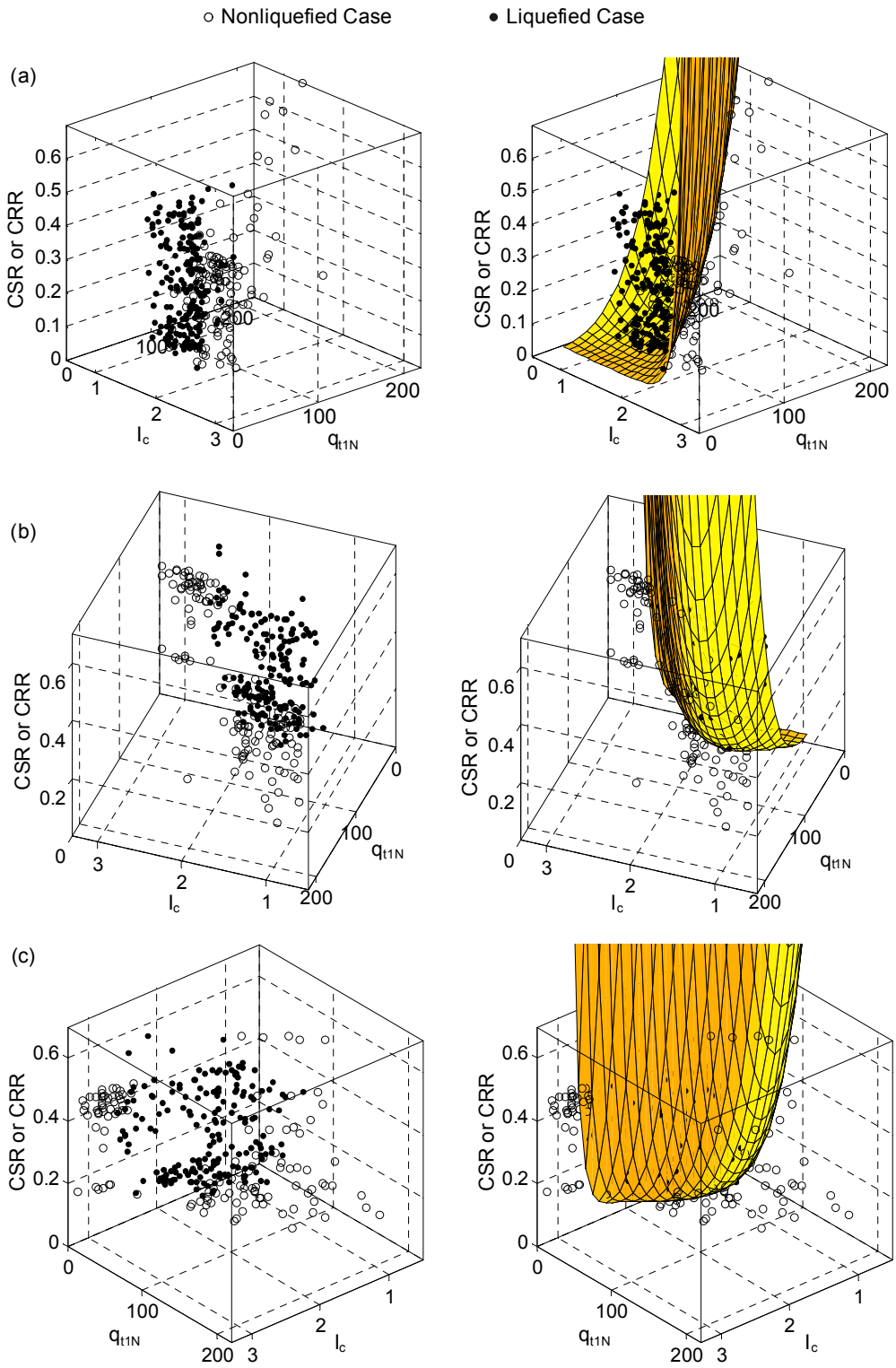

Figure 1-4. Boundary surface at three different angles with case history data

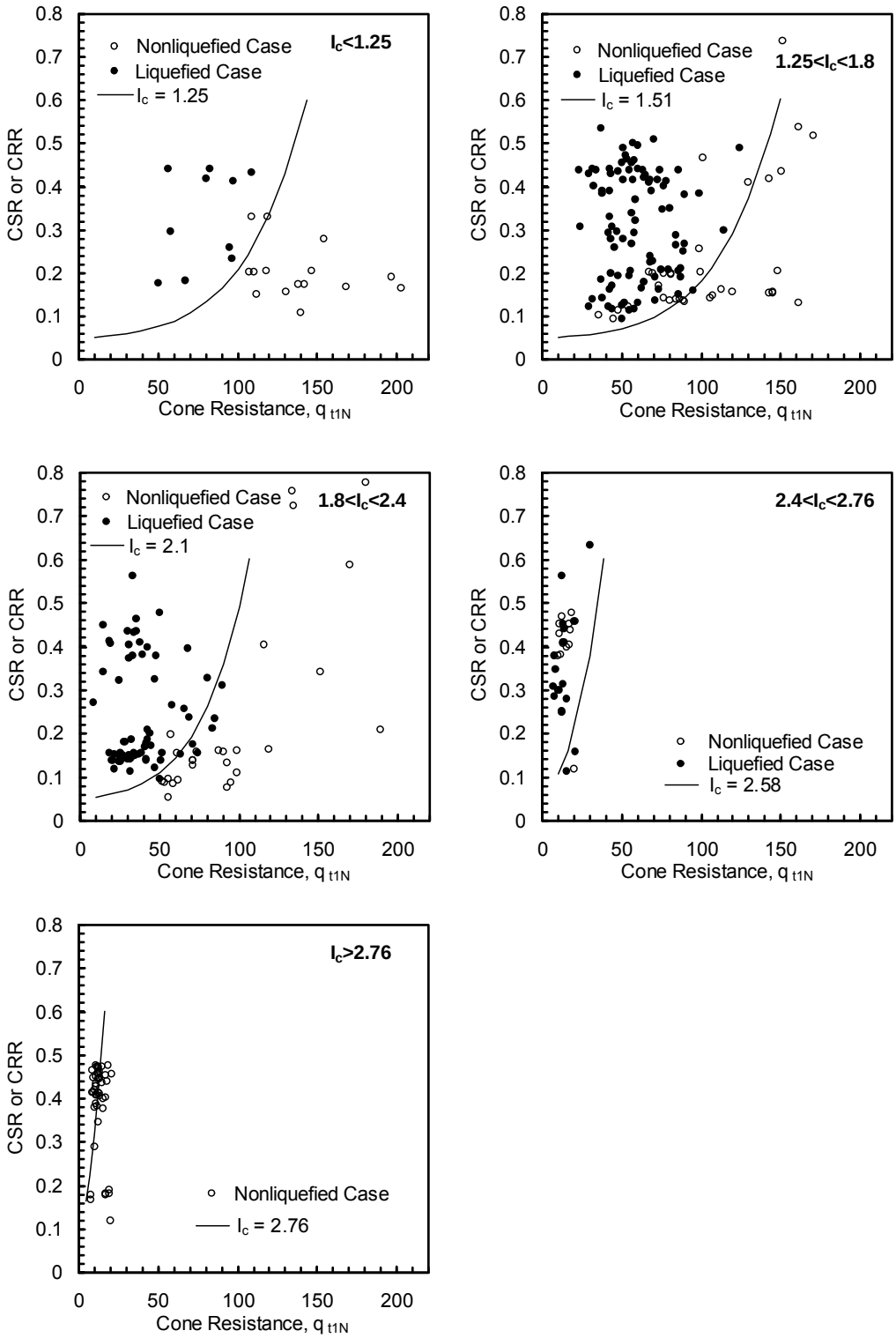

Figure 1-5. 2-D graphs of the proposed model - CRR (or CSR) versus q_{t1N} (as defined in Equation 1-2)

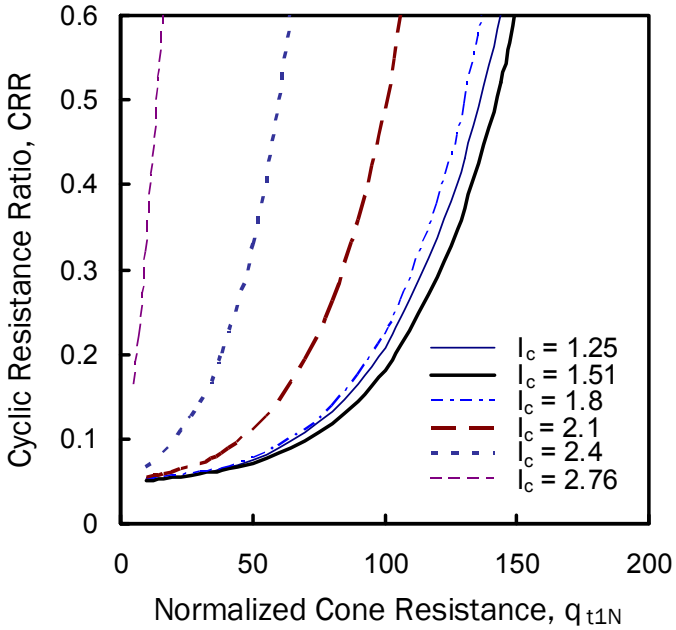

Figure 1-6. Family boundary curves of the proposed model - CRR versus q_{t1N} (Equation 1-2)

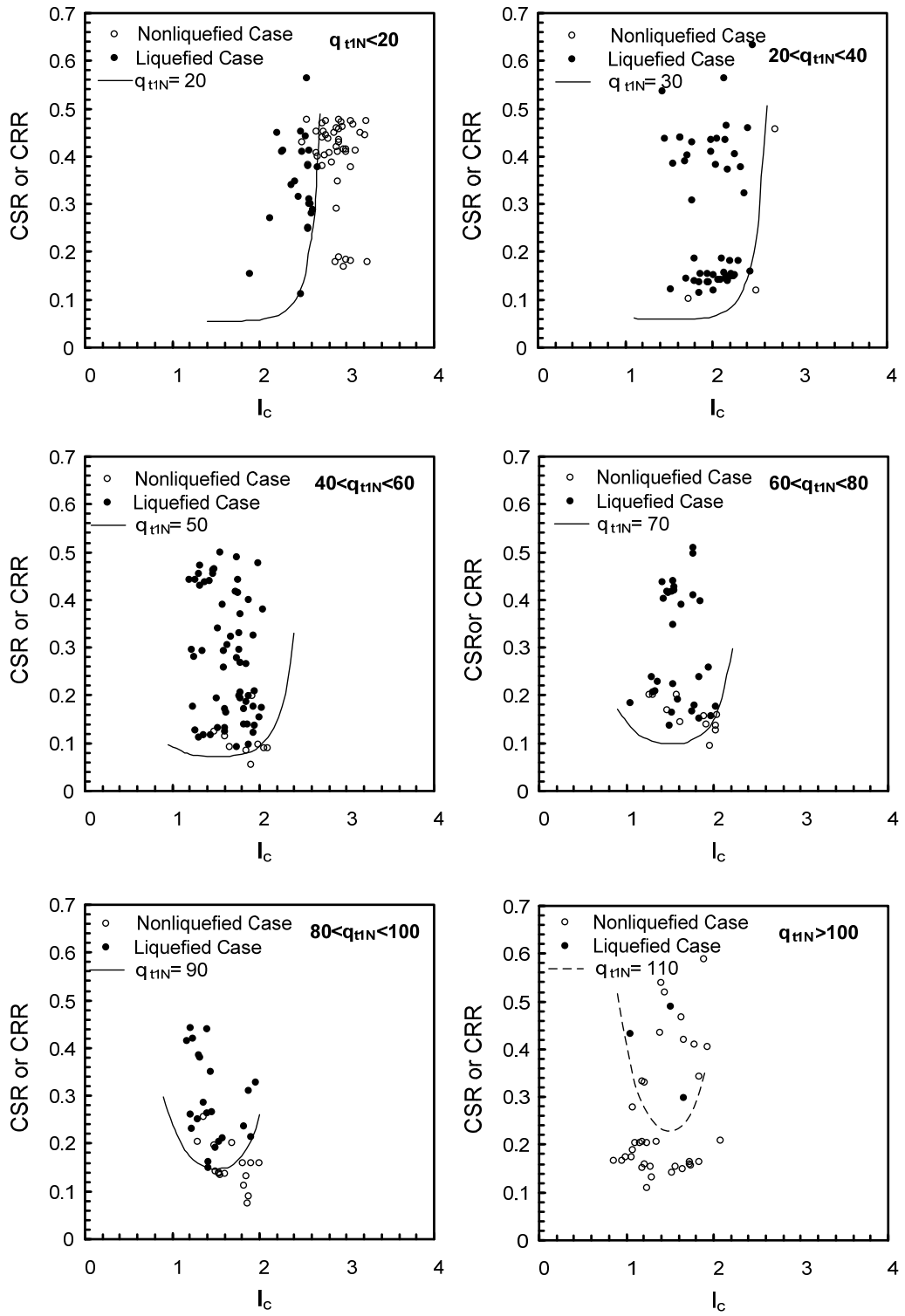

Figure 1-7. 2-D graphs of the proposed model - CRR (or CSR) versus I_c (as defined in Eq. 1-3)

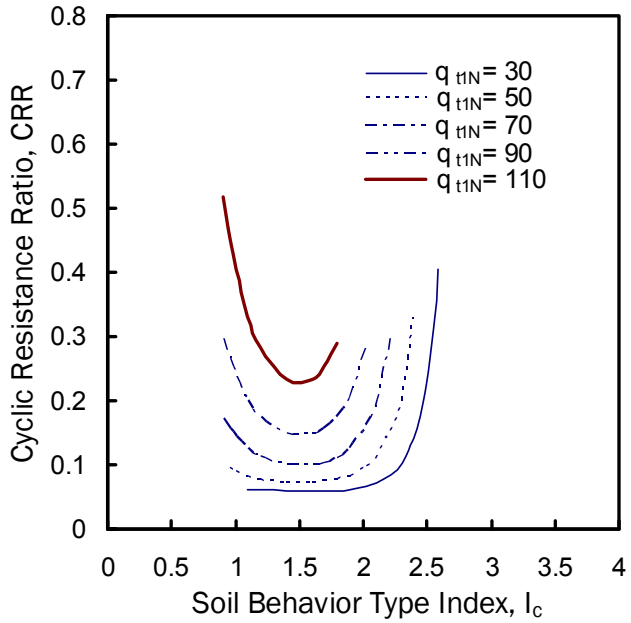

Figure 1-8. Family boundary curves of the proposed model - CRR versus I_c (Eq. 1-3)

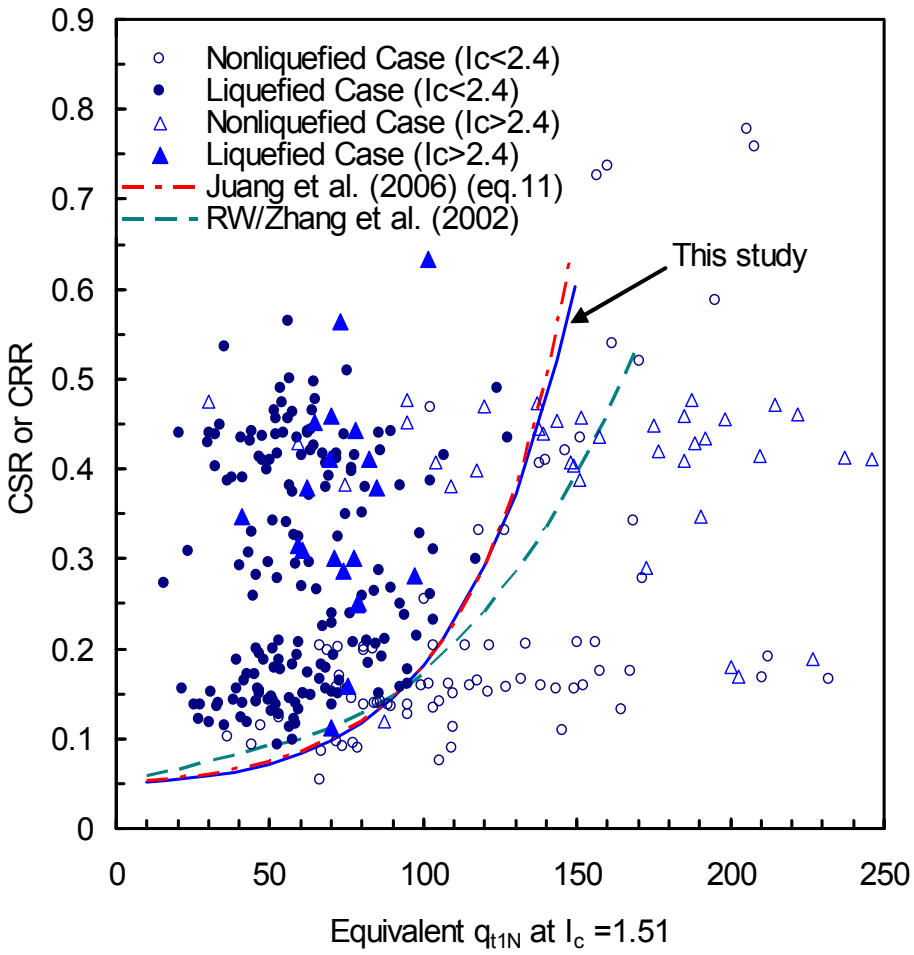

Figure 1-9. Base boundary curve with transformed data

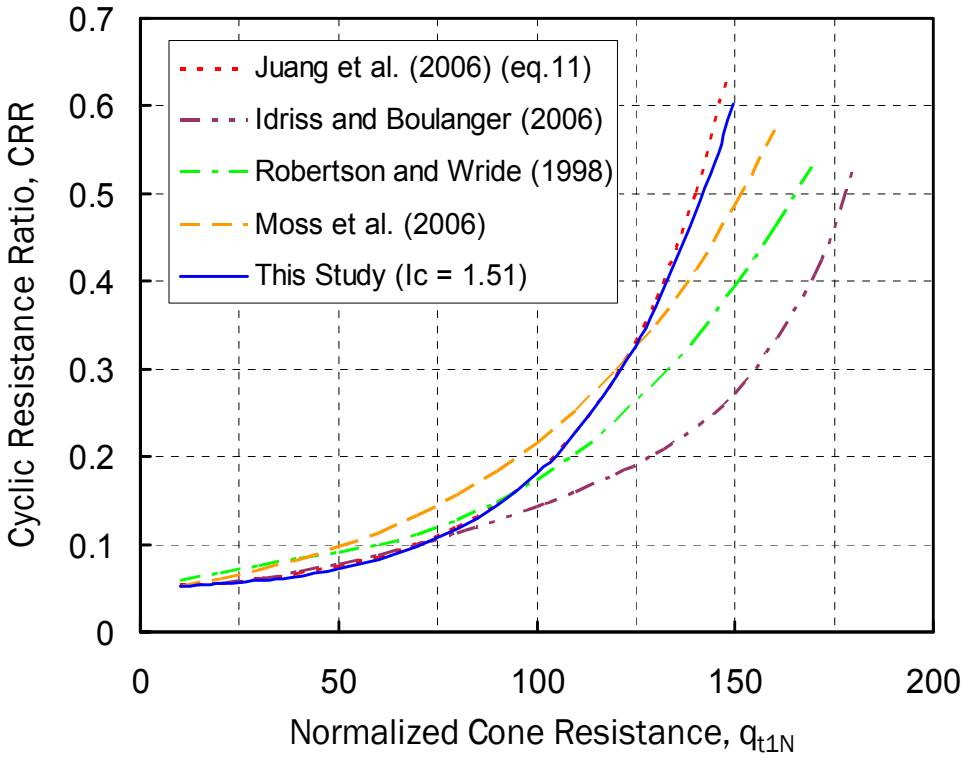

Figure 1-10. Comparison of base boundary curves from various models

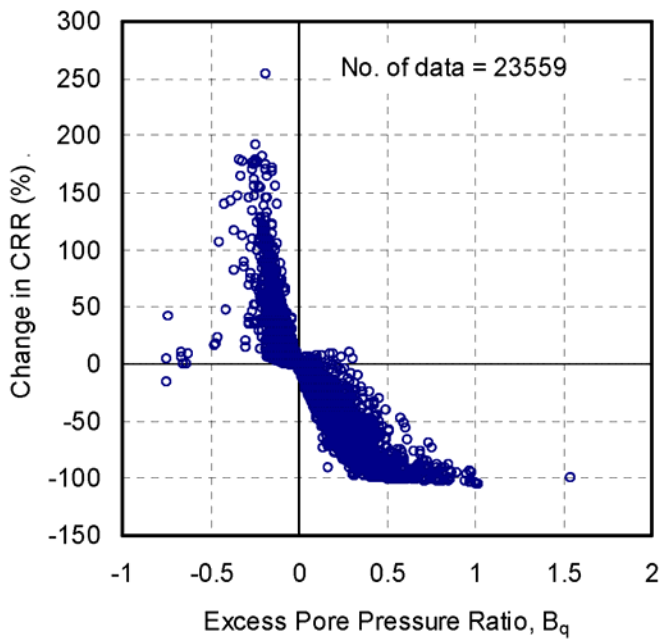

Figure 1-11. Percentage change in CRR as a result of ignoring B_q in the proposed model

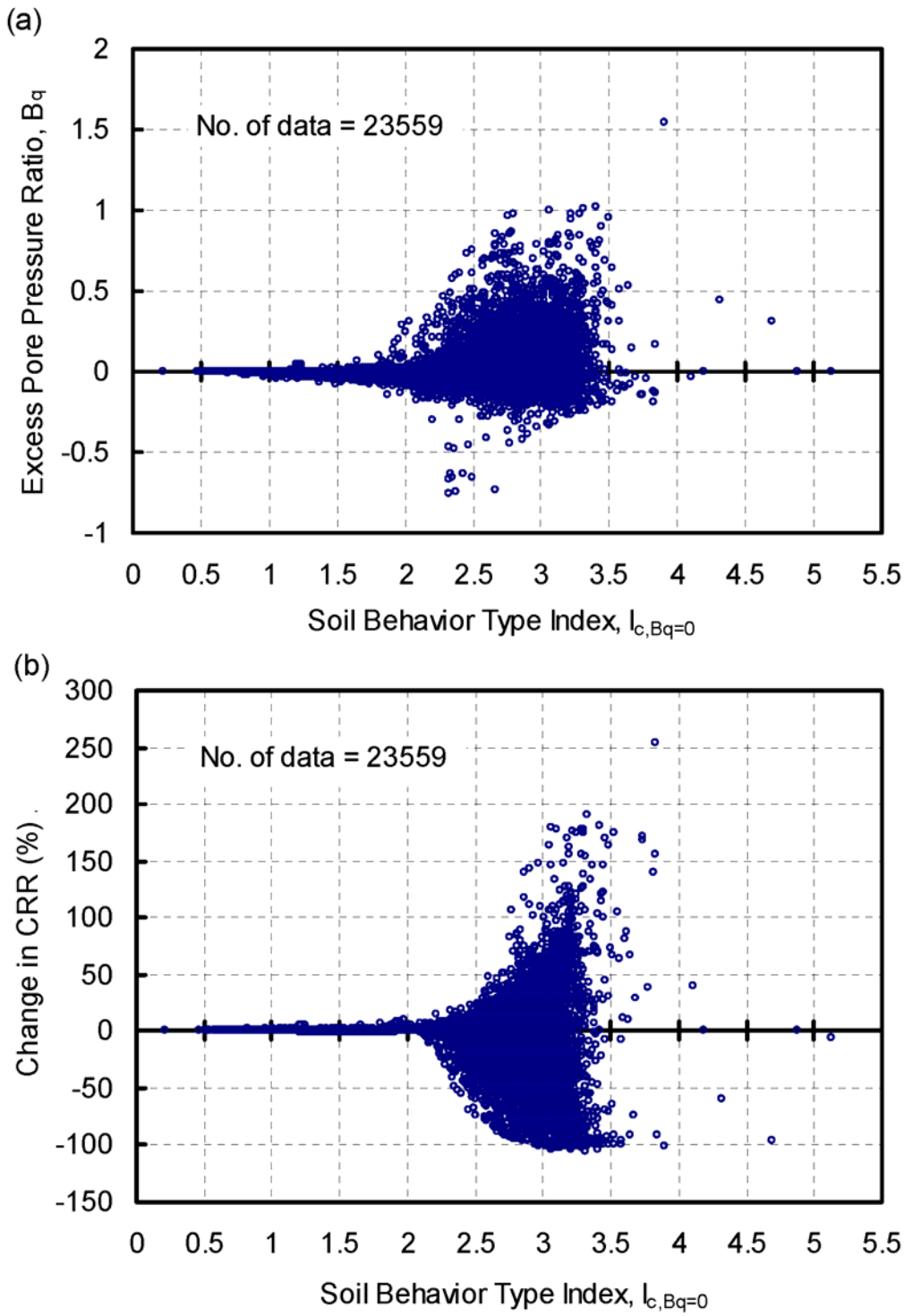

Figure 1-12. Percentage change in CRR as a result of ignoring B_q – a different angle

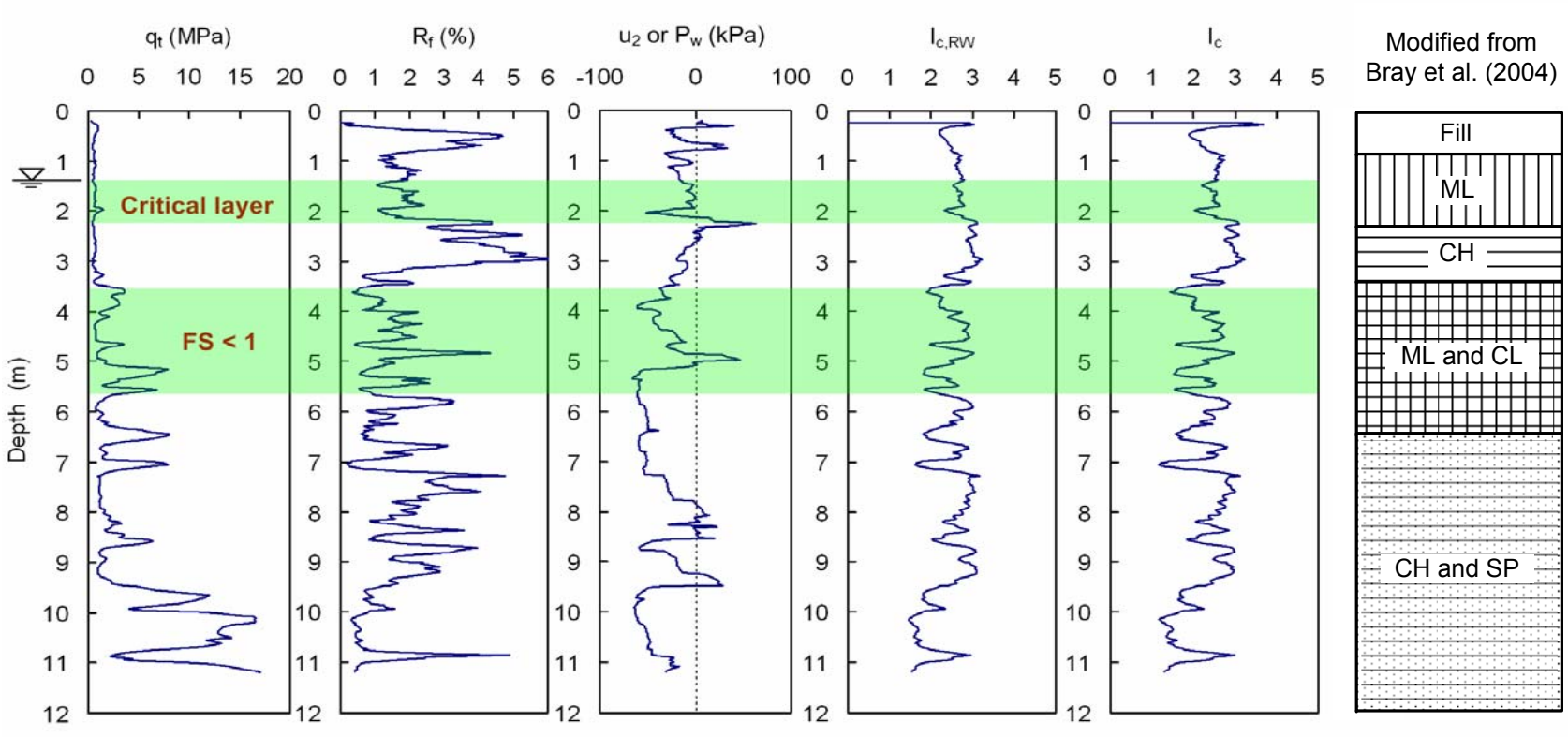

Figure 1-13. CPTu sounding profiles and soil classification at location CPT-C4 in Adapazari

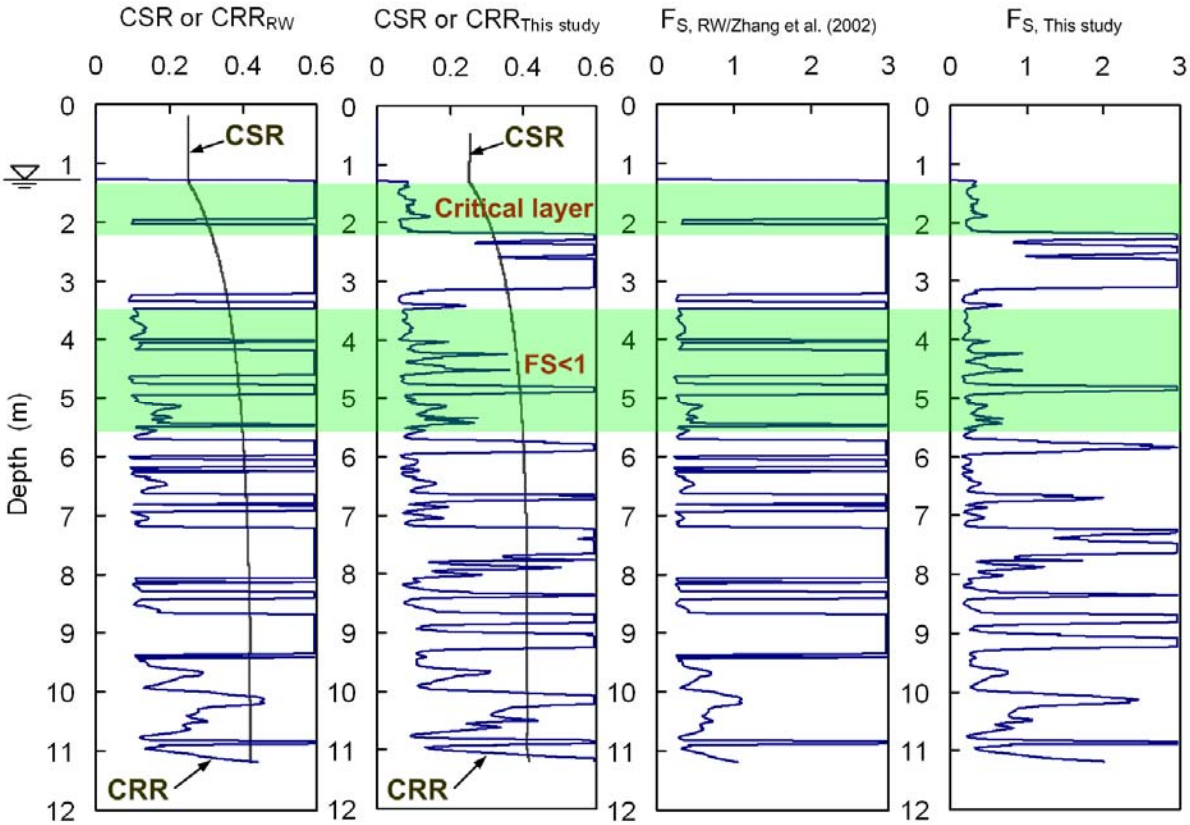

Figure 1-14. Results of the analysis of Adapazari CPT-C4 using the Robertson and Wride (R-W) method and the proposed method

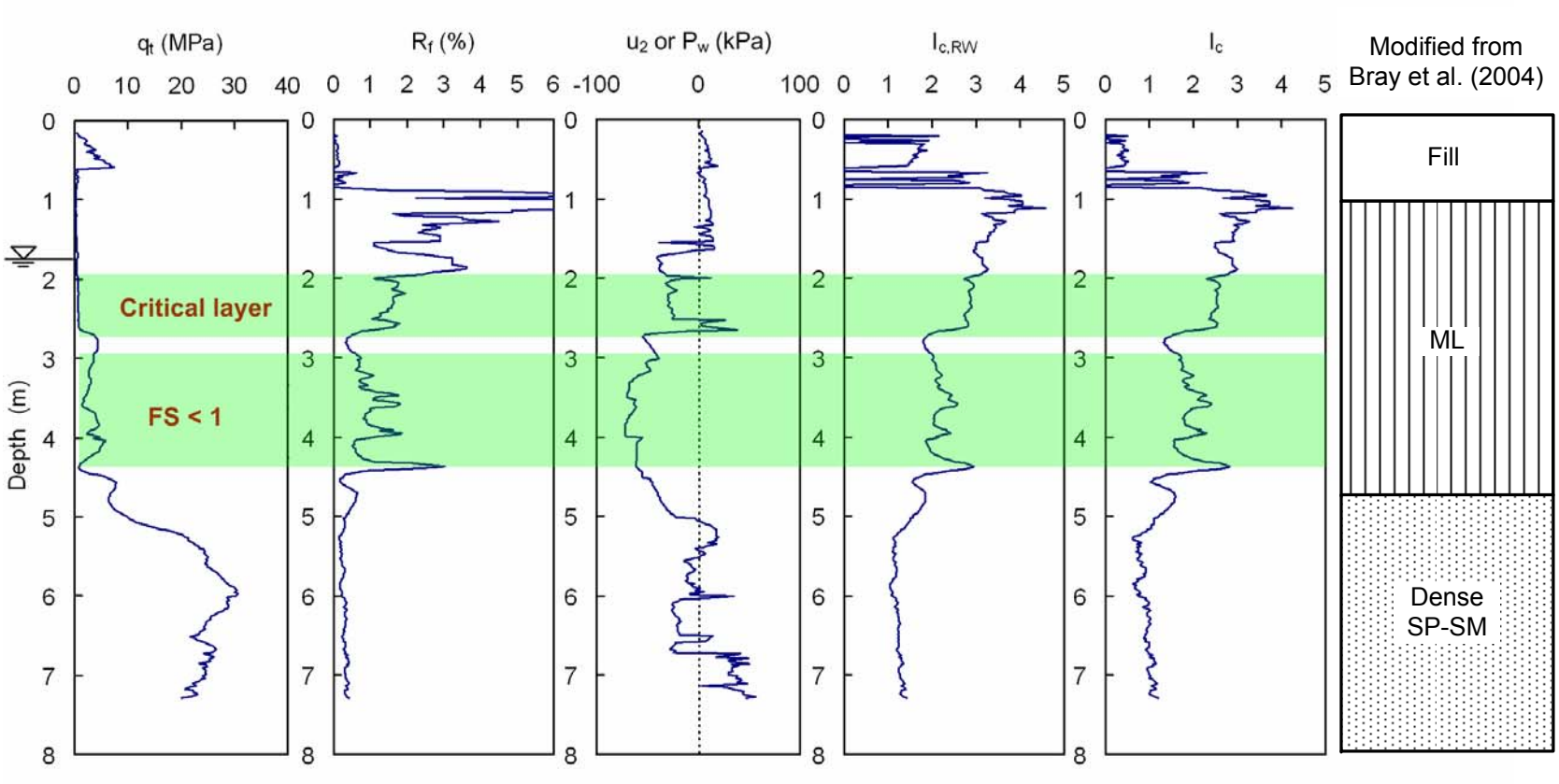

Figure 1-15. CPTu sounding profiles and soil classification at location CPT-B4 in Adapazari

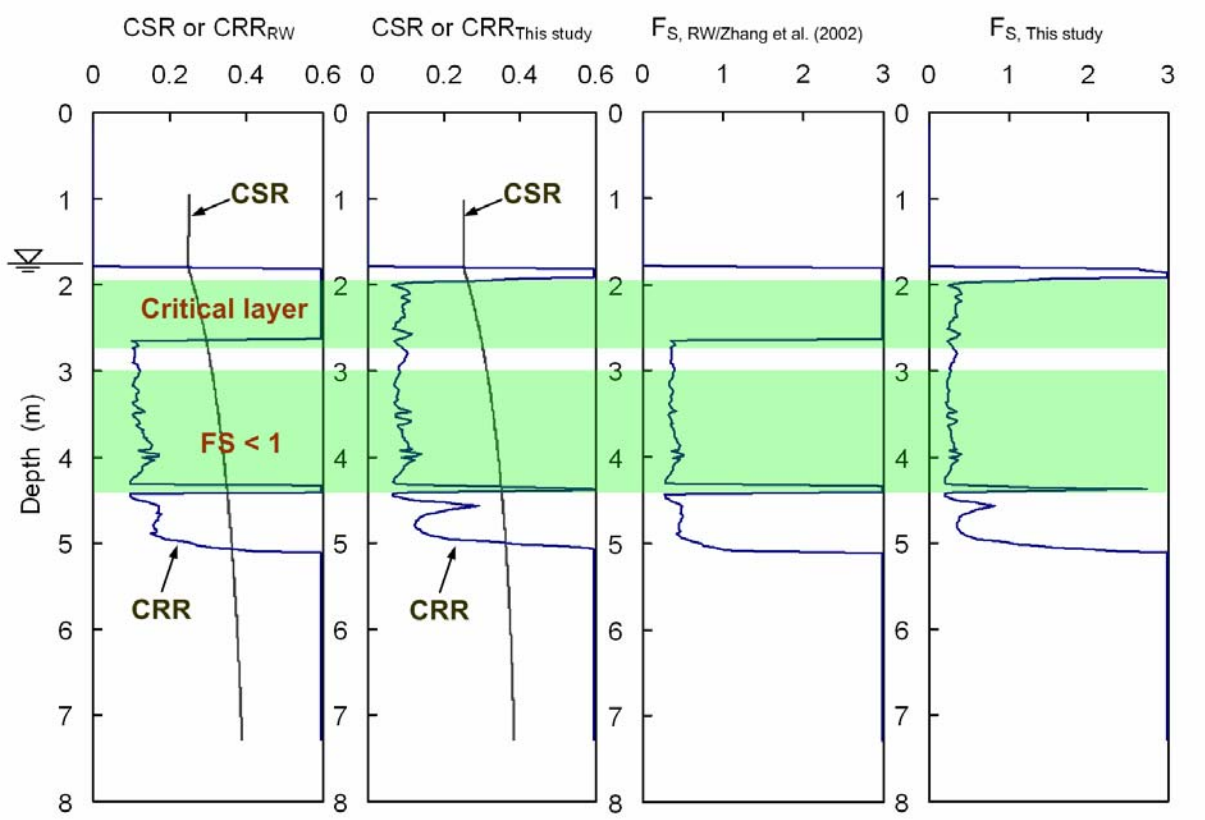

Figure 1-16. Analytical results of CPT-B4 using the Robertson and Wride (R-W) method and the proposed CPTu method

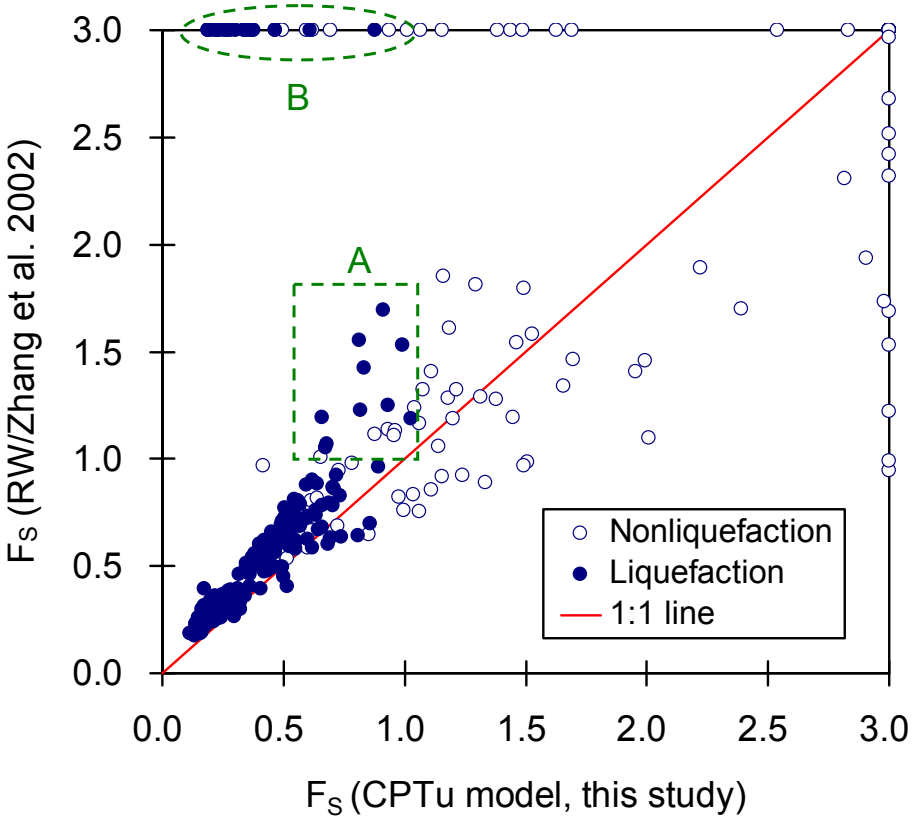

Figure 1-17. Comparison of the F_S values computed with the two methods; liquefied cases in Zones A and B are more accurately predicted by the CPTu model.

Part II:
Calibration of Liquefaction Potential Index: A Re-visit Focusing on a New CPTU Model

Part II of the Report presents a review of the state-of-the-art of Liquefaction Potential Index (LPI), a parameter created by Iwasaki and his co-workers to characterize the potential for surface manifestation of liquefaction, and the results of an extensive calibration of the LPI with a focus on a new model based on piezocone testing (CPTU). The results show that the threshold criteria developed by Iwasaki and his co-workers for interpreting the calculated LPI are not universally applicable. To the contrary, the LPI must be re-calibrated when any component model of the LPI framework is replaced with a new model. The new CPTU model is a significant advance in the cone penetration-based liquefaction evaluation; in fact, it is the first simplified model that explicitly incorporates pore pressure measurement as one of its input parameters. This CPTU model is applicable to a wide range of soil types and thusly enables a more convenient and effective modeling of liquefaction effects within the LPI framework. Finally, the results of the calibration of the LPI calculated with this CPTU model are presented and discussed.

---

*The contents of this part (Part II) of the report have been published as a Technical Paper in Engineering Geology. The article citation is as follows: Juang, C. H., et al. (2008c), "Calibration of liquefaction potential index: A re-visit focusing on a new CPTU model," *Engineering Geology*, Vol. 102, No. 1-2, 2008, pp. 19-30.

1. Introduction – An Overview of Liquefaction Potential Index

Liquefaction hazard maps have increasingly been incorporated into the seismic safety plans of communities and also used for regulatory purposes (CDMG 1997). Early maps of liquefaction hazards were mostly based on surficial geologic parameters and qualitative rankings (Youd and Hoose 1977; Youd and Perkins 1987). Later, use of field penetration data for mapping liquefaction hazards was proposed (Kavazanjian et al. 1985; Elton and Hadj-Hamou 1990), where the liquefaction potential for a specific location and depth within the soil was assessed using the simplified procedure developed by Seed and Idriss (1971, 1982). In recent years, use of the Liquefaction Potential Index (LPI), developed by Iwasaki et al. (1978, 1982), as a parameter to characterize the potential for the occurrence of damaging liquefaction in a geologic unit has received greater attention (Frost et al. 1997; Luna and Frost 1998; Divakarla et al. 1998; Holzer et al. 2002). Toprak and Holzer (2003) suggested that LPI is also useful for describing the geographic variability of liquefaction hazards; together with Geographical Information System (GIS) applications, LPI can greatly facilitate the preparation of liquefaction hazard maps. In fact, this index has been used in several U.S. Geological Survey (USGS) liquefaction hazard mapping projects (e.g., Holzer et al. 2006a).

Liquefaction Potential Index (LPI), as formulated by Iwasaki et al. (1978, 1982), is computed by integrating the "contribution" of liquefaction potential, in terms of factor of safety (F_S) against the initiation of liquefaction, over the depth at a "borehole" location. Symbolically, this index is expressed as follows:

$$\mathrm{LPI} = \int_0^{20} F \cdot w(\mathrm{z})\, d\mathrm{z} \qquad (2\text{-}1)$$

in which the depth weighting factor, $w(z) = 10 - 0.5z$ where z = depth (m). Thus, the weighting factor is 1.0 at z = 0 and linearly decreases to 0 at z = 20 m, which implies that the severity of surface manifestation of liquefaction (such as sand boils, lateral spreads, and settlement) is proportional to the proximity of the liquefied "layer" to the ground surface. The variable F is defined as follows:

$$F = 1 - F_S, \text{ for } F_S < 1; \text{ and}$$

$$F = 0 \text{ for } F_S \geq 1. \tag{2-2}$$

in which F_S is the factor of safety against the ignition of liquefaction of a soil element at a given depth. This definition of variable F implies that only soils with $F_S < 1$ "contribute" to the severity of liquefaction at the ground surface. Finally, the integration (or summation) over the depth of 20 m implies that the severity of liquefaction is proportional to the thickness of the liquefied layer, and that no contribution from soils below 20 m. Figure 2-1 shows an example of the calculation of LPI based on the cone penetration sounding profiles, which is the focus of this study and the details will be presented later.

In the formulation by Iwasaki et al. (1982), the factor of safety (F_S) is determined using a standard penetration test (SPT)-based simplified method established by the Japan Road Association (1980). On the basis of field observations at liquefaction sites in Japan, Iwasaki et al. (1982) concluded that severe liquefaction is very likely at sites with LPI > 15 and that severe liquefaction is very unlikely at sites with LPI < 5. In other words, the liquefaction risk is low if the LPI < 5, and high if the LPI > 15. This criterion with the two threshold values of 5 and 15 is referred to herein as the *Iwasaki criterion*.

Toprak and Holzer (2003) computed LPI values from cone penetration test (CPT) at sites with surface manifestations of liquefaction during the 1989 Loma Prieta, California, earthquake. In their calculations, they used the same formulation of LPI as defined by Iwasaki et al. (1982) except that factor of safety (F_S) was calculated using the CPT-based method by Robertson and Wride (1998), which employs the simplified procedure pioneered by Seed and Idriss (1971 & 1982). Toprak and Holzer (2003) reported that sand boils typically occurred at soundings where the LPI ≥5, and that lateral spreads typically occurred where the LPI ≥12. They emphasized that these threshold values are *median* LPI values, and the lower and upper *quartiles* were 3 and 10 for sand boils, and 5 and 17 for lateral spreads, respectively (Figure 2-2). They suggested that LPI ≥5 can be used as a threshold for the surface manifestation of liquefaction, which is consistent with the original suggestion by Iwasaki et al. (1982) and supported by findings of subsequent studies of Holzer et al. (2005 & 2006a,b). These studies by Holzer and his co-workers, made possible by the enormous efforts by the U.S. Geological Survey in collecting *in situ* data at liquefaction and no-liquefaction sites in recent earthquakes, represent an important milestone of LPI calibration. These studies showcase the advantages of using LPI in the regional mapping of liquefaction hazards.

In a recent comprehensive study, Lenz and Baise (2007) computed LPI values for geologic units across the East Bay of the San Francisco California Bay Area using both CPT and SPT data sets. They found that CPT-based LPI characterization results in higher hazard in the same study area than those derived from the SPT. They suggested that the bias could be caused by either misclassification of soil type in the CPT or a bias in the CPT-based simplified procedure for liquefaction potential. They attributed the latter to the finding by Juang et al. (2002) that soils with an equal F_S value, determined with different simplified

methods, may not have the same liquefaction potential due to the different degrees of model bias associated with these methods. Another important finding of the Lenz and Baise study (2007) is that the CPT-based LPI values have a much higher degree of *spatial correlation* and a lower variance over a greater distance than those estimated from SPTs (Figure 2-3). Thus, they determined that only CPT-based LPI values allowed for direct interpolation between data through ordinary kriging; the SPI-based LPI values showed no spatial correlation and kriging was not possible. They concluded that CPT is a more reliable and consistent measure of liquefaction potential. This is perhaps the first time direct evidence is presented that showcases the advantage of using the CPT over the SPT in the LPI framework. Furthermore, CPT has been shown to have a much higher degree of repeatability than SPT (Jefferies and Davies 1993), and it also provides a continuous profile while SPT does not [note: Because LPI is computed by integrating the "contribution" of liquefaction potential over depth, a continuous profile is desirable].

Lenz and Baise (2007) also showed that many geologic units in their study area had broad LPI distributions with considerable overlap between units. Similar results have been reported by many others, including Toprak and Holzer (2003) and Hayati and Andrus (2007). Lenz and Baise (2007) recommended that liquefaction classifications for these geologic units be expressed in terms of *distributions* rather than simple hazard ratings that mask the true variability within a region.

The research work summarized previously accentuates the need for fundamental and extensive calibration of LPI, especially for the purpose of mapping liquefaction hazards. Indeed, the importance of calibration has also been emphasized in recent years in several other studies. Based on their study of the 72 CPTs at sites with field observations in the 1999

Chi-Chi, Taiwan, earthquake, Lee et al. (2004) reported that when the CPT-based method by Robertson and Wride (1998) was used to determine the factor of safety (F_S), the calculated LPI values did not match either the Iwasaki criterion or the results by Toprak and Holzer (2003). The results by Lee et al. (2004) showed that 50% of liquefied cases had an LPI >15 with only 10% of liquefied cases having an LPI <5. To the contrary, 85% of non-liquefied cases had an LPI >5, and 30% of non-liquefied cases even had an LPI >15. These results, summarized in Figure 2-4, suggest that the Iwasaki criterion is not "universally" applicable. Their results are further confirmed in the contour map of liquefaction hazards prepared using the LPI values calculated for the 72 CPTs in a small town of Yuanlin, Taiwan in which several zones without surface manifestations of liquefaction showed an LPI >15. Based on these results, Lee et al. (2004) suggested that if the Robertson and Wride method is used to determine F_S, the two threshold values of the Iwasaki criterion, 5 and 15, should be modified to 13 and 21, respectively. Thusly, liquefaction risk is high for sites with LPI > 21 and low for sites with LPI < 13.

The discrepancy between the results by Toprak and Holzer (2003) and those by Lee et al. (2004) is significant. Further research is needed to determine the cause of this discrepancy. One postulation for such discrepancy is that the sites examined by Toprak and Holzer (2003) are mostly deposits of sands with modest fines content, where the sites examined by Lee et al. (2004) are mostly deposits of silty sands and sandy silts with high fines content, and this difference is critical in the application of the Robertson and Wride method in terms of screening out non-liquefiable layers. Similar opinion is presented by Papathanassiou (2008), which is reviewed later.

Important works on LPI calibration were also conducted by Sonmez and his co-workers. Sonmez (2003) classified liquefaction potential in five LPI classes, from "Non-liquefiable," to "Low", "Moderate", to "High" and "Very high." Although the LPI framework (Equation 2-1) was retained, he modified the formulation of the variable *F* as a means to calibrate LPI to the Iwasaki criterion. Partly because of the recognition that soils with an equal F_S value determined with different simplified methods may not have the same liquefaction potential, Sonmez and Gokceoglu (2005) concluded that the use of a probability-based factor for variable *F* was more realistic. They suggested a *variant* of LPI, known as the Liquefaction Severity Index (L_s). This new index was utilized in a subsequent study by Sonmez et al. (2008), in which the liquefaction-induced failures on ground surface was assessed using two parameters, the liquefaction severity index (L_s) and the thickness of capping non-liquefied layer (H_1). The assessment procedure, presented in a chart form (Sonmez et al. 2008), was shown to be effective in identifying liquefaction-induced failures on ground surface. The inclusion of the thickness of capping non-liquefied layer (H_1) in this assessment may be traced back to the findings by Ishihara (1985) and Yuan et al. (2003).

Papathanassiou et al. (2005) conducted an LPI-based microzonation mapping study for the town of Lefkada after the 2003 Lefkada earthquake. Papathanassiou (2008) conducted another significant investigation on the topic of LPI calibration. In this study, LPI values were computed using SPT data from liquefied and non-liquefied sites in Taiwan, Turkey and Greece. The LPI framework (Equation 2-1) was retained, although the factor of safety was computed using the SPT-based method by Youd et al. (2001). Furthermore, the liquefaction susceptibility criteria by Seed et al. (2003), as opposed to the so-called Chinese criteria, were used to screen out non-liquefied layers (soils with high fines content) in the computation of

LPI. The computed LPI values were presented in a box-whisker plot, which showed that for cases with "high" degree of liquefaction failures, the median LPI value is 38, and for cases with "medium" severity and "no failure," the median LPI values are 24 and 14, respectively (Figure 2-5). Significant overlap between the three categories was obvious; the first and third quartiles for cases with "high" degree of liquefaction failures are 32 and 45, respectively; and for cases with "medium" severity, the first and third quartiles are 19 and 29, respectively; and finally, for cases with "no failure," the first and third quartiles are 10 and 19, respectively. For the assessment of liquefaction hazards, Papathanassiou (2008) suggested threshold LPI values of 19 and 32, as opposed to 5 and 15 as iterated in the Iwasaki criterion. Though there are reasons for the existence of such discrepancies, Papathanassiou (2008) emphasized the impact of using different liquefaction susceptibility criteria (for example, the criteria by Seed et al. 2003 as opposed to the Chinese criteria) on the computed LPI value. Furthermore, Papathanassiou (2008) also showed that the accuracy in the "prediction" of surface manifestations of liquefaction can be improved by considering both LPI and the thickness of capping non-liquefied layer as the assessment parameters.

Finally, a fundamental study of LPI by Li et al. (2006) is reviewed below. In this study, 155 CPT soundings with field observations of liquefaction/no-liquefaction in various seismic events in the United States, Taiwan, and Turkey were analyzed. LPI values were computed using a CPT-based method by Juang et al. (2006). To investigate the effect of adopting different models for F_S in the LPI framework on the computed LPI value, four models of liquefaction resistance (and thus F_S) were examined. These models were all variants of the CPT-based method by Juang et al. (2006) and each with a different degree of conservatism (characterized with a different mean probability, ranging from 0.15 to 0.50, as

shown in Figure 2-6). The results of the LPI calibration analyses showed the obvious effect of adopting different models for F_S (Figure 2-7). Moreover, the F_S model that was characterized with a mean probability of approximately 0.35 (labeled as Model #3 in Figure 2-6) yielded the "best" results.

Another point of interest in the Li study (2006) was the investigation of possible use of probability of liquefaction (P_L) at a given depth, in lieu of factor of safety (F_S), in the LPI framework. In their work, Equation 2-1 was retained but variable F was defined based on the probability of liquefaction at a given depth as follows:

$$F = P_L - 0.35, \text{ for } P_L \geq 0.35; \text{ and}$$

$$F = 0 \text{ for } P_L < 0.35. \tag{2-3}$$

Equation 2-3 is conceptually parallel to Equation 2-2. A soil "layer" with $P_L < 0.35$ is assumed to have negligible contribution to surface manifestations of liquefaction. This cut-off value was chosen for two reasons. First, according to a classification criterion by Chen and Juang (2000), the liquefaction potential of a soil is rated as "low" if $P_L < 0.35$. Thusly, the contribution of a soil layer with $P_L < 0.35$ to surface manifestations could be negligible. Second, a sensitivity analysis involving five different cut-off probabilities ranging from 0.15 to 0.50, conducted by Li et al. (2006), showed that use of the cut-off probability of 0.35 yielded the best results (in terms of being able to distinguish liquefaction severity based on the calculated LPI).

Based on the results of their extensive calibration, Li et al. (2006) recommended use of the probability-based variable F (Equation 2-3) for computing LPI, which is consistent with the conclusion of Sonmez and Gokceoglu (2005) and Sonmez et al. (2008).

Furthermore, in view of the possible variation in the calculated LPI value, Li et al. (2006) developed an empirical equation that relates the computed LPI to probability of surface manifestations of liquefaction. The equation, the form of which is almost identical to that obtained by Papathanassiou (2008) through logistic regression, provided a simple means for interpreting the computed LPI in terms of probability of surface manifestations of liquefaction.

2. Objective of the present study

CPTU simplified model for liquefaction potential evaluation has been developed and presented in Part I of this report. One of the unique features of this study is the inclusion of pore pressure measurement from CPTU, in terms of pore pressure ratio (B_q), in the formulation of soil behavior type index (I_c). This form of I_c was originally developed by Jefferies and Davies (1993). It should be noted that the more well-known soil behavior type index used in the Robertson and Wride (1998) method is actually a simplification (by removing the B_q term) of the original 1993 definition by Jefferies and Davies. The inclusion of B_q in the formulation of I_c (as will be shown later in Equation 2-6) is essential to allow for the evaluation of liquefaction resistance for a wider range of soils, including soils that are previously described as "too clay-rich to liquefy." A CPTU-based method that can accurately evaluate the liquefaction resistance of soils over a wide range of I_c values (where B_q is included in the formulation) would enable a more meaningful modeling of liquefaction effects within the framework of LPI. Considering that no sample is taken in a CPTU, being able to accurately evaluate the liquefaction resistance over a full range of I_c values is very beneficial in the computation of LPI.

Furthermore, there has been some concern over the use of soil behavior type index (where B_q is omitted) as a proxy to the effect of "fines" on liquefaction resistance (Idriss and Boulanger 2004 &2006). The CPTU model developed in this study (Part I) essentially removed this concern. The results of the analysis of cases from critical layers at selected ground failure sites in Adapazari using this CPTU model agreed well with field observations in the 1999 Kocaeli earthquake. The results showed that those liquefied cases previously identified as "too clay rich to liquefy" based on the Robertson and Wride (1998) method can be correctly "predicted" using this CPTU model. This model has been shown to be applicable to soils with a wide range of I_c.

In light of the previous discussions of LPI and the availability of the CPTU model for liquefaction potential evaluation, it is of particular interest to calibrate the LPI computed with new results of variable *F* that is based on this CPTU model. Thus, the objective of this study is to revisit the issue of LPI calibration with a focus on the CPTU model developed in this study (Part I; also see Chen et al., 2008 and Juang et al. 2008b).

3. Summary of the CPTU model (Juang et al. 2008b)

This CPTU model is a simplified method that follows the general outline of the simplified procedure pioneered by Seed and Idriss (1971 & 1982). As such, two components are needed to determine the liquefaction potential of a soil element or finite layer; one is a model for cyclic stress ratio (CSR) and the other is a model for cyclic resistance ratio (CRR). For historic perspective, the reader is referred to Seed and Idriss (1982), Seed et al. (1985), Youd et al. (2001), and Idriss and Boulanger (2004). The model for CSR adopted in the

present study is one recommended by Idriss and Boulanger (2004 & 2006). Symbolically, this CSR model is expressed as:

$$CSR = 0.65\left(\frac{\sigma_v}{\sigma'_v}\right)\left(\frac{a_{max}}{g}\right)(r_d)\left(\frac{1}{MSF}\right)\left(\frac{1}{K_\sigma}\right) \tag{2-4}$$

where σ_v and σ'_v are the total stress and the effective stress, respectively, of the soil of concern at a given depth, *g* is the acceleration of gravity, which is the unit for peak ground surface acceleration a_{max}, r_d is the depth-dependent shear stress reduction factor, MSF is the magnitude scaling factor, and K_σ is the overburden correction factor for cyclic stress ratio. Both σ_v and σ'_v are in same units, and r_d, MSF, and K_σ are dimensionless. It should be noted that this definition of CSR (Equation 2-4) is already adjusted to the conditions of moment magnitude $M_w = 7.5$ and $\sigma'_v = 100$ kPa. This adjustment is essential to process case histories that were collected from different earthquakes of various magnitudes and to unify the influence of confining pressures. The intermediate parameters, r_d, K_σ, and MSF as defined by Idriss and Boulanger (2006) are employed herein. The formulations of these parameters are listed in Appendix II.

Following the convention of the simplified procedure, the CRR is the "limiting" CSR beyond which liquefaction is expected to occur. Thus, the "boundary curve" or the CRR model can be developed through "calibration" with sufficient case histories where CSR levels are known. In the CPTU model developed in the present study, the CRR model is expressed as (with modification to the original form):

$$CRR = 0.05 + \exp\left[A + B \times (q_{t1N}/100)^C\right] \tag{2-5}$$

where

$$A = I_c \cdot (q_{t1N}/100) - 10.455$$

$$B = 0.669 \cdot I_c^3 - 5.55 \cdot I_c + 12.993$$

$$C = 0.284 - 0.0214 \cdot I_c^2$$

and where the soil behavior type index I_c is defined as (after Jefferies and Davies 1993):

$$I_c = \sqrt{\left[3 - \log_{10}\left\{Q_t\left(1 - B_q\right) + 1\right\}\right]^2 + \left[1.5 + 1.3\left(\log_{10} F_R\right)\right]^2} \tag{2-6}$$

The parameters Q_t, B_q, and F_R are the normalized cone tip resistance, excess pore pressure ratio, and normalized friction ratio, respectively. These are derived parameters from CPTU measurements. Finally, the parameter q_{t1N} is the adjusted cone tip resistance defined by Idriss and Boulanger (2004 & 2006). This parameter along with other "raw" and derived parameters of the CPTU is defined in Appendix I.

As with the conventional approach, liquefaction potential of a soil element is measured with factor of safety, which is determined as F_S = CRR/CSR where CSR is calculated with Equation 2-4 and CRR with Equation 2-5.

The developed CPTU model has been shown applicable to a wide range of soils, including soils that were previously considered "too clay-rich to liquefy." Figure 2-8 shows the data points that were used for the development of the CPTU model plotted on the soil behavioral classification chart. Figure 2-9 shows three-dimensional graphs of boundary surfaces (3-D view of the CRR model) along with data points; the capability of this model to distinguish liquefied cases from nonliquefied cases is shown.

The most significant feature of this CPTU model is the inclusion of the porewater pressure ratio B_q in the formulation of CRR through I_c. This enables the model to be applicable to a wide range of soils. An example to demonstrate the superiority of this CPTU model is given herein. This example concerns a case history from a ground failure site in Adapazari during the 1999 Kocaeli earthquake. Figure 2-10 shows the CPTU soundings, the I_c values, and the soil profile as determined by the SPT borehole sampling at the location designated CPT-C4. The critical layer marked in this figure is the layer that was judged by Bray et al. (2004 & 2006) through their field investigation, laboratory testing and finite element analysis as the one responsible for surface manifestation of liquefaction. However, this layer would have been identified as non-liquefiable had the Robertson and Wride method (1998) been employed. The layer marked with "F_S <1" in Figure 2-10 is a layer that was determined to be liquefiable using the Robertson and Wride method. Figure 2-11 shows the results of the analyses using both the Robertson and Wride method and the newly developed CPTU model. The results show that the critical layer previously identified as "too clay rich to liquefy" based on the Robertson and Wride (1998) method can be correctly "predicted" using the new CPTU model. The overall F_S-profile determined with the new CPTU model shows significant improvement over the F_S-profile determined by the Robertson and Wride method.

4. Probabilistic characterization of the new CPTU model

As noted in Section 1, one possibility of computing LPI is to define variable *F* based on the probability of liquefaction of a soil element at a given depth, as reflected in Equation 2-3. The new CPTU model is a deterministic method. To develop a mapping function that can provide an estimate of the conditional probability of liquefaction (P_L) for a given factor of

safety (F_S), the procedure described in Juang et al. (2002) is applied. Figure 2-12 shows the distribution of the computed F_S values of non-liquefied cases, while Figure 2-13 shows the distribution of the computed F_S values of liquefied cases. By applying Bayes' theorem of condition probability, the procedure of which was described in detail by Juang et al. (2002), the following mapping function is obtained (Figure 2-14):

$$P_L = \frac{1}{1 + e^{-3.64+5.37F_S}} \tag{2-7}$$

It should be noted that sensitivity analysis was performed involving different assumptions of prior probability ratio (1.0 and 0.82) and different class widths (0.2, 0.25, and 0.3) in the discretization of probability density function of the F_S values that were computed for both groups of liquefied and non-liquefied cases. In general, the prior probability ratio, defined as the ratio of the prior probability of liquefaction over the prior probability of no liquefaction, should be 1.0 based on the *principle of maximum entropy* as explained by Juang et al. (2000b & 2002). Because of sampling disparity in the database, some compensation in the assumed prior probability ratio might be appropriate, and in this study, a ratio of 0.82 (Wilson Tang 2007, personal communication) was also used to examine any possible difference. The results of sensitivity analysis, however, show that these changes in the class widths and prior probability ratios yielded negligible difference in the developed mapping function. Thus, Equation 2-7 is considered satisfactory.

5. Calibration of LPI with a focus on new CPTU model

The discussions so far allow for calculation of LPI at any site characterized by CPTU soundings and subject to a given seismic loading. The CPTU model (Equations 2-4 and 2-5) allows for the determination of F_S at a given depth, and the Iwasaki framework (Equations 2-1 and 2-2) allows for the determination of LPI at this site. Alternatively, LPI can be calculated by replacing variable *F* defined in Equation 2-2 with Equation 2-3, and in such scenario, the probability of liquefaction (P_L) at a given depth with a known F_S is obtained first from Equation 2-7.

For calibration of the LPI calculated in the manner just described, 75 CPTU soundings are used. These are CPTU conducted at sites with or without liquefaction surface manifestation in the 1999 Chi-Chi, Taiwan and Kocaeli, Turkey earthquakes. The cases with surface manifestations are referred to herein as liquefied cases, and those without surface manifestations are referred to as nonliquefied cases. It should be noted that many other case histories in the existing database, particularly those from cleaner sand sites, are not included in this calibration analysis because of their lack of pore pressure sounding profile. Thus, a bias may exist in this calibration analysis because the sites investigated are largely underlain by fine-grained soils, and thusly, caution should be exercised when extending the results to cleaner sand sites. Table 2-1 lists relevant data of these CPTUs.

Figure 2-15 shows the box-whisker plot of the LPI values calculated with variable *F* defined by both Equation 2-2 and Equation 2-3. In these calculations, the CPTU sounding profiles as listed in Table 2-1 are used. As shown in Figure 2-15, the P_L-based LPI (variable *F* based on Equation 2-3) yields smaller variation in the calculated LPI than does the F_S-based LPI (variable *F* based on Equation 2-2). Moreover, the distinction between the LPI values of

the liquefied group and those of the non-liquefied group is more obvious in the P_L-based formulation than in the F_S-based formulation. Therefore, for the calibration of the LPI computed with the new CPTU model, only the P_L-based formulation is considered.

To interpret the computed LPI, the same Bayes' theorem as employed for the development of Equation 2-7 can be used. As demonstrated by Li et al. (2006), a function that relates the computed LPI to the conditional probability of surface manifestation of liquefaction (P_G) can be established based on the distribution of the LPI of liquefied cases and the distribution of the LPI of nonliquefied cases. Figure 2-16 shows the histograms and cumulative distributions of liquefied and non-liquefied groups for three chosen class widths. By means of Bayes' theorem, the following mapping function is obtained (in reference to Figure 2-17):

$$P_G = \frac{1}{1 + e^{6.75 - 0.57(LPI)}} \tag{2-8}$$

To examine the accuracy of the developed mapping function (Equation 2-8), all cases in Table 2-1 are evaluated for their probabilities of surface manifestations (P_G). The computed P_G values are shown in Figure 2-18 along with the five risk levels (categories) proposed by Li et al. (2006). The results indicate that the calculated P_G values can distinguish the cases with surface manifestations of liquefaction from those without surface manifestations. Among the cases without surface manifestation, approximately 83% is in the "extremely low" and "low" risk categories, 17% in the "medium" risk category, and none in the "high" and "extremely high" categories. Among the cases with surface manifestation, approximately 82% is in the "extremely high" and "high" risk categories, 16% in "medium"

risk category, and 2% in the "low" and "extremely low" risk categories. A summary of these results is listed in Table 2-2.

In summary, the procedure for estimating the probability of surface manifestations of liquefaction has been developed through calibration of LPI and is recommended herein. This recommended procedure is summarized in the following. At a site with CPTU sounding profiles, the CRR profile is obtained through Equation 2-5 and the associated definitions of parameters, and the CSR profile is obtained through Equation 2-4 and the associated definitions of parameters. The profile of F_S can be determined next, followed by the profile of P_L (through Equation 2-7). Then, by applying Equations 2-1 and 2-3, a value of the LPI for the CPTU site can be determined. Finally, the probability of surface manifestations of liquefaction is determined with Equation 2-8. It should be emphasized that the entire process and the associated component models must be followed with no substitution of any component model, as they were calibrated as a whole.

The calculated P_G values may be used along with other more abundant data such as surficial geologic parameters for mapping regional liquefaction hazards. On the other hand, as a site-specific design tool, the calculated P_G should be applied with a conservative bias. A "tolerable" level of risk (or P_G) should be selected considering both safety and economic aspects of the project and the need of the client, affected public, and regulators. For *ordinary* engineering projects, the criterion of $P_G \leq 0.2$ (note: this threshold value is at the midpoint of the "Low" risk category) may be adopted; for important or critical structures, a threshold value of $P_G \leq 0.1$ or much lower may be appropriate. Ultimately, the need of the client, affected public, and regulators must be satisfied.

Finally, it is interesting to note that the concept of the probability of surface manifestations of liquefaction was also employed in the latest development of probabilistic liquefaction hazards maps at the U.S. Geological Survey (for example, Holzer et al. 2006a & 2006b), although their formulation is different from that presented in this report. In these USGS studies, they used the Robertson and Wride method (1998) and the CPT data (without porewater pressure parameter) to calculated the F_S, and Equations 2-1 and 2-2 to integrate the LPI. They developed the complementary cumulative distributions of LPI to establish liquefaction probability curves of geologic units; the latter was then used to prepare probabilistic maps.

6. Summary and Conclusions

A summary of the state-of-the-art of the Liquefaction Potential Index (LPI) is presented, following by the results of a calibration of LPI that is computed with the newly developed CPTU model. This CPTU model is the first of its kind that incorporates explicitly the pore pressure measurements in a piezocone penetration testing (CPTU) as one of its input parameters. The new CPTU model is applicable to a wide range of soils and thusly enables a more convenient and effective modeling of liquefaction effects within the framework of LPI. The procedure for determining the probability of surface manifestation of liquefaction based on the results of the LPI calibration is presented and readily applicable.

The following conclusions are reached based on the results presented in this report. Firstly and most importantly, the Iwasaki criterion, in which LPI = 5 and 15 were chosen as the threshold values for low and high liquefaction risk, respectively, is found to be "not universally applicable." Thus, the LPI must be re-calibrated when any component model of

the LPI framework is replaced with a new model. This is no difference from the need to re-calibrate equipment for laboratory or in situ testing when a part of the equipment has been replaced with a new design or the testing procedure has been changed.

The newly developed CPTU model is characterized probabilistically by means of Bayes' theorem using case histories. Sensitivity analysis involving different class widths in the discretization of probability density function of the F_S values computed for both groups of liquefied and non-liquefied cases, and different assumptions of prior probability ratio, shows that modest changes in the chosen class width and prior probability ratio yielded negligible difference in the developed mapping function. Thus, the developed mapping function, which relates the factor of safety to the conditional probability of liquefaction, is considered satisfactory.

In this study, the LPI is calculated with Equation 2-1, in which variable *F* is defined by Equation 2-3 based on P_L that is computed from the probabilistic CPTU model. The calibration analysis shows that satisfactory interpretation of the computed LPI can be achieved with the concept of probability of surface manifestation of liquefaction (P_G). In this regard, a mapping function that relates LPI to P_G is developed, which is shown to be able to distinguish cases with surface manifestations of liquefaction from cases without surface manifestations.

The calculated P_G values may be used along with other more abundant data such as surficial geologic parameters for mapping regional liquefaction hazards. On the other hand, as a site-specific design tool, the calculated P_G should be applied with a conservative bias. A "tolerable" level of risk (or P_G) should be selected considering both safety and economic aspects of the project and the need of the client, affected public, and regulators. For ordinary

engineering projects, the criterion of $P_G \leq 0.2$ may be adopted, although ultimately the need of the client, affected public, and regulators must also be satisfied.

Table 2-1. CPTU soundings that were used in the analysis and calibration of LPI

Sounding ID	Sounding depth (m)	LPI ($F = P_L - 0.35$)	Liq?	Earthquake	a_{max} (g)	Location	Reference
BLC3	20.0	6.7	No	Chi-Chi[a]	0.12	Changbin	Ku (2004)
BLC5	20.0	5.2					
BLC6	20.0	6.0					
LWA3	20.0	7.7					
LWA5	20.0	7.9					
LWA7	20.0	5.5					
LWA9	20.0	3.8					
LWC2	20.0	4.1					
LWD2	20.0	9.0					
NT-C-16	18.8	2.8	No	Chi-Chi	0.38	Nantou	Ku (2004)
YLC10	30.0	12.5	No	Chi-Chi	0.18	Yuanlin	Ku (2004)
YLC11	27.9	12.1					
YLC13	30.0	11.6					
YLC16	30.0	10.0					
YLC28	30.0	8.9					
YLC36	30.1	6.9					
YLC8	30.0	7.4					
YLC9	30.0	9.4					
CPT-C4	11.0	22.9	Yes	Izmit[b]	0.40	Adapazari	Bray et al. (2004 & 2006)
CPT-C6	11.6	21.8					
CPT-E1	25.2	27.0					
CPT-F1	26.4	34.4					
CPT-G1	24.3	37.5					
CPT-G3	11.0	29.9					
CPT-H2	28.1	18.0					
CPT-H3	10.1	16.9					
CPT-J2	24.7	29.4					
CPT-J4	10.1	26.0					
CPT-K2	10.0	19.9					
LK0	20.0	20.8	Yes	Chi-Chi	0.12	Lukang	Ku (2004)
LK1	20.0	13.4					
LK2	20.0	14.2					
LK46	20.0	17.4	Yes	Chi-Chi	0.12	Lukang	Ku (2004)
LK5	20.0	14.1					
LK-E3	20.0	19.6					
LK-E4	20.0	12.5					

Table 2-1. Continued

Sounding ID	Sounding depth (m)	LPI (F = PL – 0.35)	Liq?	Earthquake	a_{max} (g)	Location	Reference
LK-N3	20.0	18.0	Yes	Chi-Chi	0.12	Lukang	Ku (2004)
LWA2	20.0	12.2	Yes	Chi-Chi	0.12	Changbin	Ku (2004)
LWA8	20.0	8.8					
LWC1	20.0	12.8					
NT-1	11.4	15.5	Yes	Chi-Chi	0.38	Nantou	Ku (2004)
NT-C-02	16.4	22.0					
NT-C-03	26.2	20.4					
NT-C-07	25.1	26.6					
NT-C-15	18.3	29.8					
TH1-02	25.6	25.0	Yes	Chi-Chi	0.16	Taichung Harbor	Lai et al. (2004)
TH1-03	12.8	17.8					
TH1-07	30.1	11.5					
TH2-01	30.0	11.8					
TH2-02	30.1	20.4					
TH2-04	11.9	12.2					
TH3-01	21.9	27.8					
TH3-02	10.5	15.6					
TH3-04	11.7	13.5					
TH4-01	22.7	24.8					
TH4-02	13.6	17.4					
TH4-03	27.0	13.5					
THI-03	12.8	17.8					
WF-1	11.4	30.0	Yes	Chi-Chi	0.67	Wufeng	Ku (2004)
WF-5	14.8	23.7					
WF-C10	12.1	31.2					
WF-C15	19.3	15.2					
WF-C7	12.4	13.8					
YL1	29.1	16.7	Yes	Chi-Chi	0.18	Yuanlin	Ku (2004)
YL3	30.2	15.6					
YLC19	30.0	21.3					
YLC2	18.4	12.8					
YLC22	30.0	21.4					
YLC24	30.0	21.3					
YLC25	12.9	17.0					
YLC31	29.1	23.9					
YLC32	30.0	24.2					
YLC35	13.0	12.3					
YLC4	18.3	14.3					
YLC43	30.0	10.4					

[a] 1999 Chi-Chi earthquake of Taiwan (M_w = 7.6);
[b] 1999 Kocaeli (Izmit) Earthquake of Turkey (M_w = 7.4)

Table 2-2. Distribution of the P_G values in the group of cases with surface manifestation (liquefied cases) and in the group of cases without surface manifestation (non-liquefied cases)

Category (or level) of risk of surface manifestation of liquefaction	P_G	Distribution of cases without surface manifestation	Distribution of cases with surface manifestation
Extremely low	0.0 – 0.1	61%	0
Low	0.1 – 0.3	22%	2%
Medium	0.3 – 0.7	17%	16%
High	0.7 – 0.9	0	19%
Extremely high	0.9 – 1.0	0	63%

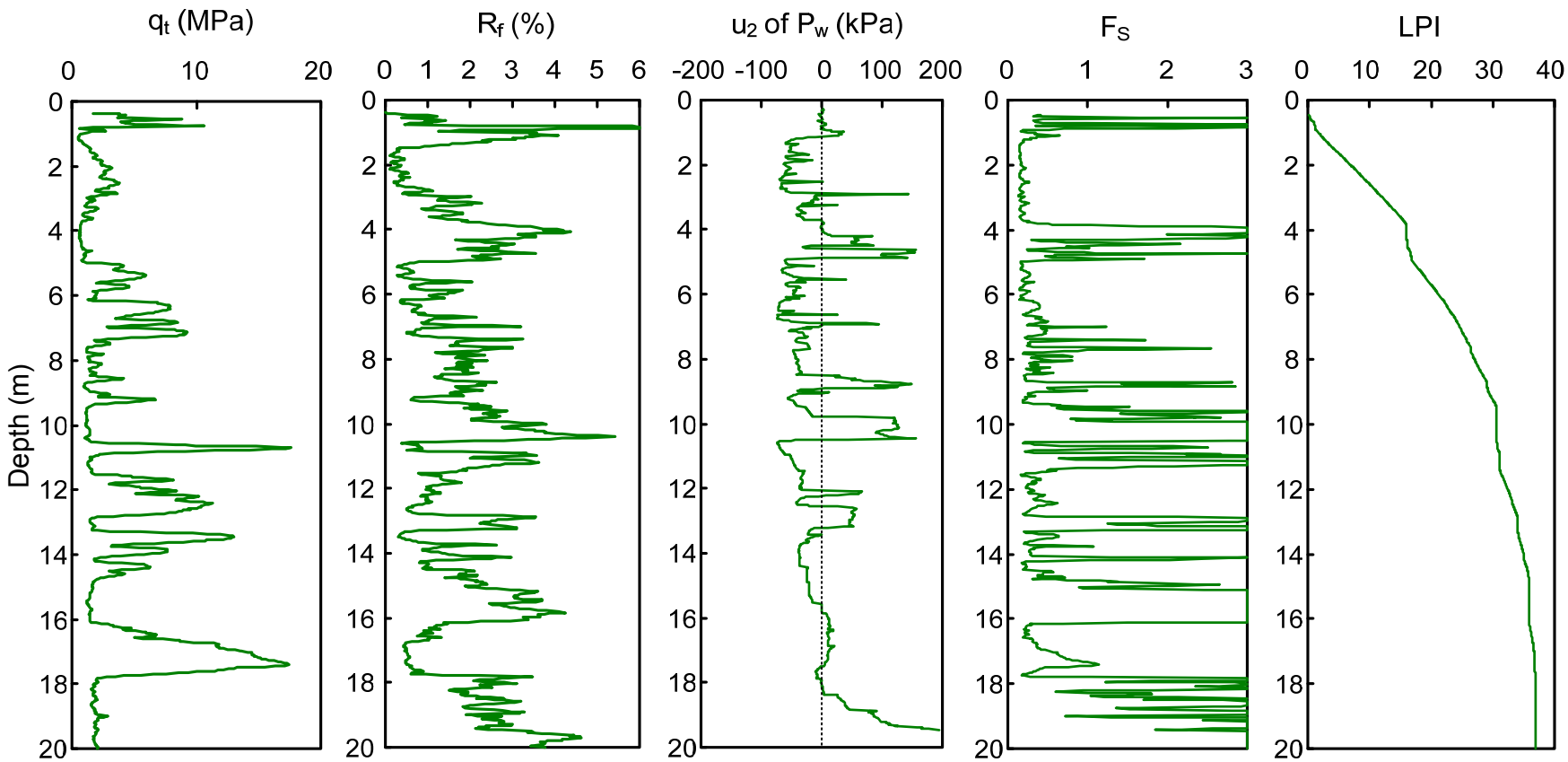

Figure 2-1. CPTU soundings and the analysis results at location CPT-G1 in Adpazari (source data from Bray et al., 2004)

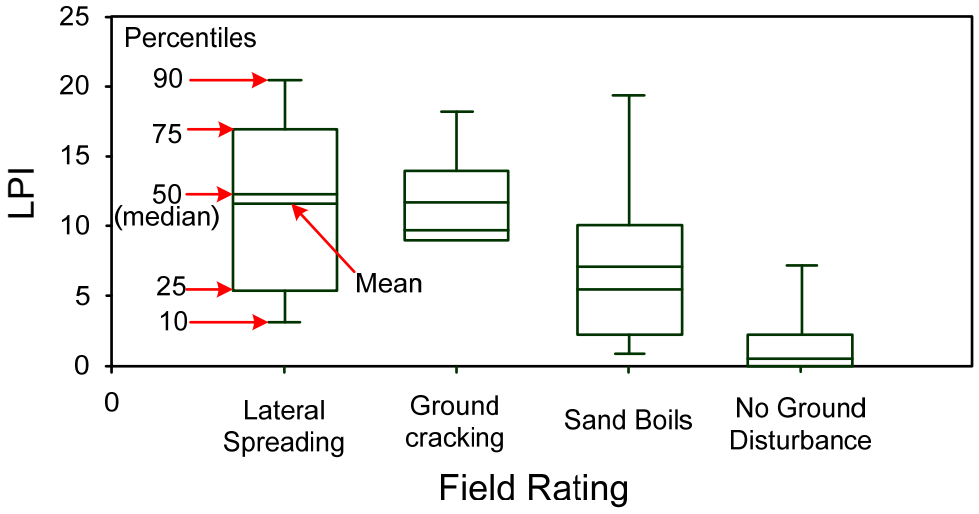

Figure 2-2. Correlation of LPI values with surface effects for the 1989 Loma Prieta Earthquake (Toprak and Holzer, 2003)

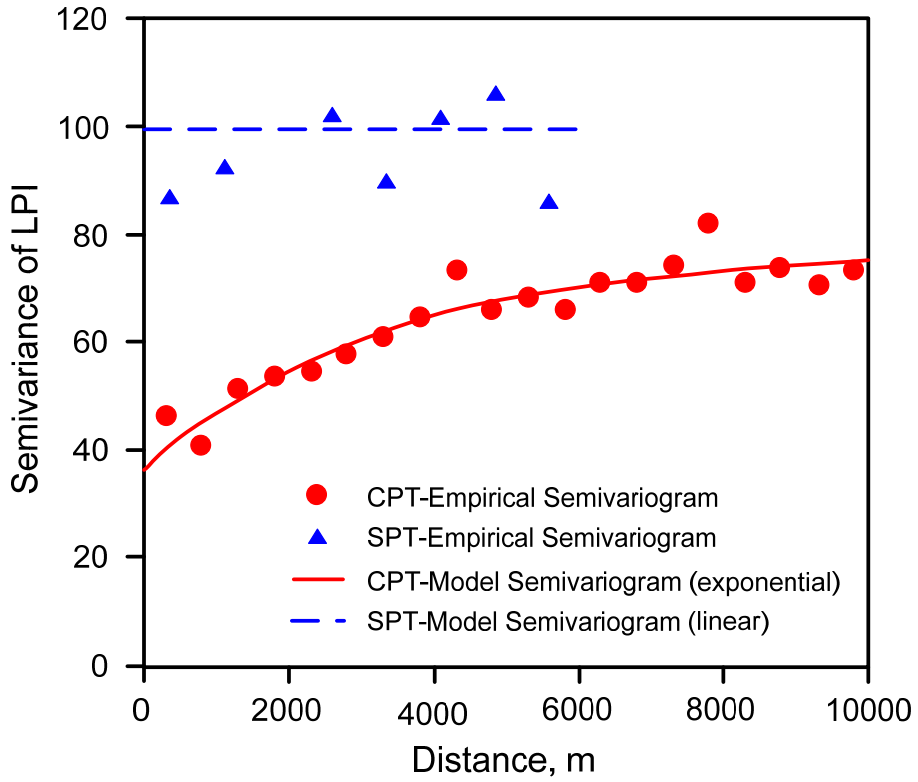

Figure 2-3. Empirical semivariograms of LPI for CPT and SPT (Lenz and Baise, 2007)

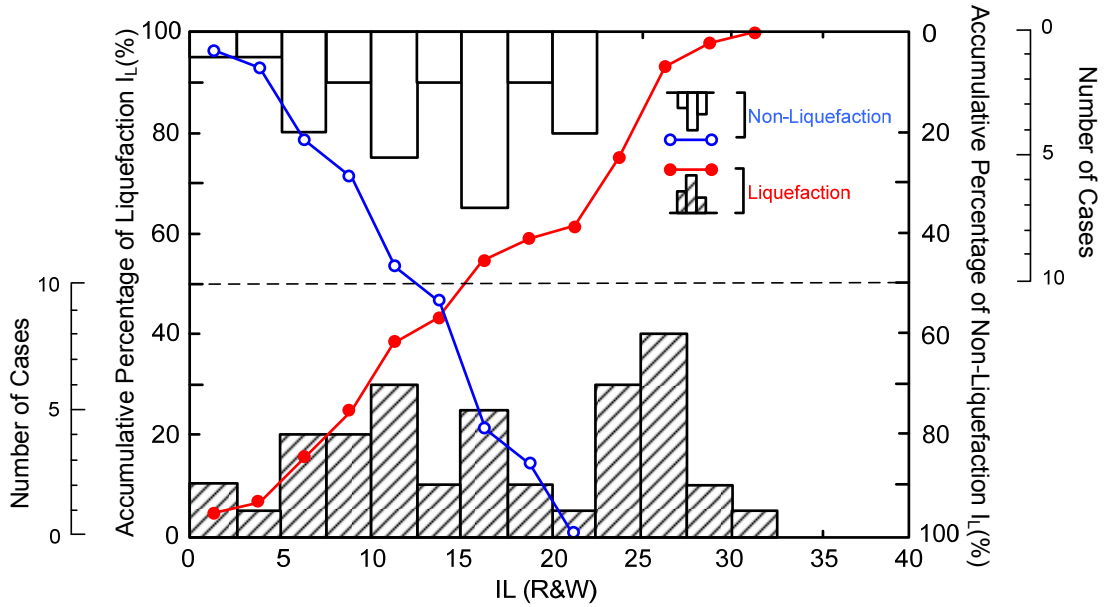

Figure 2-4. Distribution of calculated LPI (or I_L) of liquefied group and non-liquefied group of cases using the Robertson and Wride method (Lee et al. 2004)

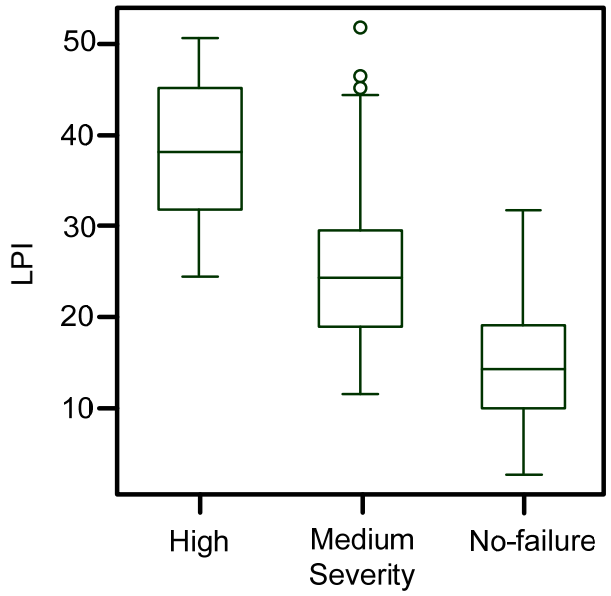

Figure 2-5. LPI values with severity of liquefaction-induced deformations box–whisker plot (Papathanassiou, 2008)

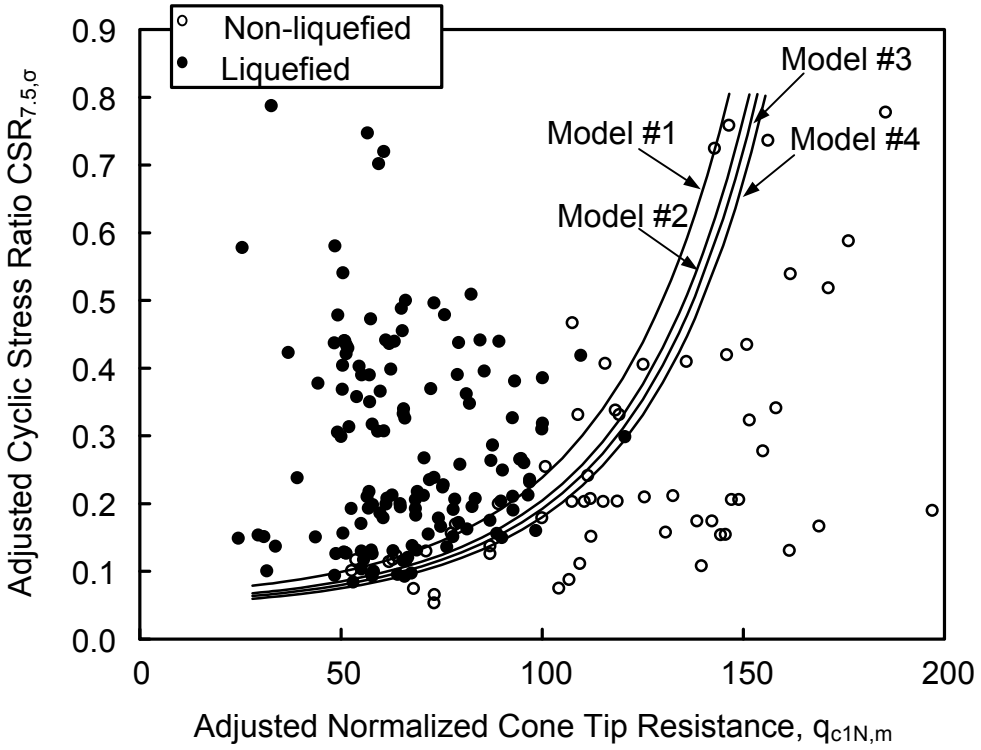

Figure 2-6. A family of CRR models with different degrees of conservatism (Li et al. 2006)

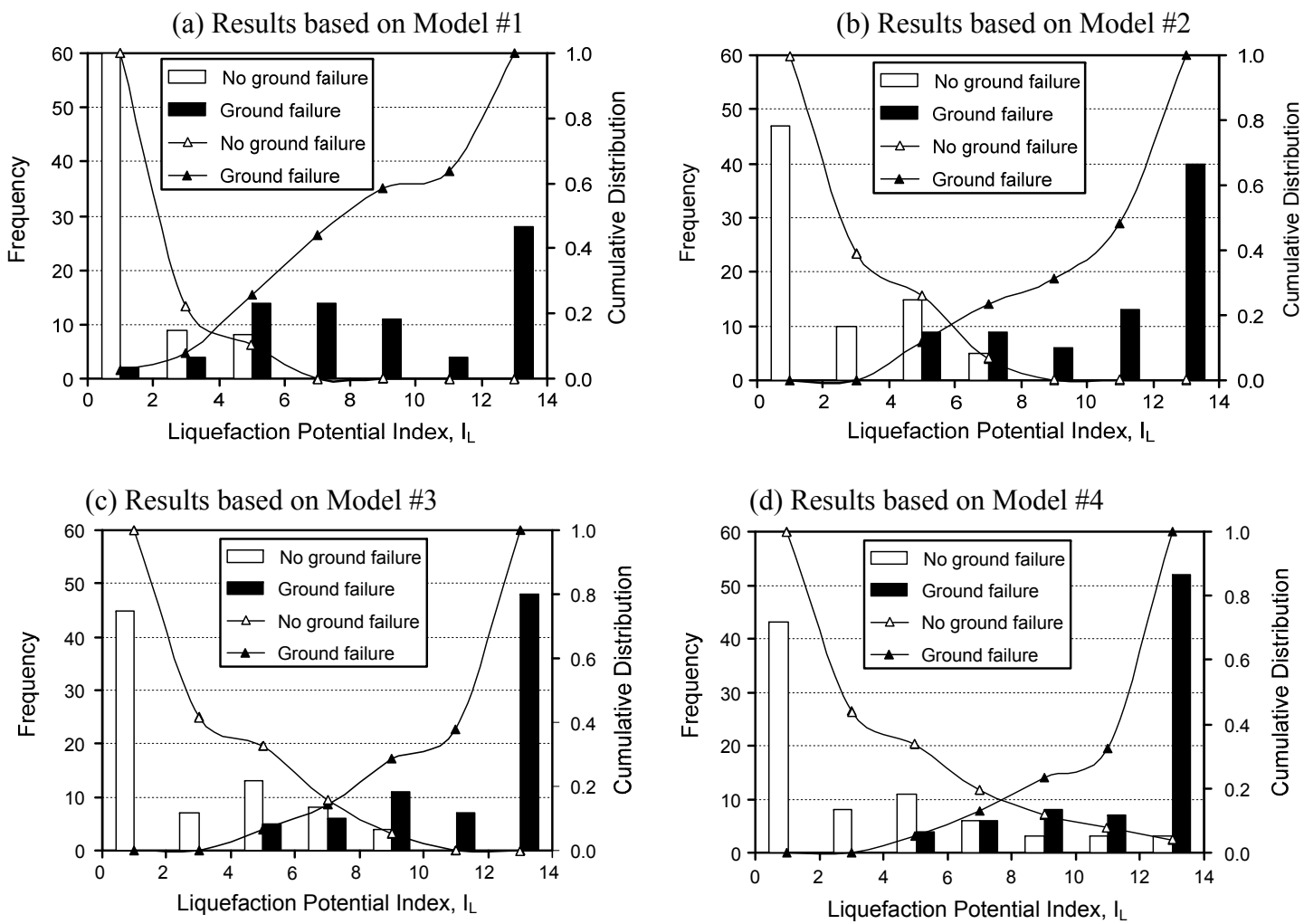

Figure 2-7. Frequency distributions of LPI (or I_L) of liquefied (ground failure) group and non-liquefied (no failure) group calculated with each of the four CRR models (Li et al. 2006)

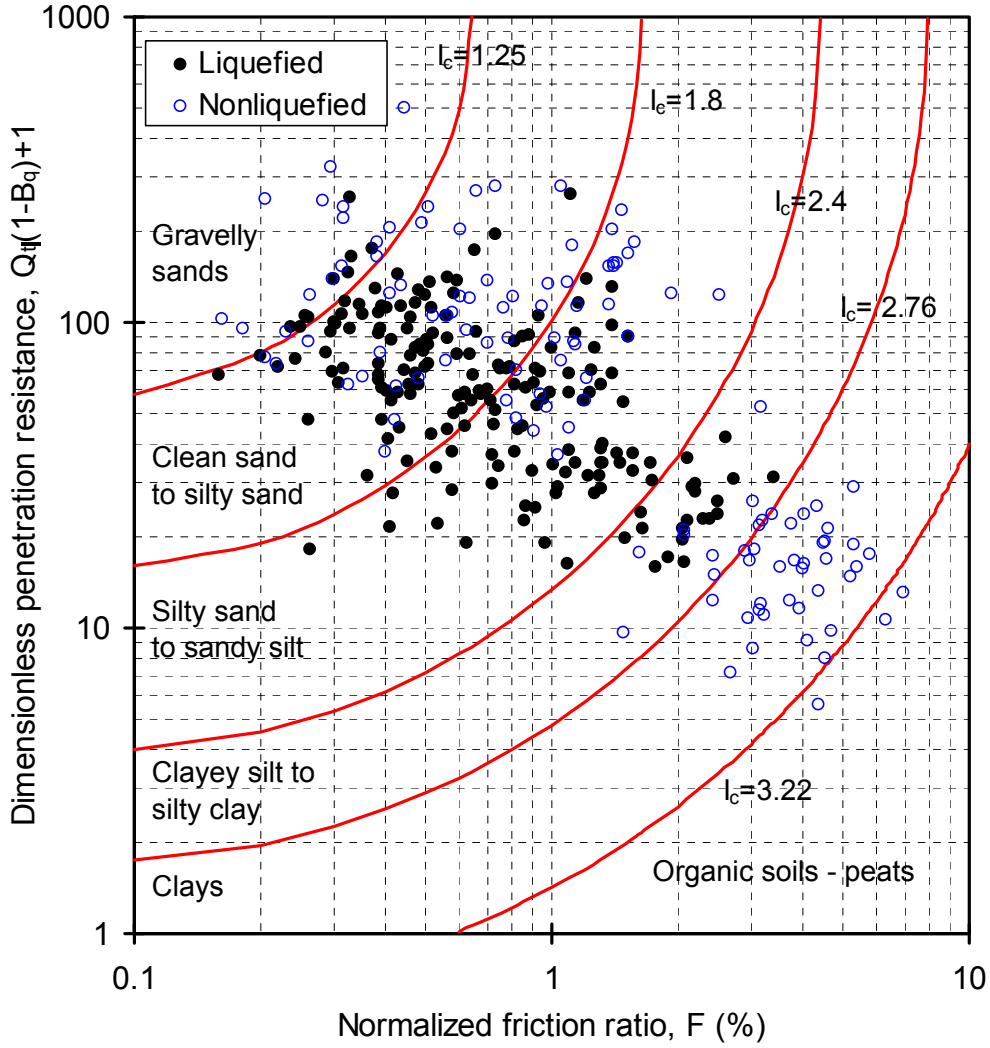

Figure 2-8. Source data for the CPTU model

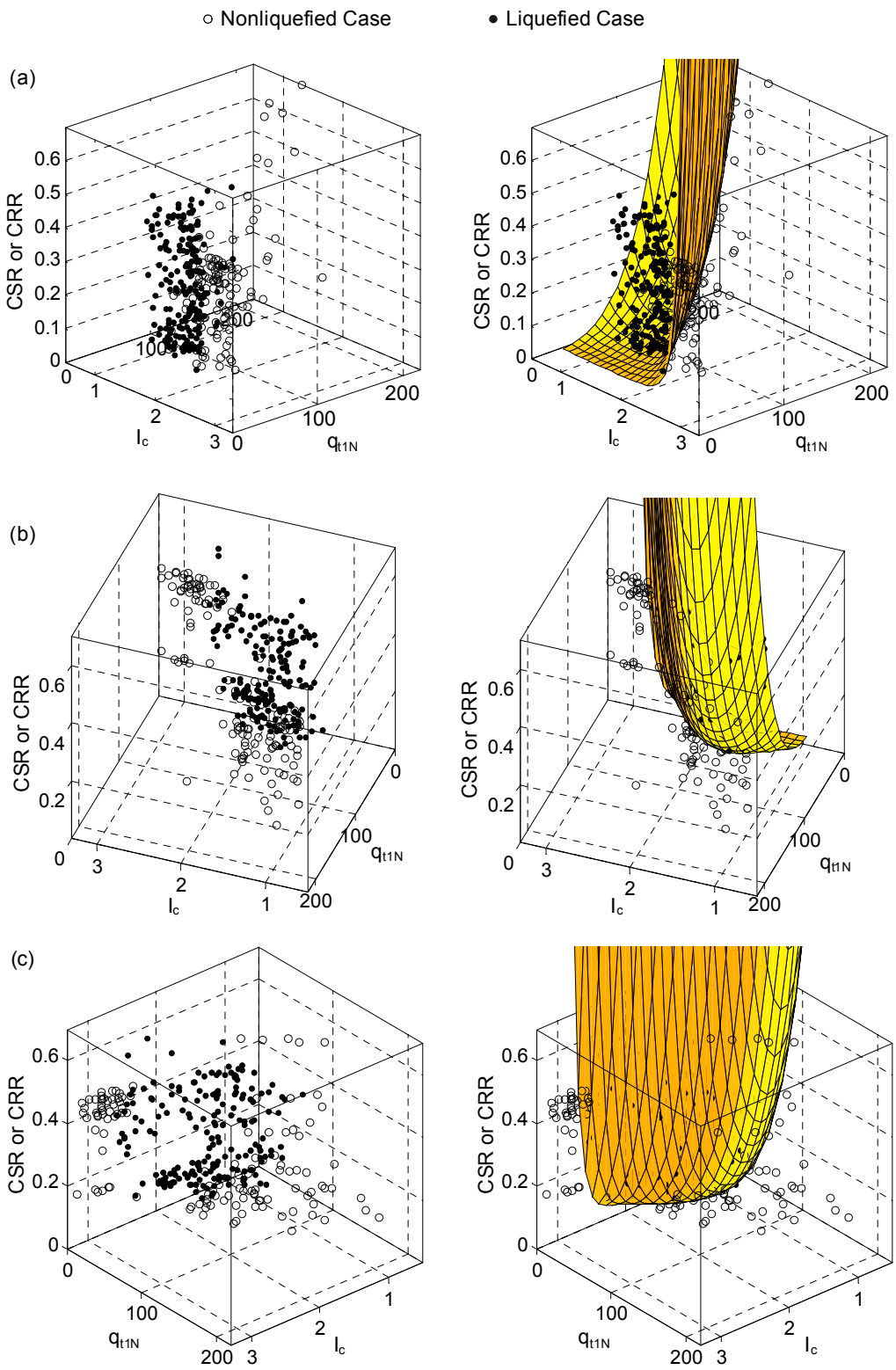

Figure 2-9. Boundary surface at three different angles with case history data points

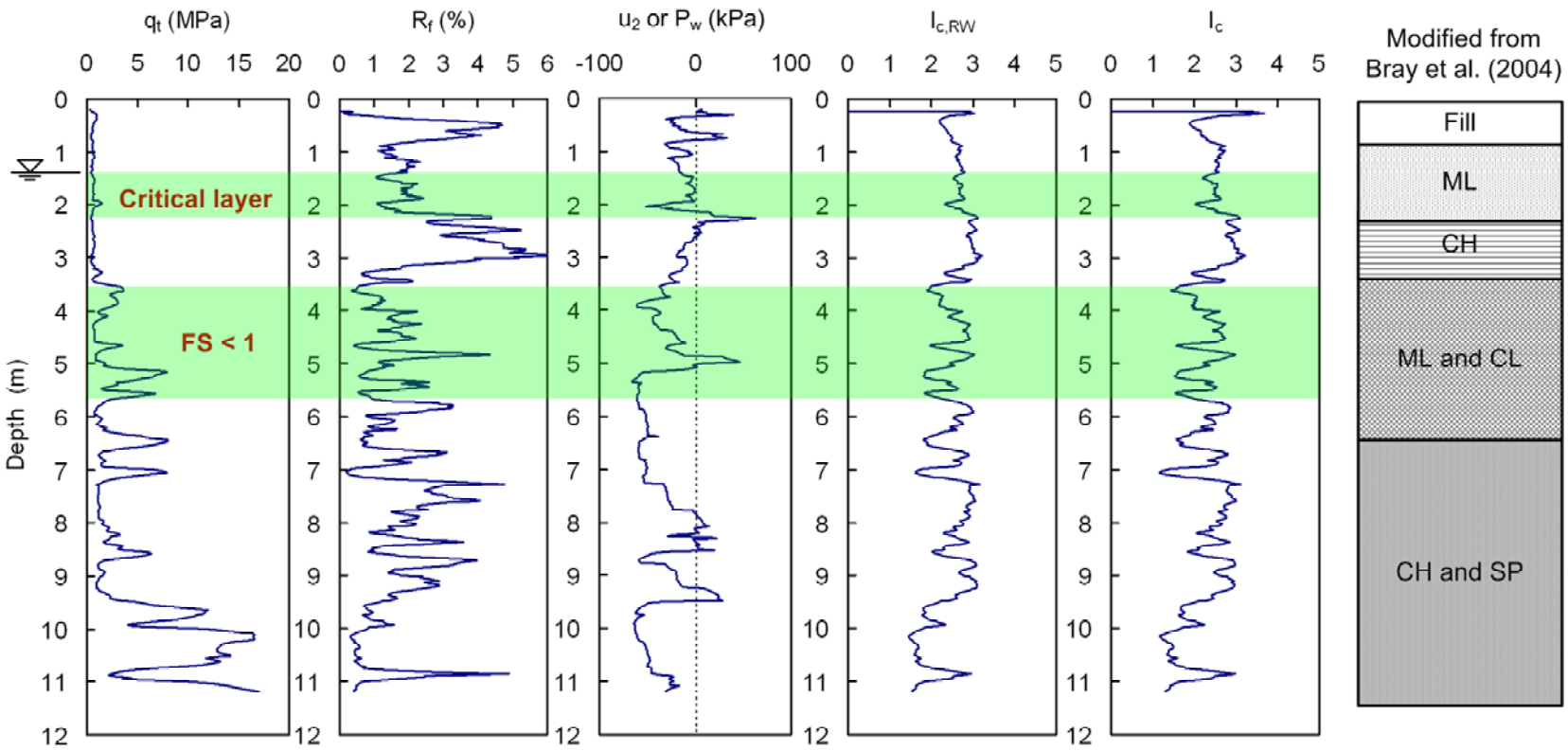

Figure 2-10. CPTU sounding profiles and soil classification at location CPT-C4 in Adapazari (Source data from Bray et al. 2004)

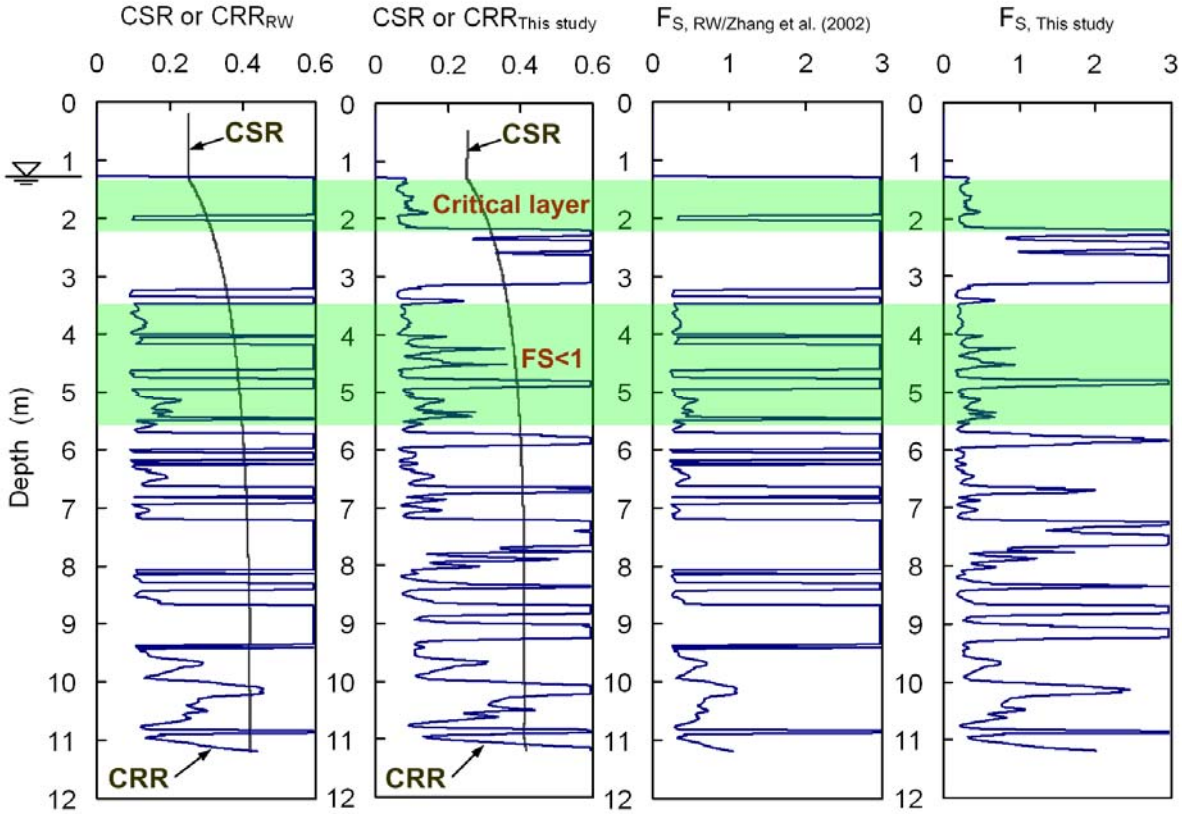

Figure 2-11. Results of the analysis of Adapazari CPT-C4 using two methods: the Robertson and Wride (RW) method the new CPTU model

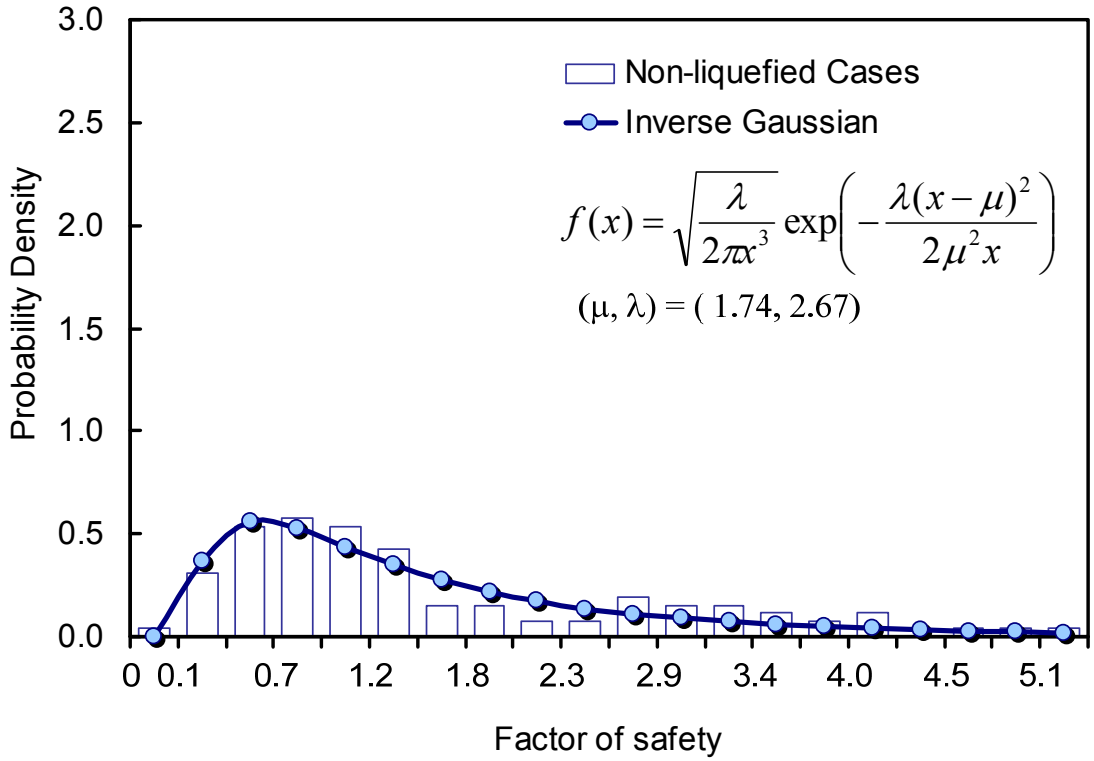

Figure 2-12. Distribution of factor of safety (F_S) of 123 nonliquefied cases

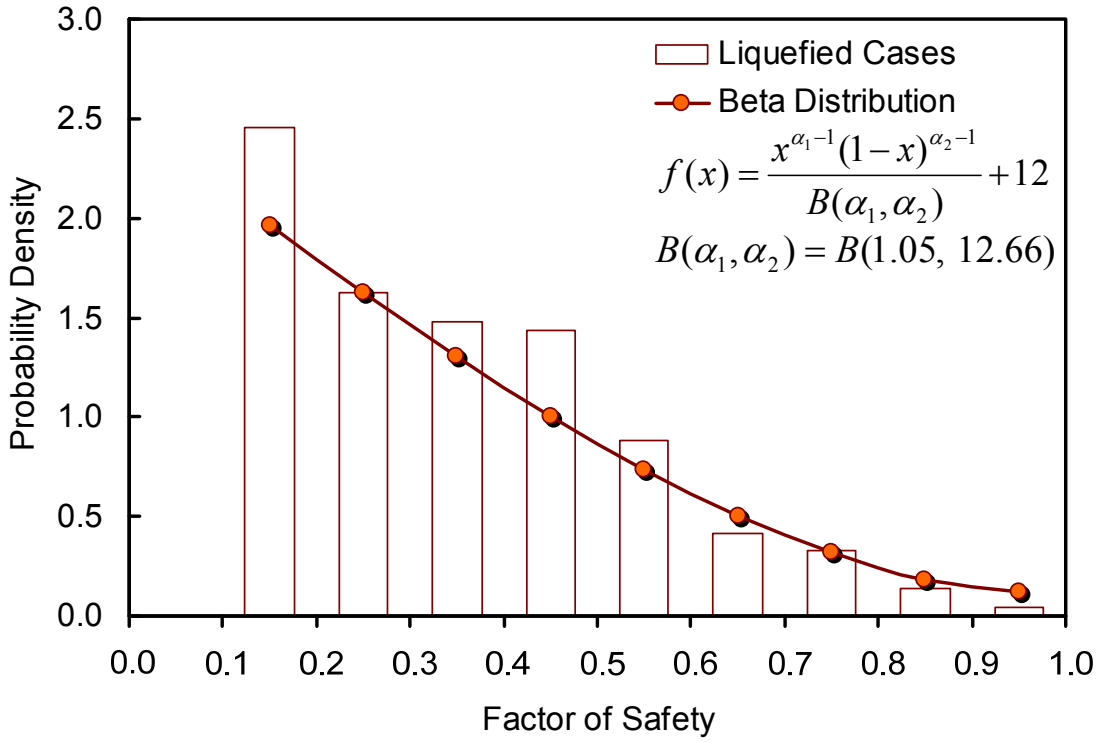

Figure 2-13. Distribution of factor of safety (F_S) of 190 liquefied cases

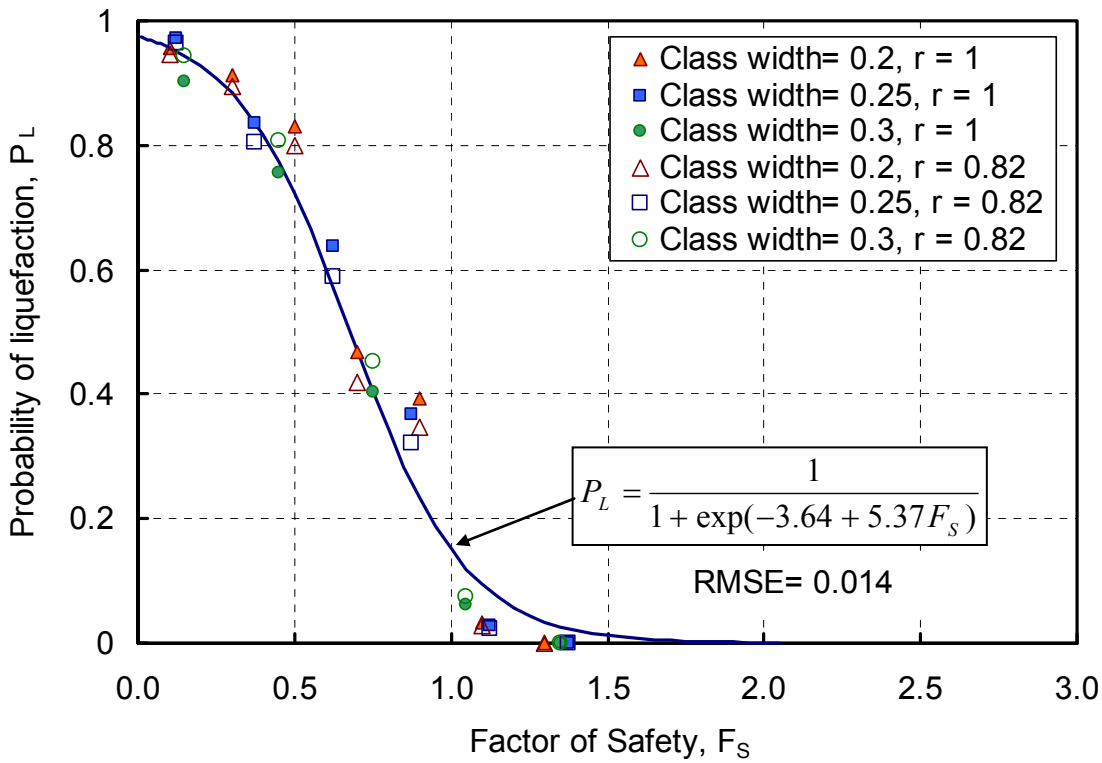

Figure 2-14. Mapping function that relates factor of safety to probability of liquefaction

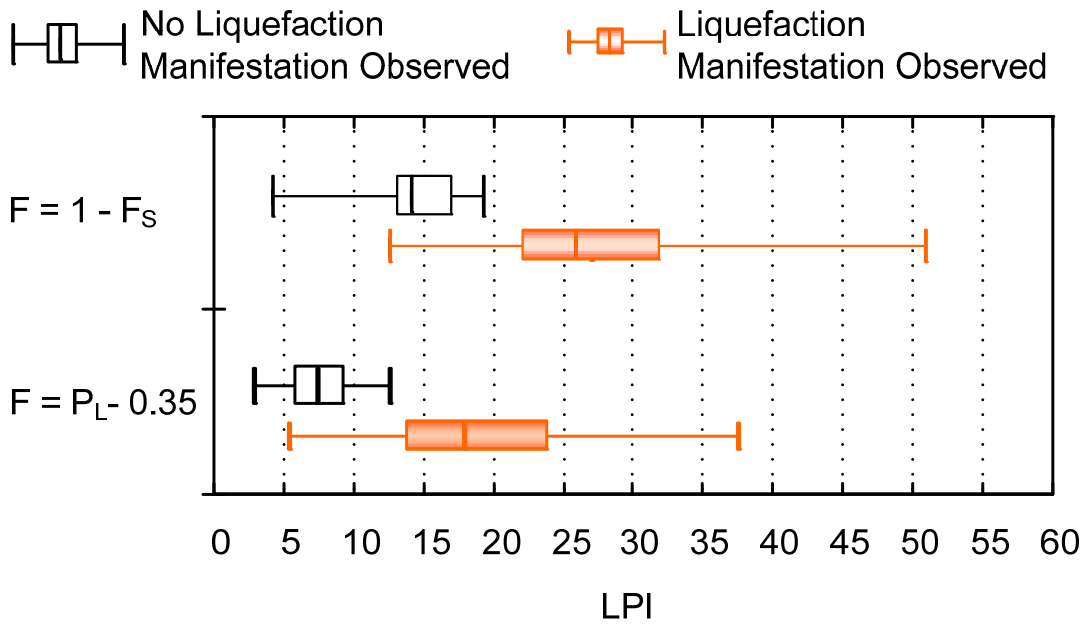

Figure 2-15. Box- whisker plots of the calculated LPI values for liquefied and nonliquefied groups with two definitions of F ($F = P_L - 0.35$ versus $F = 1 - F_S$)

(a) Class width = 0.3

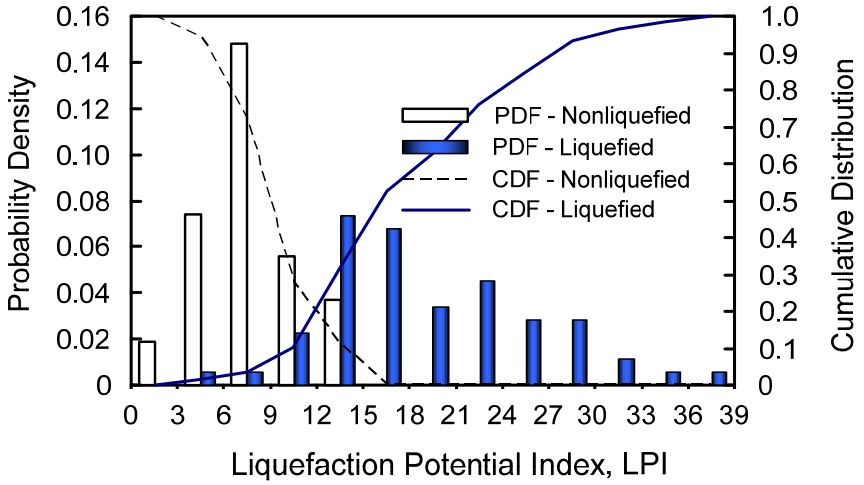

(b) Class width = 0.35

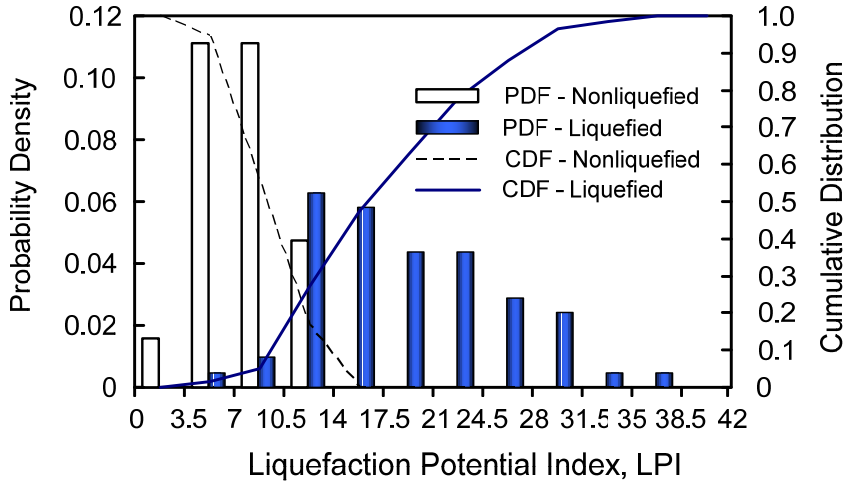

(c) Class width = 0.4

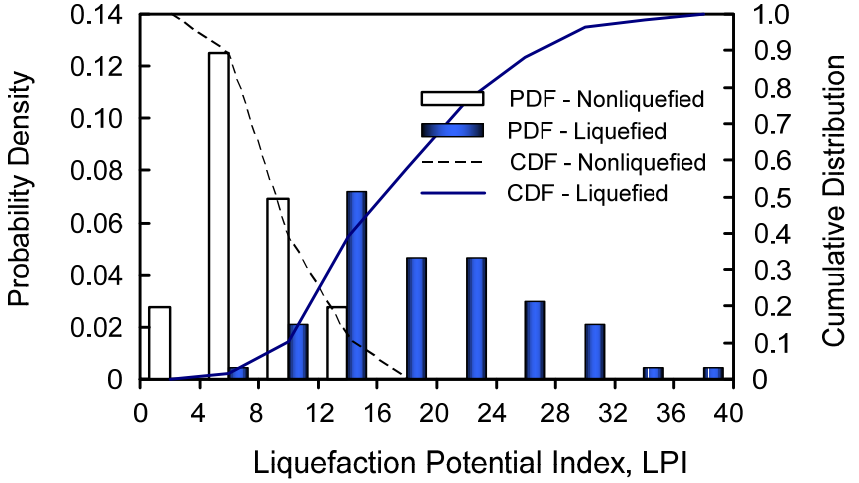

Figure 2-16. Histograms and cumulative distributions of liquefied and nonliquefied groups

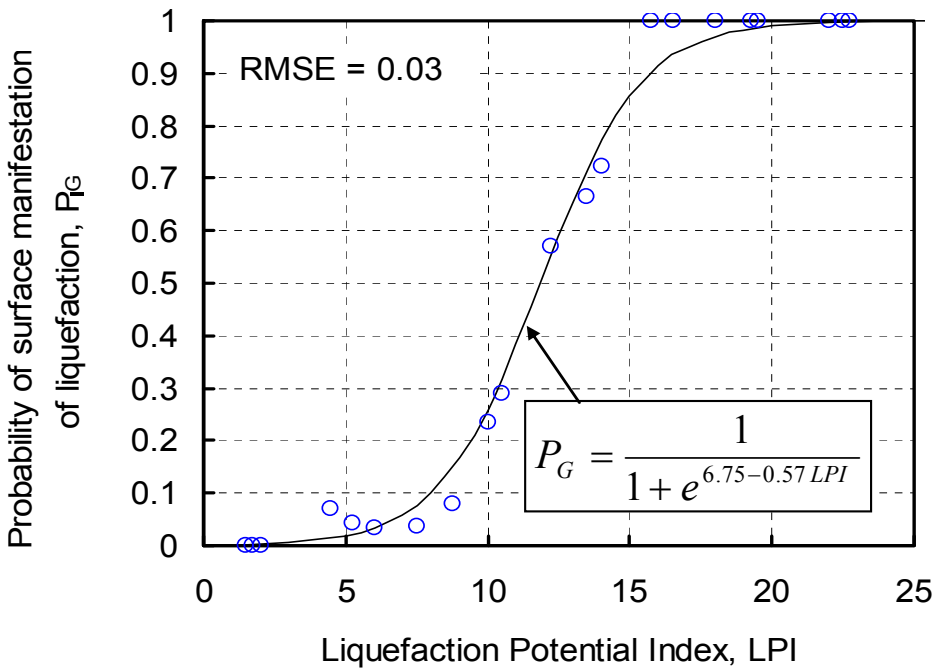

Figure 2-17. Probability of surface liquefaction manifestation (LPI calculated with Equations 2-1 and 2-3 where $F = P_L - 0.35$)

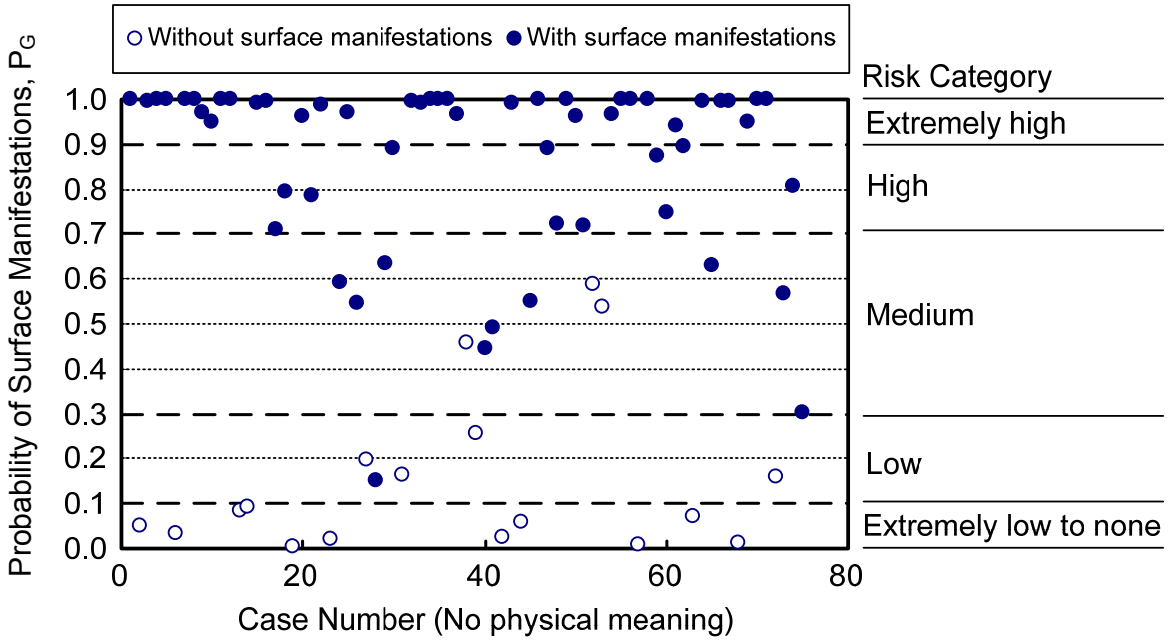

Figure 2-18. Distribution of the calculated P_G values for all cases analyzed

Part III:
Assessing Probability of Surface Manifestation of Liquefaction at a Given Site in a Given Exposure Time Using CPTU*

ABSTRACT

Part III of the Report is a follow-up to Part II on the subject of liquefaction potential index (LPI), a parameter that is often used to characterize the potential for surface manifestation of liquefaction at a given site subjected to a given shaking level (represented by a pair of peak ground surface acceleration a_{max} and moment magnitude M_w). In Part II, the LPI was re-calibrated for a piezocone penetration test (CPTU) model, and a simplified model based on LPI was created for computing the conditional probability of surface manifestation of liquefaction (P_G). In Part III, the model for this conditional probability P_G is extended into a complete framework for assessing the probability of surface manifestation of liquefaction *in a given exposure time* at a given site subjected to *all possible ground motions at all seismic hazard levels*. This new framework is formulated and demonstrated with an example site in 10 different seismic regions in the United States.

---

*The contents of this part III have been published as a Technical Paper in Engineering Geology. The article citation is as follows: Juang, C. H., et al. (2008d), "Assessing Probability of Surface Manifestation of Liquefaction at a Given Site in a Given Exposure Time Using CPTU," *Engineering Geology* (2008), doi:10.1016/j.enggeo.2008.10.011. (in press)

1. Introduction

In engineering practice, the liquefaction potential of a *soil element* at a given depth in a given site is most often evaluated using the simplified procedure pioneered by Seed and Idriss (1971) and those that followed this classic method. In today's terminology, at a soil element, liquefaction "loading" is expressed as *cyclic stress ratio* (CSR) and liquefaction "resistance" is expressed as *cyclic resistance ratio* (CRR). The liquefaction potential of this soil element is generally expressed as factor of safety (F_S), defined as the ratio of CRR over CSR. For historic perspectives of this simplified procedure, the reader is referred to Seed and Idriss (1971), Seed et al. (1985), Youd et al. (2001), Seed et al. (2003), and Idriss and Boulanger (2004).

In a given soil element, the CSR is mainly a function of peak ground surface acceleration (a_{max}) and moment magnitude (M_w). In the simplified procedure, the CRR is determined from an empirical model that relates the CRR to some in situ test data. The piezocone penetration test (CPTU)-based model developed in the present study (Part I) is one of the more recent models for evaluation of liquefaction resistance and potential of a soil element.

In recent years, use of the Liquefaction Potential Index (LPI), proposed by Iwasaki et al. (1978, 1982), as a parameter to characterize the potential for the occurrence of damaging liquefaction in a geologic unit has received greater attention (Frost et al. 1997; Luna and Frost 1998; Divakarla et al. 1998; Holzer et al. 2002). While the simplified procedure is used to evaluate the liquefaction potential of a soil element at a given depth (or critical layer) in a given site, the LPI is used to evaluate the potential of a soil "column" (the first 20 m from the ground surface) for surface manifestation of liquefaction, such as sand boils, settlement and lateral

spreads. Toprak and Holzer (2003) suggested that LPI is also useful for describing the geographic variability of liquefaction hazards; together with Geographical Information System (GIS) applications, LPI can greatly facilitate the preparation of liquefaction hazard maps. In fact, this index has been used in several U.S. Geological Survey (USGS) liquefaction hazard mapping projects (e.g., Holzer et al. 2005 & 2006a,b). Other examples of LPI-related studies include Sonmez, H. (2003), Lee et al. (2004), Sonmez and Gokceoglu (2005), Papathanassiou et al. (2005), Lenz and Baise (2007), Papathanassiou (2008), and Juang et al. (2008c).

The conventional liquefaction evaluation procedures, be it the simplified procedure for liquefaction potential of a soil element at a given depth or the LPI-based method for potential of surface manifestation of liquefaction of a soil column, consider only the ground motion that corresponds to a *single* seismic hazard level. In a performance-based earthquake engineering design, however, it is often required to determine the probability of liquefaction subjected to all possible ground motions in a specified exposure time of, say, 50 years (Marrone et al. 2003; Kramer and Mayfield 2005; Kramer et al. 2006; Kramer and Mayfield 2007).

Building on the foundation of the studies by Kramer and his coworkers, Juang et al. (2008a) developed an algorithm for establishing the joint distribution of a_{max} and M_w for a given site in a specified exposure time using the National Seismic Hazard Map data by the U.S. Geological Survey (USGS). The algorithm for developing the joint distribution of a_{max} and M_w and the procedure for computing the total probability of liquefaction of a soil element at a given depth subjected to all possible ground motions are documented by Juang et al. (2008a).

In the present study, the framework for computing the LPI and the conditional probability of surface manifestation of liquefaction (P_G) for a *single* seismic hazard level formulated by Juang et al. (2008c) is extended using the concept of the joint distribution of a_{max}

and M_w to evaluate the total probability of surface manifestation of liquefaction in a given exposure time that considers all possible ground motions at all hazard levels. The extended framework is illustrated with example applications and its versatility is demonstrated.

2. Joint Distribution of a_{max} and M_w and Fully Probabilistic Framework

Using the USGS websites data (USGS 2002 a&b), the joint distribution of a_{max} and M_w at a given site in a specified exposure time can be established. Figure 3-1 illustrates an algorithm created by Juang et al. (2008a) for developing the joint distribution of a_{max} and M_w.

As shown in Figure 3-1, a seismic hazard curve for a specified exposure time (say, 50 years) at a given site (with known longitude and latitude) is first obtained from the USGS website (USGS 2002a). Figure 3-2 shows an example of a seismic hazard curve for a typical site in San Jose, CA. It is noted that the hazard curve is provided in the form of discrete data points in the USGS website. Based on this hazard curve, the probability density function of the rock outcrop *PGA* can be derived. This *PGA* is usually assumed to follow lognormal distribution. However, in this study the hazard curve is curve-fitted with "cubic splines" (Figure 3-2). Thus, the probability density (Figure 3-3) needs to be computed numerically. Use of cubic splines to represent the hazard curve yields more accurate probability density function than the commonly assumed lognormal distribution, and in some cases, the difference is quite significant.

The USGS de-aggregation website (USGS 2002b) provides M_w distribution at six seismic hazard levels as shown in Table 3-1. For example, for a given site in San Jose, the conditional probability mass function of M_w for each of the six hazard levels (listed in Table 3-

1) is shown in Table 3-2. These data are interpolated, and extrapolated if necessary, to obtained M_w distribution for other hazard levels. Then, by considering the amplification and applying rigorous mathematics (last three steps in Figure 3-1; referred to Juang et al. 2008a for details), the joint distribution of a_{max} and M_w at a given site in a specified exposure time can be established. For example, Figure 3-4 shows the joint distribution of a_{max} and M_w for a typical site in San Jose.

With the knowledge of the joint distribution of a_{max} and M_w, a fully probabilistic framework can be established to compute the probability of liquefaction (P_{LT}) of a soil element at a given depth in a given exposure time (*T*). Symbolically, this framework can be expressed as follows (Juang et al. 2008a):

$$P_{LT} = \sum_{\text{All pairs of } (a_{\max}, M_w)} \{p[L \mid (a_{\max}, M_w)] \cdot p(a_{\max}, M_w)\} \tag{3-1}$$

where the term, $p[L \mid (a_{\max}, M_w)]$, is the *conditional* probability of liquefaction given a pair of seismic parameters a_{max} and M_w; and the term, $p(a_{\max}, M_w)$, is the joint probability of a_{max} and M_w. It is noted that the joint probability $p(a_{\max}, M_w)$ may be thought of as the *likelihood* of an event (a_{max}, M_w), and the conditional probability of liquefaction $p[L \mid (a_{\max}, M_w)]$ as the *consequence* of the event. Thus, the product of $p[L \mid (a_{\max}, M_w)]$ and $p(a_{\max}, M_w)$ is a *weighted probability* of liquefaction of a single event. The sum of all weighted probabilities in Equation 3-1 yields the total probability of liquefaction P_{LT} at the given site.

In this study, the framework expressed in Equation 3-1 is extended to consider the potential of a soil "column" for surface manifestation of liquefaction subjected to all possible ground motions in a given exposure time.

3. Probability of Surface Manifestation of Liquefaction – Proposed Framework

The framework expressed in Equation 3-1 is originally developed for computing the probability of liquefaction (P_{LT}) of a soil element at a given depth in a given exposure time (*T*). Using the same likelihood-consequence concept, Equation 3-1 can be extended to considering the potential of a soil "column" for surface manifestation of liquefaction in a given exposure time:

$$P_{GT} = \sum_{\text{All pairs of}(a_{\max}, M_w)} \{p[G \mid (a_{\max}, M_w)] \cdot p(a_{\max}, M_w)\} \tag{3-2}$$

where the term, $p[G \mid (a_{\max}, M_w)]$, is the *conditional* probability of surface manifestation of liquefaction given a pair of seismic parameters a_{max} and M_w. It is noted that the surface manifestation of liquefaction such as sand boils, settlement, and lateral spreads, is considered as *ground failure*, and accordingly, the symbol *G* is used in the conditional probability term. This equation can be interpreted essentially the same way as Equation 3-1. However, in Equation 3-1, both the conditional probability $p[L \mid (a_{\max}, M_w)]$ and the total probability P_{LT} concern a soil element at a given depth, whereas in Equation 3-2, both the conditional probability $p[G \mid (a_{\max}, M_w)]$ and the total probability P_{GT} concern the entire soil column.

To determine the conditional probability of surface manifestation of liquefaction $p[G\,|\,(a_{\max}, M_w)]$, or P_G for short, for a given shaking level represented by a pair of (a_{max},M_w), the following relationship that relates the P_G to the LPI may be used (Juang et al. 2008c):

$$P_G = \frac{1}{1 + e^{6.75 - 0.57(LPI)}} \tag{3-3}$$

It should be noted that Equation 3-3 was derived through calibration of the LPI with field observations using Bayes' theorem, and thusly, to employ this equation, the LPI must be computed using exactly the same procedure as described in Juang et al. (2008c). However, this framework (Equation 3-2) is set up in such a general way that any model similar to Equation 3-3 can be used, so long as a "consistent" set of models for computing the P_G and LPI are employed. For example, the P_G may be computed from the LPI using an empirical model developed by Papathanassiou (2008); and in such scenario, the standard penetration test (SPT)-based procedure for computing the LPI as per Papathanassiou (2008) must be employed.

Figure 3-5 shows the calibration of the conditional probability of surface manifestation of liquefaction P_G that was computed using Equation 3-3. The cases included in this figure were derived from the 1999 Chi-Chi earthquake of Taiwan (M_w = 7.6) and 1999 Kocaeli (Izmit) Earthquake of Turkey (M_w = 7.4). The reader is referred to Juang et al. (2008c) for details of these data. The risk level or category that is used to interpret the computed conditional probability P_G for a single event, listed in Table 3-3, was proposed by Li et al. (2006). The results shown in Figure 3-5 indicate that the calculated P_G values can distinguish the cases with surface manifestations of liquefaction from those without surface manifestations.

Among the cases without surface manifestation, approximately 83% is in the "extremely low" and "low" risk categories, 17% in the "medium" risk category, and none in the "high" and "extremely high" categories. Among the cases with surface manifestation, approximately 82% is in the "extremely high" and "high" risk categories, 16% in "medium" risk category, and 2% in the "low" and "extremely low" risk categories.

In the present study, as well as in Juang et al. (2008c), the LPI is computed based on a CPTU model that explicitly considers the pore water pressure measured with piezocone penetration soundings. The CPTU-based procedure for computing the LPI presented in Juang et al. (2008c) is briefly summarized in the following. At a given depth, the CPTU soundings yield three parameters, cone tip resistance (q_t), sleeve friction (f_s) and pore water pressure (u_2). These parameters can be combined into a single parameter, the equivalent normalized cone resistance, q_{t1N}^{*} (see Appendix III for its formulation). The parameter q_{t1N}^{*} is then used to compute the CRR. On the other hand, the CSR at this depth is computed with the model by Idriss and Boulanger (2004 & 2006). The formulation of this CSR model is listed in Appendix II. Finally, the conditional probability of liquefaction (P_L) at this depth is computed as follows (Juang et al. 2008b):

$$P_L = \frac{1}{1 + e^{-3.64+5.37F_S}} \tag{3-4}$$

Thus, a plot of the conditional probability versus the depth can be prepared for each CPTU sounding, an example of which is shown in Figure 3-6. Finally, the formulation by Iwasaki et al. (1978 & 1982) is used to compute the LPI:

$$\mathrm{LPI} = \int_0^{20} F \cdot w(\mathrm{z})\, d\mathrm{z} \tag{3-5}$$

in which the depth weighting factor, $w(z) = 10 - 0.5z$ where z = depth (m). The variable F is used to "measure" the contribution of a soil element at a depth z to the severity of liquefaction at the ground surface. The "original" definition of F is based on the factor of safety (F_S). However, the F_S value computed for a given case is method-dependent; different methods tend to yield different F_S values depending on the degrees of conservatism in these methods (Juang et al. 2002; Li et al. 2006). To ease this concern, Li et al. (2006) suggested use of the probability of liquefaction (P_L) to define variable F because P_L is more method-independent. Thus, the following definition for variable F is used:

$$F = P_L - 0.35, \text{ for } P_L \geq 0.35; \text{ and}$$

$$F = 0 \text{ for } P_L < 0.35. \tag{3-6}$$

Equation 3-6 implies that a soil "layer" with $P_L < 0.35$ will have negligible contribution to surface manifestations of liquefaction. This cut-off value was chosen for two reasons. First, according to a classification criterion by Chen and Juang (2000), the liquefaction potential of a soil is rated as "low" if $P_L < 0.35$. Thusly, the contribution of a soil layer with $P_L < 0.35$ to surface manifestations should be negligible. Second, a sensitivity analysis involving five different cut-off probabilities ranging from 0.15 to 0.50, conducted by Li et al. (2006), showed that use of the cut-off probability of 0.35 yielded the best results. Ultimately, the appropriateness of the definition of variable F depends on whether satisfactory results can be obtained in the calibration of the computed LPI. The results of the calibration of the entire set

of equations (Equations 3-3, 3-4, 3-5, and 3-6), as reflected in Figure 3-5, are deemed satisfactory.

Therefore, in this report the LPI is computed using Equations 3-4, 3-5 and 3-6, and then interpreted with Equation 3-3 for the conditional probability of surface manifestation of liquefaction. Figure 3-6 shows the "accumulation" of the LPI with depth at a site with CPTU sounding profiles.

In summary, at a given site with CPTU sounding profiles, the probability of surface manifestation of liquefaction in a given exposure time can be computed with the proposed framework (Equation 3-2). The evaluation of Equation 3-2 requires the knowledge of the joint distribution of a_{max} and M_w and the conditional probability of surface manifestation of liquefaction for any given pair of a_{max} and M_w. The former has been addressed previously by Juang et al. (2008a) and the latter by Juang et al. (2008c). The formulations for these two components are integrated into the proposed framework.

4. Analysis of an Example Subsurface Profile Indexed by CPTU Soundings

To illustrate the proposed framework (Equation 3-2) for computing the probability of surface manifestation of liquefaction at a site in a given exposure time, typical CPTU sounding profiles at a given site, as shown in Figure 3-6, are used as an example for the analysis. This site is assumed to locate in each of 10 different locations in the U.S. As an example, assume that this site is located in San Jose, CA. The first step in the analysis is to develop the joint distribution of a_{max} and M_w at "this" San Jose, CA site in a given exposure time of, say, $T = 50$ years. Following the procedure described previously, this joint distribution can be established

and the result is shown in Figure 3-4. The next step is to compute the conditional probability of surface manifestation of liquefaction (P_G). Here, the conditional probability P_G is computed for each given pair of (a_{max}, M_w). Thus, the joint distribution shown in Figure 3-4 is first discretized into 7455 pairs of (a_{max}, M_w), with a_{max} ranging from 0.01 g to 2.13 g (upper bound of the hazard curve from the USGS) in an increment of 0.01 g and M_w ranging from 4.8 to 8.2 (upper bound at this site from the USGS) in an increment of 0.1. Subjected to a given pair of (a_{max}, M_w), the LPI value can be computed using Equations 3-4, 3-5, and 3-6, and the conditional probability P_G can be determined with Equation 3-3. This process is repeated for all 7455 pairs of (a_{max}, M_w), and the distribution of the conditional probability P_G is thus obtained. Figure 3-7 shows the distribution of the computed conditional probability of surface manifestation of liquefaction (P_G).

The distribution of the conditional probability of surface liquefaction manifestation P_G is an interesting concept. First, the result is site-specific; meaning that the distribution is developed for a specific site. Second, the two-dimensional (2-D) contour of the distribution, as shown in Figure 3-8, can be a practical tool, particularly when it is used along with the liquefaction hazards levels defined in Table 3-3 (Li et al. 2006). For example, if an engineer is required to design with a seismic hazard level corresponding to, say, a return period of 475 yrs (which would lead to a "representative" pair of a_{max} and M_w at the site), he or she can use this chart (Figure 3-8) to estimate the liquefaction hazard level at this site. If the liquefaction hazard level is deemed too high and unacceptable, countermeasures such as ground improvement may be recommended. On the other hand, the chart may also be used to examine the appropriateness of the local code in terms of the seismic hazard level or return period specified for the site (or

the area). In this scenario, acceptable pairs of (a_{max}, M_w), and thusly the seismic hazard level, can be selected based on an acceptable liquefaction hazard level.

Next, the product of the joint probability distribution (Figure 3-4), as the likelihood, and the conditional probability of surface liquefaction manifestation (Figure 3-7), as the consequence, is the weighted probabilities of surface liquefaction manifestation. Figure 3-9 shows the distribution of the weighted probabilities of surface liquefaction manifestation for this site in San Jose. The volume under the distribution surface is the probability of surface manifestation of liquefaction P_{GT} in 50 years at this site, and in this case, $P_{GT} = 0.486$. If the earthquake events are assumed to follow the Poisson's processes, the annual rate of the surface manifestation of liquefaction at this site will be 0.0133, and the return period of the surface manifestation of liquefaction at this site will be approximately 75 yrs. It should be noted that the return period of the surface manifestation of liquefaction is different from the return period of a given hazard level (i.e., an earthquake that would produce a rock outcrop *PGA* exceeding some certain value).

To further illustrate the proposed framework, the site with CPTU sounding profiles shown in Figure 3-6 is assumed to be in Butte, MT and Seattle, WA, respectively. It is noted that for a given pair of (a_{max}, M_w), the *conditional* probability of surface liquefaction manifestation P_G depends on the CPTU sounding profiles, but not the seismicity at the site. Thus, the distributions of the computed conditional probability of surface manifestation of liquefaction for these two cases are the same as the one shown in Figure 3-7. For the Butte, MT site, the joint distribution of a_{max} and M_w is shown in Figure 3-10 and the weighted probabilities of surface liquefaction manifestation is shown in Figure 3-11. The probability of

surface manifestation of liquefaction P_{GT} in 50 years at this site is P_{GT} = 0.025. Thus, the annual rate of the surface manifestation of liquefaction at this site is 0.000496 and the return period of the surface manifestation of liquefaction at this site is approximately 2016 yrs.

For the Seattle, WA case, the joint distribution of a_{max} and M_w is shown in Figure 3-12 and the weighted probabilities of surface liquefaction manifestation is shown in Figure 3-13. The probability of surface manifestation of liquefaction P_{GT} in 50 years at this site is P_{GT} = 0.275. Thus, the annual rate of the surface manifestation of liquefaction at this site is 0.0064 and the return period of the surface manifestation of liquefaction at this site is approximately 156 yrs.

5. Effect of the Variation in the CPTU Parameters

Two sets of input data are required in the evaluation of Equation 3-2 for the probability of surface manifestation of liquefaction P_{GT} at a site in a given exposure time (*T*). They are seismic data and soil data. In the formulation for P_{GT}, the uncertainty of a_{max} and M_w is already reflected in the joint distribution. Thus, in this section, the focus is on the sensitivity of the computed P_{GT} to the variation in CPTU parameters q_t, f_s, and u_2. However, these parameters are correlated and the study of their individual effects on the CRR (and thusly P_{GT}), by varying one parameter while keeping the other parameters constant, is less meaningful. In this study, the effect of the combined parameter, q_{t1N}^*, is examined.

To investigate the effect of the uncertainty of these input parameters, the CPTU sounding profiles shown in Figure 3-6 are again analyzed. The analysis is carried out to

compute the P_{GT} value for this site assuming that it is located in each of the 10 locations listed in Table 3-4. The same procedure as presented previously is applied. For each location, five analyses are conducted to investigate the effect of the variation in q_{t1N}^{*}; one with the actual (mean) value and the other four being the mean plus 10%, the mean minus 10%, the mean plus 20%, the mean minus 20%, respectively. Figure 3-14 shows the results of these analyses, which indicate that the variation in the computed P_{GT} value (and thusly, the return period for the occurrence of surface manifestation of liquefaction) as a result of the variation in q_{t1N}^{*} is generally significant at locations with high seismic risk, such as San Jose, San Francisco, Santa Monica, Seattle, and Eureka. Using San Jose as an example, a 20% increase in q_{t1N}^{*} resulted in a 28% reduction in the P_{GT} value (i.e., a decrease from 0.49 to 0.35); and a 20% decrease in q_{t1N}^{*} resulted in a 25% increase in the P_{GT} value (i.e., an increase from 0.49 to 0.61). The results provide a basis for estimating possible error in the computed P_{GT} value due to the variation in the equivalent normalized cone resistance q_{t1N}^{*}. It also points to the importance of proper characterization of the site and accurate determination of the index properties in the liquefaction hazards analysis.

6. Concluding Remarks

A simple framework (Equation 3-2) for assessing the probability of surface manifestation of liquefaction in a given exposure time T (say, T = 50 years) that considers all possible ground motions at all seismic hazard levels is developed in this study. This framework consists of two components, an algorithm for the joint distribution of a_{max} and M_w at a given

site in a given exposure time and a model for the conditional probability of surface manifestation of liquefaction based on the concept of LPI. In this study, the two components, examined in the previous studies, are integrated into the proposed framework.

The new framework is demonstrated with an example subsurface profile (indexed by CPTU soundings) subjected to all possible ground motions at each of the 10 U.S. locations with different seismic risks. The feasibility and versatility of the proposed framework for assessing the probability of surface manifestation of liquefaction at any given site in a given exposure time is demonstrated. This framework has a potential to be a useful tool for mapping liquefaction hazards in an area or for the site-specific liquefaction hazards analysis.

The variations of the computed probability of surface manifestation of liquefaction in a given exposure time as a result of the variation in q_{t1N}^{*} are significant at locations with high seismic risk. Careful evaluation of the CPTU parameters in the site investigation to reduce the parameter uncertainty is vital in the liquefaction hazards analysis. At the very least, the possible variation in the computed P_{GT} value should be assessed.

The two dimensional contour chart of the site-specific distribution of the conditional probability of surface liquefaction manifestation can also be a useful engineering tool. The engineer can use it to determine the liquefaction hazard level at a given site for a given pair of a_{max} and M_w that is representative of a specified seismic hazard level. If the liquefaction hazard level determined from this chart is deemed too high and unacceptable, countermeasures such as ground improvement may be recommended. On the other hand, the chart may also be used to examine the appropriateness of the local code in terms of the seismic hazard level specified for the site, from the perspective of liquefaction hazards. Of course, the appropriateness of the

local code in terms of the seismic hazard level specified for the site must also satisfy other requirements such as the structural requirements.

Table 3-1. Six commonly used seismic hazard levels (for typical site in San Jose, CA)

	Description of hazard levels (in terms of probability of exceedance, PGA, and return period)					
	1	2	3	4	5	6
Probability of exceedance	1% in 50 yr	2% in 50 yr	5% in 50 yr	10% in 50 yr	20% in 50 yr	50% in 75 yr
PGA (g)	0.7749	0.6838	0.5646	0.4743	0.3828	0.2940
Return period (yrs)	4975	2475	975	475	224	108

Table 3-2. Conditional probability distribution of magnitude (M_w) for each of the six hazard levels at a typical site[a] in San Jose, CA (Source data: USGS 2002a,b)

M_w	Conditional probability or contribution (%) of M_w at hazard levels					
	1	2	3	4	5	6
5.00	1.173	1.079	1.073	1.129	1.270	1.369
5.20	2.342	2.138	2.170	2.309	2.645	2.961
5.40	2.269	2.112	2.208	2.393	2.799	3.237
5.60	2.191	2.138	2.245	2.501	2.983	3.520
5.80	2.094	2.111	2.253	2.584	3.161	3.776
6.00	3.135	3.085	3.277	3.625	4.379	5.132
6.20	16.037	14.801	13.726	12.961	12.964	13.510
6.40	7.793	7.665	8.264	9.001	9.583	9.949
6.60	13.877	13.999	14.336	15.069	15.130	15.446
6.80	19.656	23.922	25.426	19.474	23.817	20.779
7.00	6.119	2.717	1.247	6.424	1.318	2.860
7.20	3.776	3.666	3.436	3.142	2.625	2.241
7.40	3.055	2.780	2.478	2.158	1.700	1.324
7.60	2.177	2.010	1.808	1.568	1.221	0.914
7.90	13.354	14.720	14.956	14.498	13.271	11.968
8.11	0.709	0.860	0.955	1.003	1.015	1.001

[a] Location: Longitude = –121.893°, Latitude = 37.339°.

Table 3-3. Risk levels for interpreting the conditional probability of surface manifestation of liquefaction (Li et al. 2006)

P_G	Risk category
0.0 – 0.1	None to extremely low
0.1 – 0.3	Low
0.3 – 0.7	Medium
0.7 – 0.9	High
0.9 – 1.0	Extremely high to certainty

Table 3-4. Probability of surface manifestation of liquefaction in 50 years, P_{GT}, computed for each of the 10 locations using the example CPTU soundings shown in Figure 3-6

Location	Latitude(°)	Longitude(°)	P_{GT}
Butte, MT	40.003	112.533	0.025
Charleston, SC	32.776	79.931	0.094
Eureka, CA	40.802	124.162	0.520
Memphis, TN	35.149	90.048	0.083
Portland, OR	45.523	122.675	0.150
Salt Lake City, UT	40.755	111.898	0.124
San Francisco, CA	37.775	122.418	0.455
San Jose, CA	37.339	121.893	0.486
Santa Monica, CA	34.015	118.492	0.380
Seattle, WA	47.530	122.300	0.275

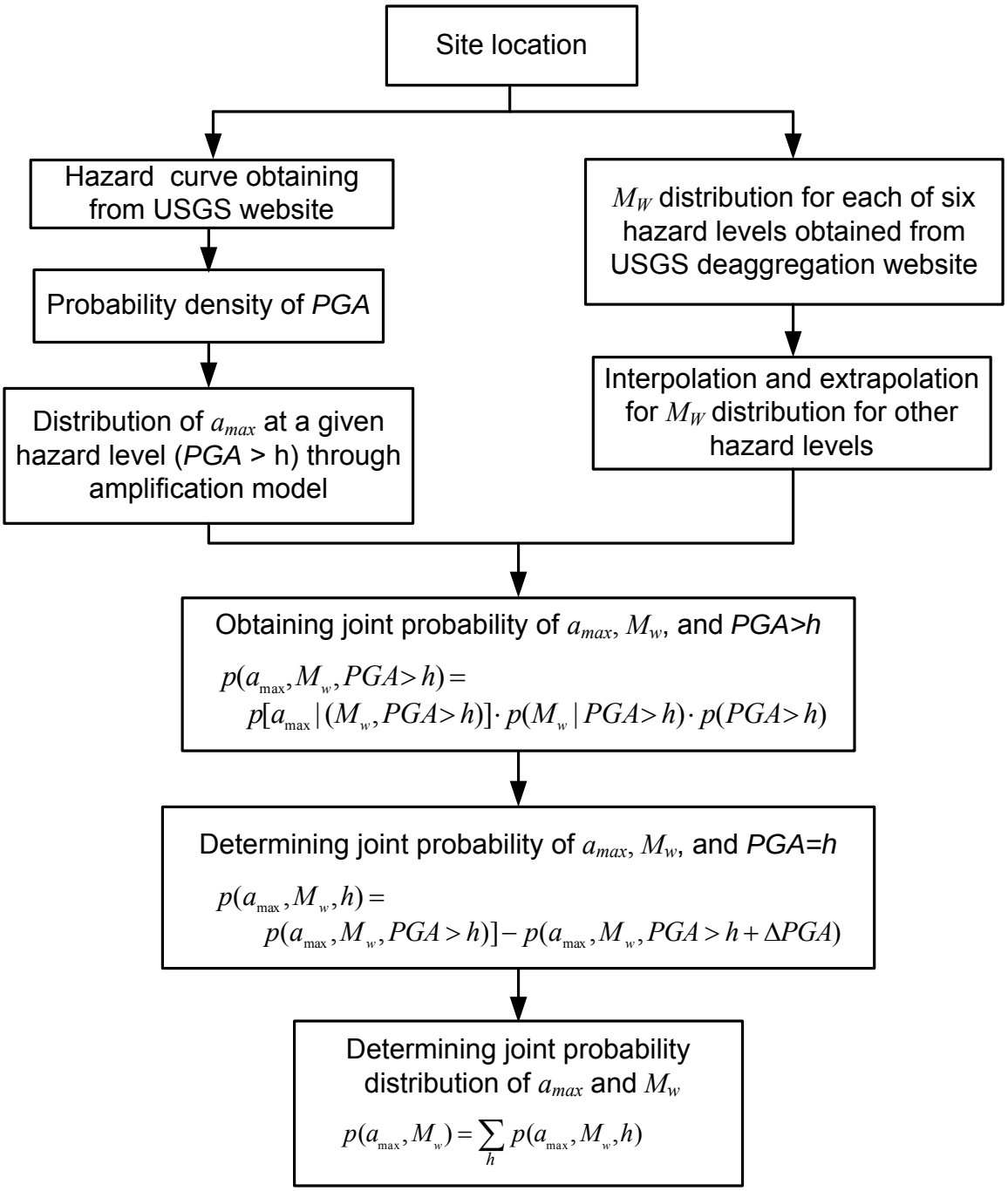

Figure 3-1. Flow chart for developing joint distribution of a_{max} and M_w

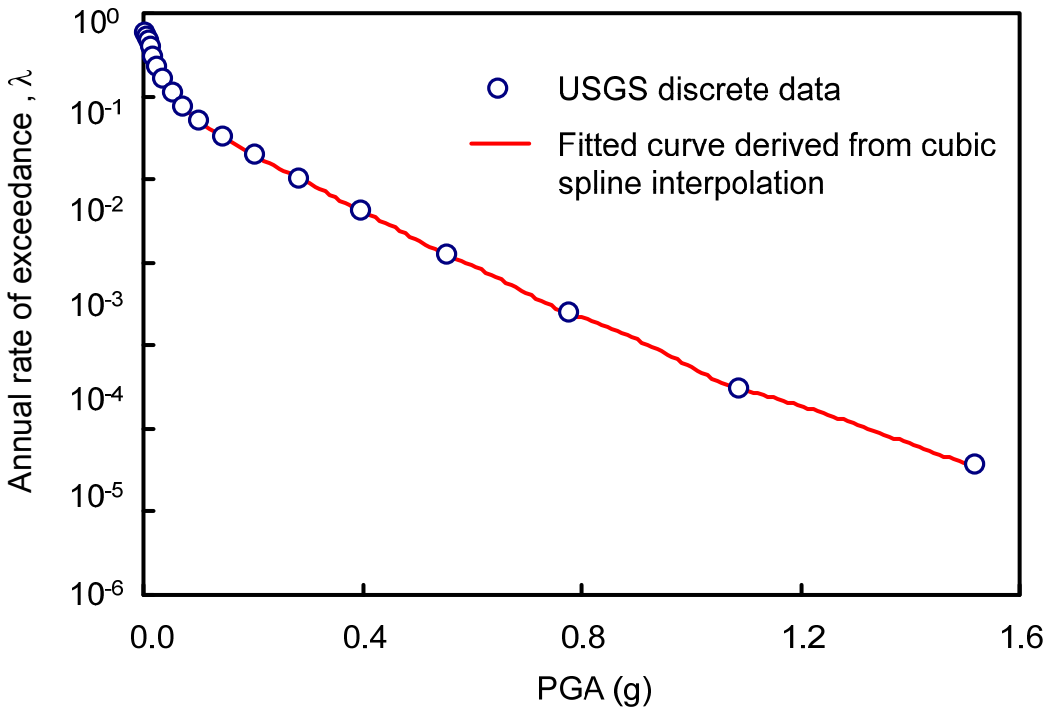

Figure 3-2. Seismic hazard curve for a typical site in San Jose, CA

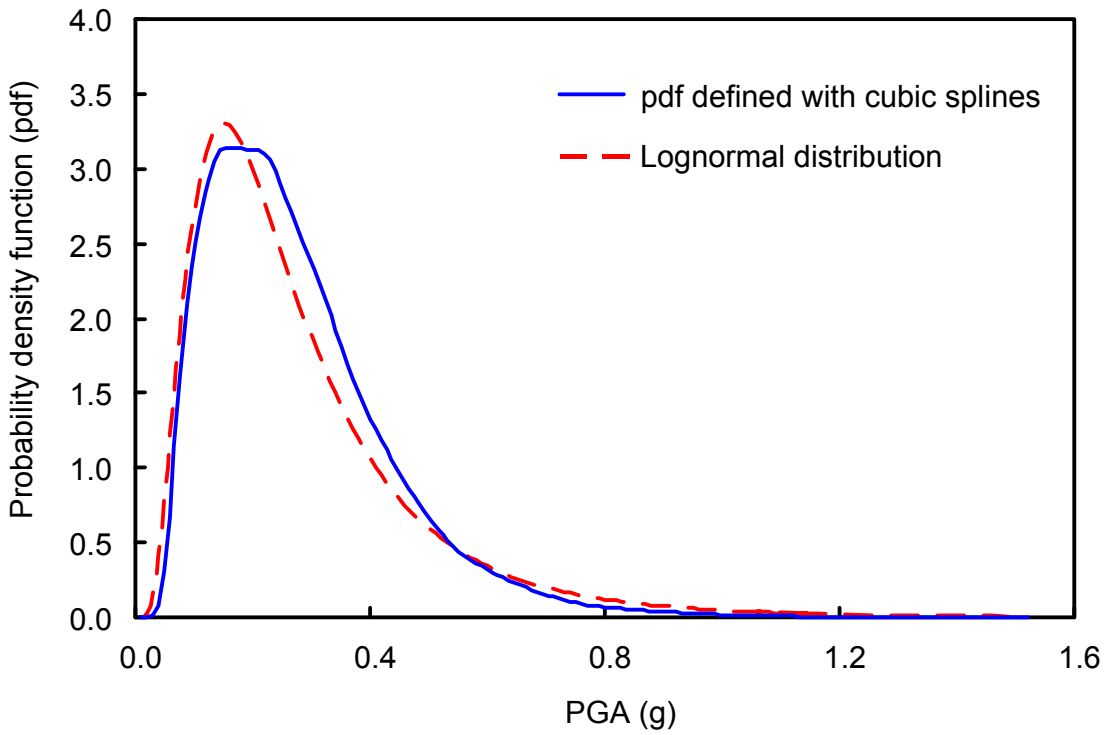

Figure 3-3. The distribution of rock outcrop PGA in an exposure time of 50 years for a typical site in San Jose, CA

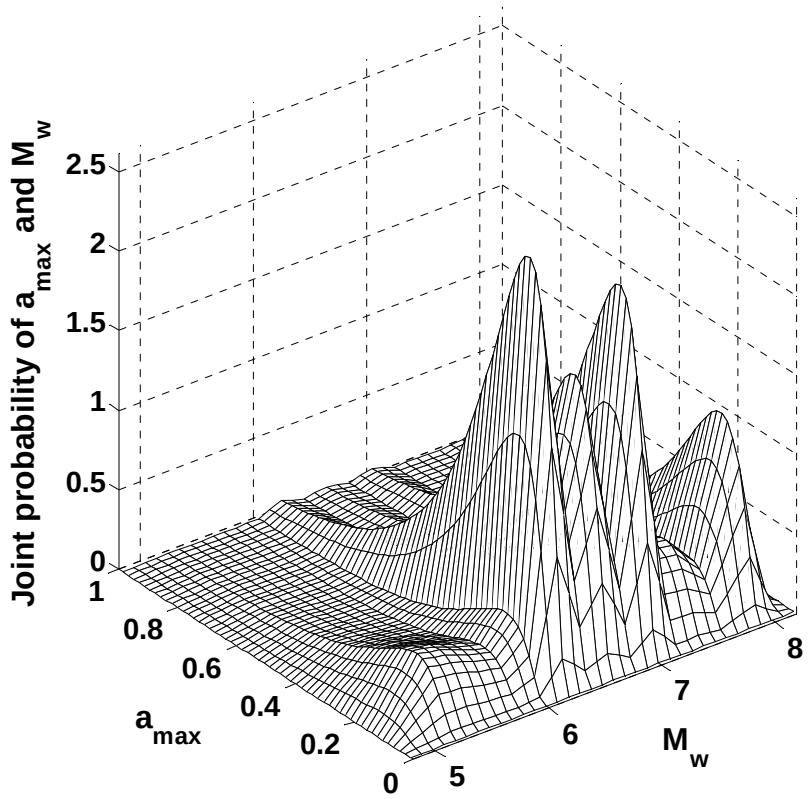

Figure 3-4. The joint probability distribution of a_{max} and M_w at a typical Quaternary alluvium site at San Jose, CA in an exposure time of 50 yrs

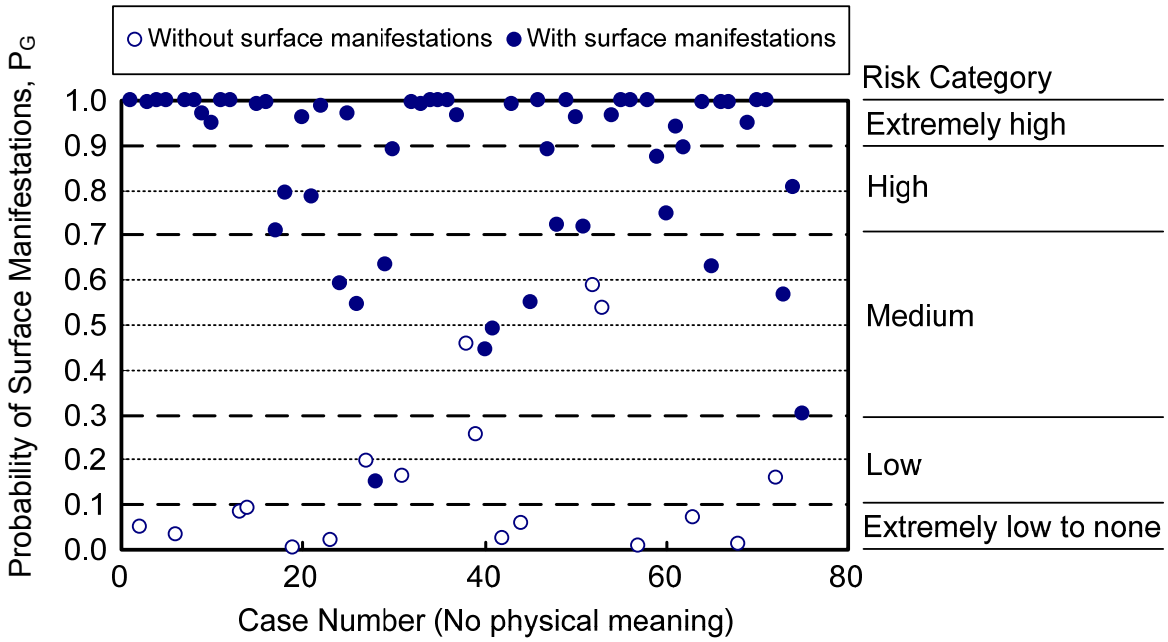

Figure 3-5. Distribution of the calculated P_G values for all cases analyzed

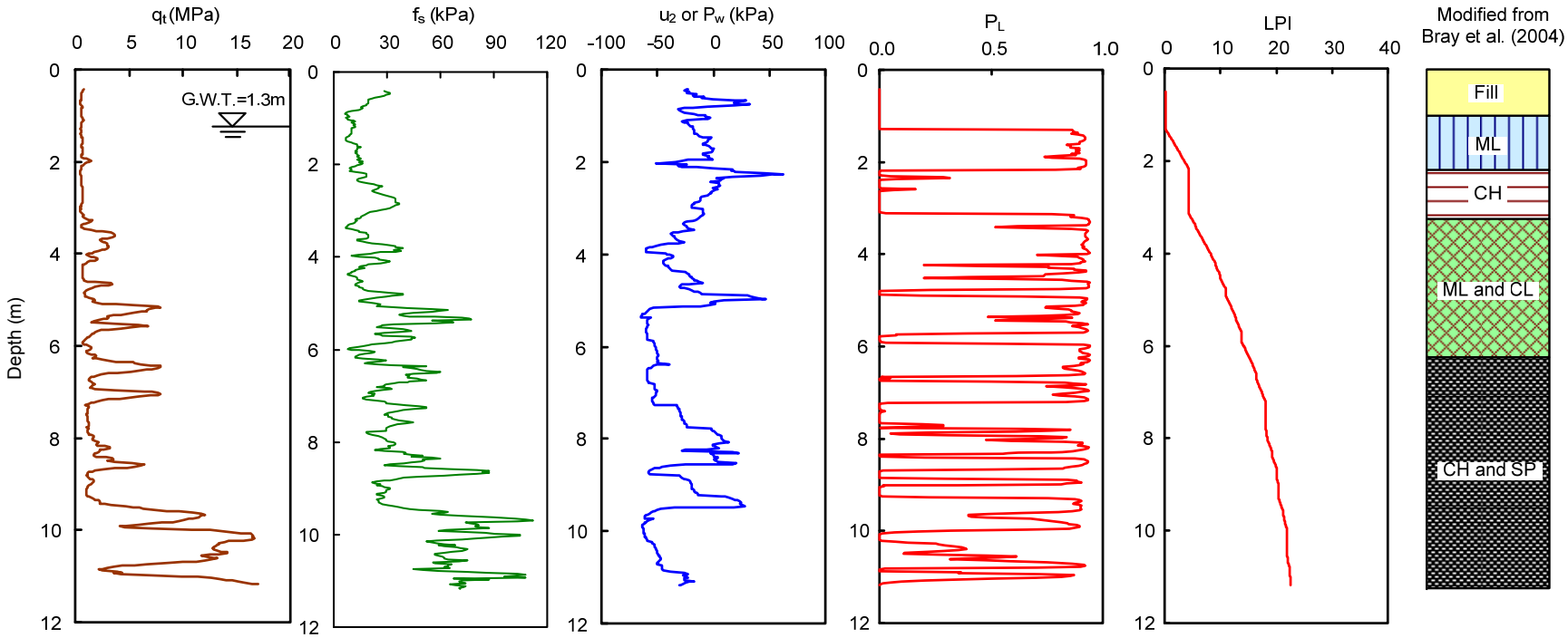

Figure 3-6. Typical CPTU sounding profiles and the LPI at a site (CPTU data from Bray et al. 2004)

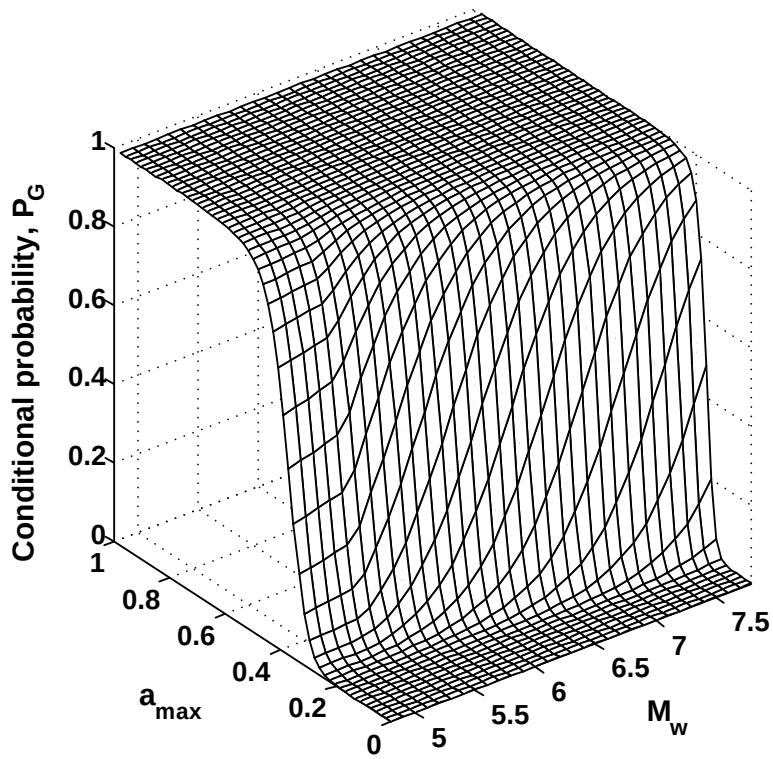

Figure 3-7. The distribution of the conditional probability of surface manifestation of liquefaction (based on CPTU sounding profiles shown in Figure 3-6)

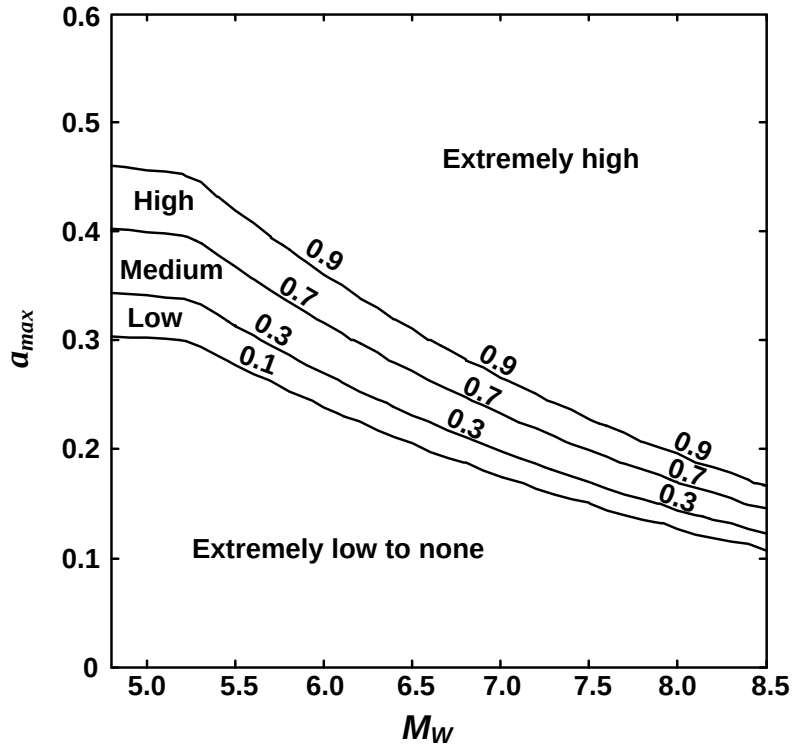

Figure 3-8. Contour of the conditional probability of surface liquefaction manifestation (P_G)

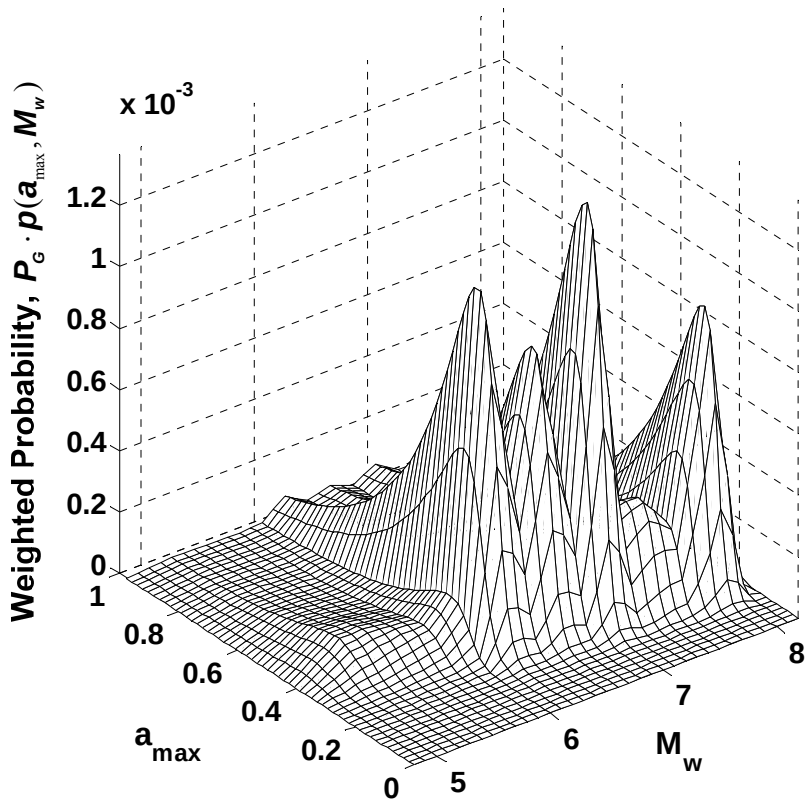

Figure 3-9. Weighted probability of surface liquefaction manifestation at a typical site at San Jose, CA

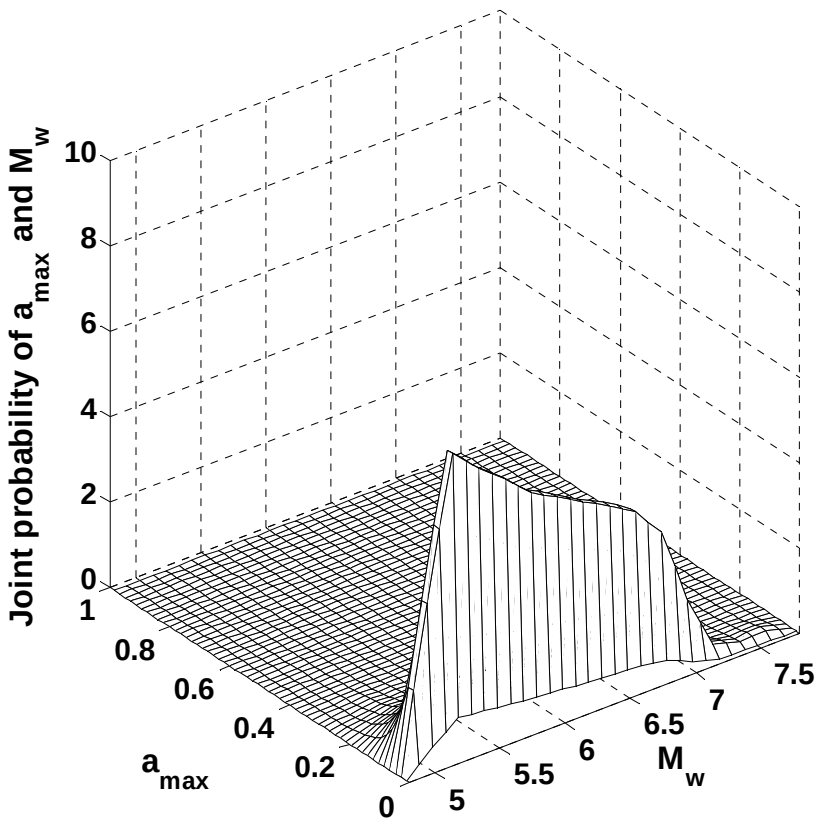

Figure 3-10. The joint probability distribution of a_{max} and M_w at a typical Quaternary alluvium site at Butte, MT

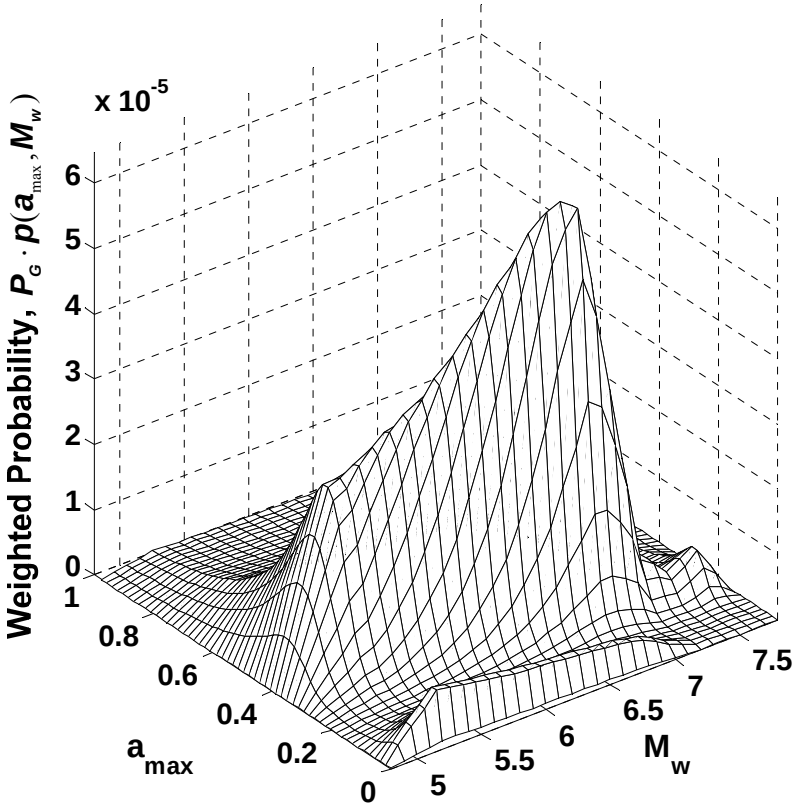

Figure 3-11. Weighted probability of surface liquefaction manifestation at a typical site at Butte, MT

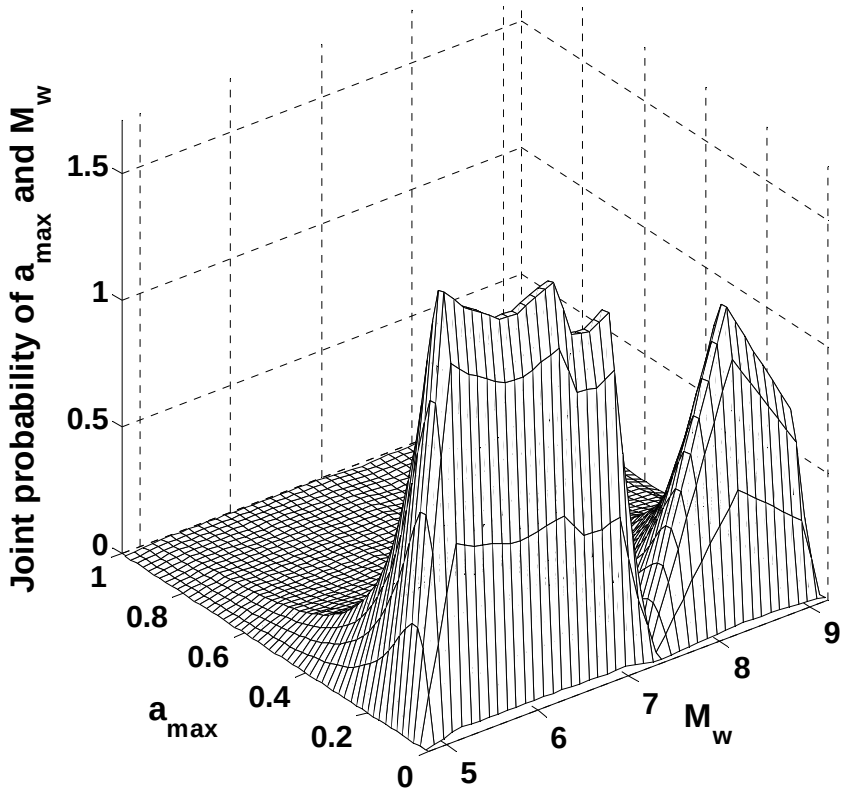

Figure 3-12. The joint probability distribution of a_{max} and M_w at a typical Quaternary alluvium site at Seattle, WA

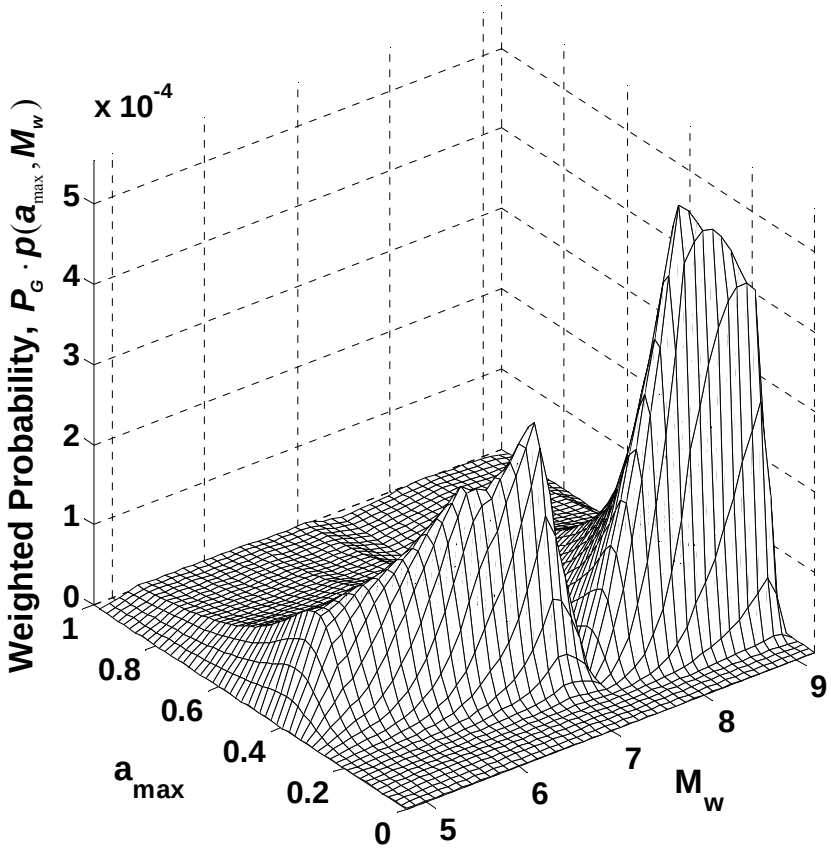

Figure 3-13. Weighted probability of surface liquefaction manifestation at a typical site at Seattle, WA

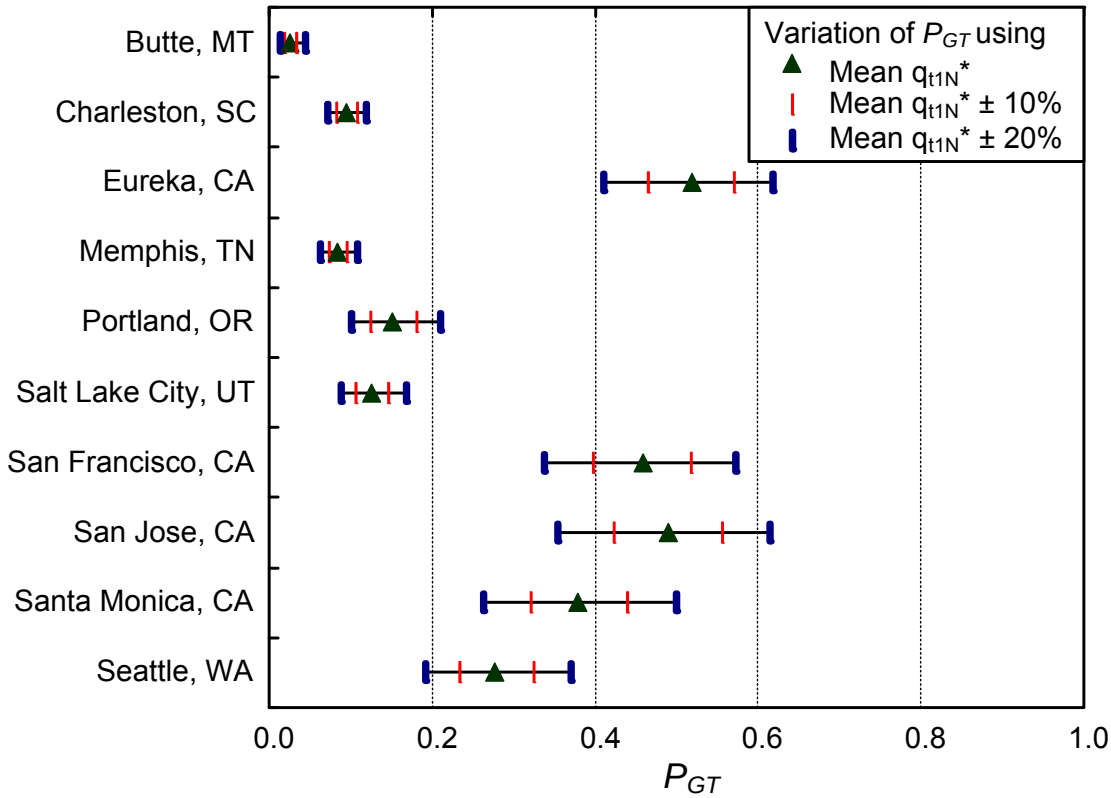

Figure 3-14. Variation of P_{GT} as a result of the variation in q^*_{t1N}

Appendix I – Definitions of CPTU parameters

q_c = raw cone tip resistance

q_t = cone tip resistance corrected for porewater pressure

f_s = sleeve friction

R_f = friction ratio = $f_s/q_t \cdot 100\%$

$u_2 = P_w$ = porewater pressure

B_q = excess porewater pressure ratio = $\dfrac{u_2 - u_o}{q_t - \sigma_{vo}}$

u_0 = hydrostatic water pressure

σ_{vo} = total vertical (overburden) stress

$Q_t = \dfrac{q_t - \sigma_{vo}}{\sigma'_{vo}}$ = normalized form of cone tip resistance

σ'_{vo} = effective vertical (overburden) stress

F = normalized sleeve friction = $\dfrac{f_s}{q_t - \sigma_{vo}} \times 100\%$

$I_{c,RW}$ = soil behavior type index defined by Robertson and Wride (1998)

$$= \sqrt{\left(3.47 - \log_{10} Q_t\right)^2 + \left(\log_{10} F + 1.22\right)^2} \qquad \text{(A-1)}$$

I_c = soil behavior type index adopted in this report (Equation 1-3)

$$= \sqrt{\left[3 - \log_{10}\left\{Q_t\left(1 - B_q\right) + 1\right\}\right]^2 + \left[1.5 + 1.3\left(\log_{10} F\right)\right]^2} \qquad \text{(A-2)}$$

q_{t1N} = stressed-adjusted cone tip resistance defined by Idriss and Boulanger (2006), which is different from q_{c1N} defined by Robertson and Wride (1998. The term q_{t1N} is defined as follows:

$$q_{t1N} = C_N\, q_t / \sigma_{atm} \qquad \text{(A-3)}$$

$$C_N = \left[\frac{\sigma_{atm}}{\sigma'_v} \right]^{\alpha} \leq 1.7 \tag{A-4}$$

$$\alpha = 1.338 - 0.249 (q_{t1N})^{0.264} \tag{A-5}$$

where σ_{atm} is the atmosphere pressure (1 atm = 1.013 bars = 101.3 kPa).

Appendix II - Intermediate Parameters for Adjusted CSR

The model for adjusted CSR adopted in this study is the one recommended by Idriss and Boulanger (2004 & 2006). Symbolically, this CSR model is expressed as:

$$\mathrm{CSR} = 0.65\left(\frac{\sigma_{\mathrm{v}}}{\sigma'_{\mathrm{v}}}\right)\left(\frac{\mathrm{a}_{\mathrm{max}}}{\mathrm{g}}\right)(\mathrm{r}_{\mathrm{d}})\left(\frac{1}{\mathrm{MSF}}\right)\left(\frac{1}{\mathrm{K}_{\sigma}}\right) \tag{A-6}$$

where σ_v and σ'_v are the total stress and the effective stress, respectively, of the soil of concern at a given depth, g is the acceleration of gravity, which is the unit for peak ground surface acceleration a_{max}, r_d is the depth-dependent shear stress reduction factor, MSF is the magnitude scaling factor, and K_σ is the overburden correction factor for cyclic stress ratio. The term r_d is defined with the following equations:

$$\ln(r_d) = \alpha + \beta M_w \tag{A-7}$$

$$\alpha = -1.012 - 1.126\sin(5.133 + z/11.73) \tag{A-8}$$

$$\beta = 0.106 + 0.118\sin(5.142 + z/11.28) \tag{A-9}$$

where z is the depth (m) and M_w is the moment magnitude (dimensionless). The term *MSF* is defined as:

$$MSF = -0.058 + 6.9\exp(-M_w/4) \le 1.8 \tag{A-10}$$

The term K_σ is defined as follows:

$$K_\sigma = 1 - C_\sigma \ln(\sigma'_v / P_a) \le 1.0 \tag{A-11}$$

where

$$C_\sigma = \frac{1}{37.3 - 8.27(q_{\mathrm{t1N}})^{0.264}} \le 0.3 \tag{A-12}$$

and where q_{t1N} is the normalized cone tip resistance defined in Appendix I.

Appendix III – Alternative Form of CPTU-based CRR Model

The CPTU-based model for CRR can also be presented in terms of the equivalent normalized cone resistance q_{t1N}^{*}. Symbolically, this CRR model is expressed as (Jianye Ching, personally communication, 2008):

$$\mathrm{CRR} = 0.05 + \exp\left[\left\{(1.51)\left(q_{t1N}^{*}/100\right) - 10.455\right\} + 2.6418\left(q_{t1N}^{*}/100\right)^{0.2352}\right] \qquad \text{(A-13)}$$

where q_{t1N}^{*} is computed as: $q_{t1N}^{*} = K \cdot q_{t1N}$ where the factor K is defined as:

$$K = \left(q_{t1N}\right)^{-0.7746+1.05I_c-0.3579I_c^2} e^{3.2691-1.5901I_c-3.0385I_c^2+2.2792I_c^3-0.3402I_c^4} \qquad \text{(A-14)}$$

The factor K is a function of two key parameters, q_{t1N} and I_c. It should be noted that in the CPTU model developed in this report, these two parameters are defined differently from those reported in the literature (see Appendix I) because of the incorporation of pore water pressure measurement in this CPTU model.

REFERENCES

Agrawal, G., Chameau, J.L., and Bourdeau, P.L. (1995), "Assessing the liquefaction susceptibility at a site based on information from penetration testing," Chapter 9, in: *Artificial Neural Networks for Civil Engineers – Fundamentals and Applications*, ASCE Monograph, New York.

Boulanger, R. W. and Idriss, I. M. (2004), "State normalization of penetration resistances and the effect of overburden stress on liquefaction resistance," *Proceedings 11th SDEE and 3rd ICEGE*, Berkeley, California, pp. 484-491.

Bray, J.D., Sancio, R.B., Durgunolu, T., Onalp, A., Youd, T.L., Stewart, J.P., Seed, R.B., Cetin, O.K., Bol, E., Baturay, M.B., Christensen, C., and Karadayilar, T. (2004), "Subsurface characterization at ground failure sites in Adapazari, Turkey," *Journal of Geotechnical and Geoenvironmental Engineering*, ASCE, Vol. 130, No. 7, pp. 673-685.

Bray, J.D. and Sancio, R.B. (2006), "Assessment of the liquefaction susceptibility of fine-grained soils," *Journal of Geotechnical and Geoenvironmental Engineering*, ASCE, Vol. 132, No. 9, pp. 1165-1177.

Bray, J.D., Sancio, R.B., Durgunolu, T., Onalp, A., Youd, T.L., Stewart, J.P., Seed, R.B., Cetin, O.K., Bol, E., Baturay, M.B., Christensen, C., and Karadayilar, T. (2006), "Closure to subsurface characterization at ground failure sites in Adapazari, Turkey," *Journal of Geotechnical and Geoenvironmental Engineering*, ASCE, Vol. 132, No. 4, pp. 541-547.

California Division of Mines and Geology (CDMG) (1997), "*Guidelines for evaluating and mitigating seismic hazards in California*," California Div. of Mines and

Geology Spec. Publ. 117, California Division of Mines and Geology, Sacramento, CA.

Carraro, J.A.H., Bandini, P., and Salgado, R. (2003), "Liquefaction resistance of clean and non-plastic silty sands based on cone penetration resistance," *Journal of Geotechnical and Geoenvironmental Engineering*, ASCE, Vol. 129, No. 11, pp. 965-976.

Cetin, K.O., Seed, R.B., Kiureghian, A.D., Tokimatsu, K., Harder, L.F., Jr., Kayen, R.E., and Moss, R.E.S. (2004), "Standard penetration test-based probabilistic and deterministic assessment of seismic soil liquefaction potential," *Journal of Geotechnical and Geoenvironmental Engineering*, ASCE, Vol. 130, No. 12, pp. 1314-1340.

Chen, C.J. and Juang, C.H. (2000), "Calibration of SPT- and CPT-based liquefaction evaluation methods," *Geotechnical Special Publication*, No. 97, ASCE, pp. 49-64.

Chen, C.H., Juang, C.H., and Schuster, M.J. (2008), "Empirical model for liquefaction resistance of soils based on artificial neural network learning of case histories," *Geotechnical Special Publication* No. 179, ASCE, Reston, VA, pp. 854-861.

Demuth H. and Beale, M. (2002), *Matlab Neural Network Toolbox, User's Guide*, The MathWorks, Inc., Natick, Mass.

Divakarla, P.K., Hoyos, L.R., and Macari, E.J. (1998), "Assessment of liquefaction potential of western Puerto Rico," *Geotechnical Special Publication* No. 75, *Geotechnical Earthquake Engineering and Soil Dynamics*, ASCE, Vol. 1, pp. 530-541.

Elton, D.J. and Hadj-Hamou, T. (1990), "Liquefaction potential map for Charleston, South Carolina," *Journal Geotechnical Engineering*, Vol. 116, No. 2, pp. 244-265.

Frost, J.D., Carrol, D.P., and Rockaway, T.D. (1997), "Spatial liquefaction analysis," *Geotechnical Special Publication*, No. 67, ASCE, pp. 70-86.

Goh, A.T.C. (1994), "Seismic liquefaction potential assessed by neural networks," *Journal of Geotechnical and Geoenvironmental Engineering*, ASCE, Vol. 120, No. 9, pp. 1467-1480.

Goh, A. T. C. (1996), "Neural network modeling of CPT seismic liquefaction data," *Journal of Geotechnical and Geoenvironmental Engineering*, ASCE, Vol. 122, No. 1, pp. 70-73.

Gratchev, I.B., Sassa K., and Fukuoka H. (2006), "How reliable is the plasticity index for estimating the liquefaction potential of clayey sands," *Journal of Geotechnical and Geoenvironmental Engineering*, ASCE, Vol. 132, No. 1, pp. 124-127.

Guo, T. and Prakash, S. (1999), "Liquefaction of silts and silt-clay mixtures," *Journal of Geotechnical and Geoenvironmental Engineering*, ASCE, 125 (8), pp. 706-710.

Hagan, M. T. and Menhaj, M. (1994), "Training feedforward networks with the Marquardt algorithm," *IEEE Transactions on Neural Networks*, Vol. 5, No. 6, pp. 989-993.

Hayati, H. and Andrus, R.D. (2007), "Liquefaction potential map of Charleston, South Carolina based on the 1886 earthquake," *Final Report to the U.S. Geological Survey*, *No. 06HQGR0058*, Clemson University, Clemson, SC.

Holzer, T.L., Bennett, M.J., Noce, T.E., Padovani, A.C., and Tinsley, J.C., III. (2002), "Liquefaction hazard and shaking amplification maps of Alameda, Berkeley,

Emeryville, Oakland, and Piedmont, California: A digital database," *U.S. Geological Survey Open-File Rep. 02-296 (version 1.0)*, U.S. Geological Survey, Menlo Park, Calif., (http://geopubs.wr.usgs.gov/open-file/of02-296).

Holzer, T.L., Noce, T.E., Bennett, M.J., Tinsley III, J.C., and Rosenburg, L.I. (2005), "Liquefaction at Oceano, California, during the 2003 San Simeon earthquake," *Bulletin of the Seismological Society of America*, Vol. 95, No. 6, pp. 2396-2411.

Holzer, T.L., Bennett, M.J., Noce, T.E., Padovani, A.C., and Tinsley III, J.C. (2006a), "Liquefaction hazard mapping with LPI in the Greater Oakland, California, Area," *Earthquake Spectra*, Vol. 22, No. 3, pp. 693-708.

Holzer, T.L., Blair, J.L., Noce, T.E., and Bennett, M.J. (2006b), "Predicted liquefaction of east bay fills during a repeat of the 1906 San Francisco earthquake," *Earthquake Spectra*, Vol. 22, No. S2, pp. S261-277.

Idriss, I.M. and Boulanger, R.W. (2004), "Semi-empirical procedures for evaluating liquefaction potential during earthquakes," *Proceedings, the 3rd International Conf. on Earthquake Geotechnical Engineering* (ICEGE), Berkeley, CA, pp. 32-56.

Idriss, I.M. and Boulanger, R.W. (2006), "Semi-empirical procedures for evaluating liquefaction potential during earthquakes," *Soil Dynamics and Earthquake Engineering*, Vol. 26, pp. 115-130.

Ishihara, K. (1985), "Stability of natural deposits during earthquakes," *Proceedings of the 11th International Conference on Soil Mechanics and Foundation Engineering*, Vol. 1, Balkema, Rotterdam, The Netherlands, pp. 321–376.

Ishihara, K. (1993), "Liquefaction and flow failure during earthquakes," *Geotechnique*, Vol. 43, No. 3, pp. 351-415.

Iwasaki, T., Tatsuoka, F., Tokida, K., and Yasuda, S. (1978), "A practical method for assessing soil liquefaction potential based on case studies at various sites in Japan," *Proceedings of the 2nd International Conference on Microzonation*, San Francisco, Vol. 2, pp.885-896.

Iwasaki, T., Arakawa, T., and Tokida, K. (1982), "Simplified procedures for assessing soil liquefaction during earthquakes," *Proceedings of the Conference on Soil Dynamics and Earthquake Engineering*, Southampton, UK, pp. 925-939.

Japan Road Association (1980), Specifications for highway bridges, Part V, *Earthquake Resistant Design,* Tokyo, Japan (in Japanese).

Jefferies, M.G. and Davies, M.P. (1993), "Use of CPTu to estimate equivalent SPT N_{60}," *Geotechnical Testing Journal,* Vol. 16, No. 4, American Society for Testing and Materials, pp. 458-468.

Jefferies, M.G. and Been, K. (2006), *Soil liquefaction – A critical state approach*, Taylor & Francis Group, New York, NY.

Juang, C.H., Chen, C. J., and Tien, Y.M. (1999a), "Appraising CPT-based liquefaction resistance evaluation methods – artificial neural network approach," *Canadian Geotechnical Journal*, Vol. 36 (3), pp. 443-454.

Juang, C.H., Rosowsky, D.V., and Tang, W.H. (1999b), "Reliability-based method for assessing liquefaction potential of sandy soils," *Journal of Geotechnical and Geoenvironmental Engineering*, Vol. 125, No. 8, pp. 684-689, 1999.

Juang, C.H., Chen, C.J., Tang, W.H., and Rosowsky, D.V. (2000a), "CPT-based liquefaction analysis, Part 1: Determination of limit state function," *Geotechnique*, Vol. 50, No. 5, pp. 583-592.

Juang, C.H., Chen, C.J., Rosowsky, D.V., and Tang, W.H., (2000b), "CPT-based liquefaction analysis, Part 2: Reliability for design," *Geotechnique*, Vol. 50, No. 5, pp. 593-599.

Juang, C.H., Jiang, T., and Andrus, R.D. (2002), "Assessing probability-based methods for liquefaction evaluation," *Journal of Geotechnical and Geoenvironmental Engineering*, ASCE, Vol. 128, No. 7, pp. 580-589.

Juang, C.H., Yuan, H., Lee, D.H., and Lin, P.S. (2003), "Simplified CPT-based method for evaluating liquefaction potential of soils," *Journal of Geotechnical and Geoenvironmental Engineering*, ASCE, Vol. 129, No. 1, pp. 66-80.

Juang, C.H., Fang, S.Y., and Khor, E.H. (2006), "First order reliability method for probabilistic liquefaction triggering analysis using CPT," *Journal of Geotechnical and Geoenvironmental Engineering*, Vol. 132, No. 3, pp. 337-350.

Juang, C.H., Li, D.K., Fang, S.Y., Liu, Z. and Khor, E.H. (2008a), "Simplified procedure for developing joint distribution of a_{max} and M_W for probability liquefaction hazard analysis," *Journal of Geotechnical and Geoenvironmental Engineering*, ASCE, Vol. 134, No. 8, pp. 1050-1058.

Juang, C.H., Chen, C.H. and Mayne, P.W. (2008b), "CPTU simplified stress-based model for evaluating soil liquefaction potential," *Soils and Foundations*, Vol. 48, No. 6, 2008, pp. 755-770.

Juang, C.H., Liu, C.N., Chen, C.H., Hwang, J.H., and Lu, C.C. (2008c), "Calibration of liquefaction potential index: A re-visit focusing on a new CPTU model," *Engineering Geology*, Vol. 102, No. 1-2, 2008, pp. 19-30.

Juang, C.H., Lu, C.C., and Hwang, J.H. (2008d), "Assessing probability of surface manifestation of liquefaction in a given exposure time using CPTU," *Engineering Geology* (2008), doi:10.1016/j.enggeo.2008.10.011.

Kavazanjian, E., Roth, R.A., and Echezuria, H. (1985), "Liquefaction potential mapping for San Francisco," *Journal of Geotechnical Engineering*, Vol. 111, No. 1, pp. 54-76.

Kim, Y.S. and Kim, B.T. (2006), "Use of artificial neural networks in the prediction of liquefaction resistance of sands," *Journal of Geotechnical and Geoenvironmental Engineering*, Vol. 132, No. 11, pp. 1502-1504.

Kishida, H. (1969), "Characteristics of liquefied sands during Mino-Owari, Tohnankai and Fukui earthquakes," *Soils and Foundations*, Vol. 9, No. 1, pp. 75-92.

Kramer, S.L. and Mayfield R.T. (2005), "Performance-based liquefaction hazard evaluation," *Geotechnical Special Publication*, No. 133, ASCE, Reston, VA, January 2005.

Kramer, S.L., Mayfield, R.T., and Anderson, D.G. (2006), "Performance-based liquefaction hazard evaluation: implications for codes and standards," *Proceedings the 8th U.S. National Conference on Earthquake Engineering*, Paper No. 888, San Francisco, CA.

Kramer, S.L. and Mayfield R.T. (2007), "Return period of soil liquefaction," *Journal of Geotechnical and Geoenvironmental Engineering*, ASCE, Vol. 133, No. 7, pp. 802-813.

Ku, C.S., Lee. D.H., and Wu J.H. (2004), "Evaluation of soil liquefaction in the Chi-Chi, Taiwan earthquake using CPT," *Soil Dynamics and Earthquake Engineering*, Vol. 24, pp. 659-673.

Lai S.Y., Hsu, S.C., and Hsieh, M.J. (2004), "Discriminant model for evaluating soil liquefaction potential using cone penetration test data," *Journal of Geotechnical and Geoenvironmental Engineering*, Vo. 130, No. 12, pp. 1271-1282.

Lee, D.H., Ku, C.S., and Yuan, H. (2004), "A study of the liquefaction risk potential at Yuanlin, Taiwan," *Engineering Geology*, Vol. 71, pp. 97-117.

Lenz, J.A. and Baise, L.G. (2007), "Spatial variability of liquefaction potential in regional mapping using CPT and SPT data," *Soil Dynamics and Earthquake Engineering*, Vol. 27, pp. 690-702.

Li, D.K., Juang, C.H., and Andrus, R.D. (2006), "Liquefaction potential index: a critical assessment," *Journal of GeoEngineering*, Taiwanese Geotechnical Society, Vol. 1, No. 1, pp. 11-24.

Li, D.K., Juang, C.H., Andrus, R.D., and Camp, W.M. (2007), "Index properties-based criteria for liequefaction susceptibility of clayey soils: a critical assessment," *Journal of Geotechnical and Geoenvironmental Engineering*, ASCE, Vol. 133, No. 1, pp. 110-115.

Luna, R. and Frost, J.D. (1998), "Spatial liquefaction analysis system," *Journal of Computing in Civil Engineering*, Vol. 12, No. 1, pp. 48-56.

Marrone, J., Osatadan, F., Youngs, R., and Litehiser, J. (2003), "Probabilistic liquefaction hazard evaluation: method and application," *Transaction of the 17th International*

Conference on Structural Mechanics in Reactor Technology, Prague, Czech Republic, August 17-22, 2003, Paper #M02-1.

MathWork, Inc. (2002), *Matlab Version 6.5*, Natick, MA.

Mitchell, J.K. and Tseng, D.J. (1990), "Assessment of liquefaction potential by cone penetration resistance," *Proceedings, H. Bolton Seed Memorial Symposium*, J.M. Duncan, ed., Vancouver, B.C., Vol. 2, pp. 335-350.

Moss, R.E.S., Seed, R.B., Kayen, R.E., Stewart, J.P., Der Kiureghian, A., and Cetin, K.O. (2006), "CPT-based probabilistic and deterministic assessment of in situ seismic soil liquefaction potential," *Journal of Geotechnical and Geoenvironmental Engineering*, ASCE, Vol. 132, No. 8, pp. 1032 - 1051.

Olsen, R.S. (1997), "Cyclic liquefaction based on the cone penetrometer test," *Proceedings of the NCEER Workshop on Evaluation of Liquefaction Resistance of Soils*, Technical report NCEER-97-0022, T. L. Youd and I. M. Idriss, eds., National Center for Earthquake Engineering Research, State University of New York at Buffalo, Buffalo, NY, pp. 225-276.

Papathanassiou, G., Pavlides, S., Ganas, A. (2005), "The 2003 Lefkada earthquake: field observations and preliminary microzonation map based on liquefaction potential index for the town of Lefkada," *Engineering Geology*, Vol. 82, pp. 12-31.

Papathanassiou, G. (2008), "LPI-based approach for calibrating the severity of liquefaction-induced failures and for assessing the probability of liquefaction surface evidence," *Engineering Geology*, Vol. 96, pp. 94-104.

PEER web site (2007), Soils and liquefaction data on 1999 Kocaeli, Turkey Earthquake, http://peer.berkeley.edu/publications/turkey/adapazari/index.html.

Perlea, V.G., Koester, J.P., and Prakash, S. (1999), "How liquefiable are cohesive soils," *Proc., 2nd Int. Conf. on Earthquake Geotechnical Engineering*, Lisbon, Portugal, pp. 611-618.

Robertson, P.K. and Campanella, R.G. (1985), "Liquefaction potential of sand using the CPT," *Journal of Geotechnical Engineering*, ASCE, Vol. 111, No. 3, pp. 384-403.

Robertson, P.K. (1990), "Soil classification using the cone penetration test," *Canadian Geotechnical Journal*, Vol. 27, No. 1, pp. 151-158.

Robertson, P.K. and Wride, C.E. (1998), "Evaluating cyclic liquefaction potential using the cone penetration test," *Canadian Geotechnical Journal*, Vol. 35, No. 3, pp. 442-459.

Rumelhart, D.E., Hinton, G.E., and Williams, R.J. (1986), "Learning internal representations by error propagation," *Parallel Distributed Processing: Foundations*, Vol.1, D.E. Rumelhart and J.L. McClelland, eds., MIT Press, Combridge, Mass, pp. 318-362.

Seed, H.B. and Idriss, I.M. (1971), "Simplified procedure for evaluating soil liquefaction potential," *Journal of the Soil Mechanics and Foundation Div*., ASCE, 97 (SM9), pp. 1249-1273.

Seed, H.B. and Idriss, I.M. (1982), *Ground motions and soil liquefaction during earthquakes*, Earthquake Engineering Research Institute Monograph, Oakland, CA.

Seed, H.B., Tokimatsu, K., Harder, L.F., and Chung, R. (1985), "The influence of SPT procedures in soil liquefaction resistance evaluations," *Journal of Geotechnical Engineering*, ASCE, Vol. 111, No. 12, pp. 1425-1445.

Seed, H. B. and de Alba, P. (1986), ‘‘Use of SPT and CPT tests for evaluating liquefaction resistance of sands,’’ *Use of In Situ Testing in Geotechnical Engineering*, Geotechnical Special Publication No. 6, ASCE, New York, pp. 281-302.

Seed, R.B., Cetin, K, O., Moss, R.E.S., Kammerer, A.M., Wu, J., Pestana, J.M., Riemer, M.F., Sancio, R.B., Bray, J.D., Kayen, R.E., and Faris, A. (2003), “Recent advances in soil liquefaction engineering: a unified and consistent framework,” *Keynote Address, 26th Annual Geotechnical Spring Seminar*, Los Angeles Section of the GeoInstitute, American Society of Civil Engineers, H.M.S. Queen Mary, Long Beach, California, USA.

Shuttle, D.A. and Cunning, J. (2007), “Liquefaction potential of silts from CPTu,” *Canadian Geotechnical Journal*, Vol. 44, No.1, pp. 1-19.

Sonmez, H. (2003), “Modification of the liquefaction potential index and liquefaction susceptibility mapping for a liquefaction-prone area (Inegol, Turkey),” *Environmental Geology*, Vol. 44, No. 7, pp. 862-871.

Sonmez, H. and Gokceoglu, C. (2005), “A liquefaction severity index suggested for engineering practice,” *Environmental Geology*, Vol. 48, No. 1, pp. 81-91.

Sonmez, B., Ulusay, R., and Sonmez, H. (2008), “ A study on the identification of liquefaction-induced failures on ground surface based on the data from the 1999 Kocaeli and Chi-Chi earthquakes,” *Engineering Geology*, Vol. 97, pp. 112-125.

Stark, T.D. and Olson, S.M. (1995), “Liquefaction resistance using CPT and field case histories,” *Journal of Geotechnical and Geoenvironmental Engineering*, ASCE, Vol. 121, No. GT 12, pp. 856-869.

Suzuki, Y., Koyamada, K., Tokimatsu, K., Taya, Y., and Kubota, Y. (1995), "Empirical correlation of soil liquefaction based on cone penetration test," *Earthquake Geotechnical Engineering*, K. Ishihara, ed., Balkema, Rotterdam, The Netherlands, pp. 369-374.

Thevanayagam, S., Fiorillo, M., and Liang, J. (2000), "Effect of non-plastic fines on undrained cyclic strength of silty sands," *Soil Dynamics & Liquefaction 2000*, Geotechnical Special Publication No. 107, ASCE, Pak, R.Y.S. and Yamamura J., Eds., Reston, VA, pp. 77-91.

Tohno, I. and Yasuda, S. (1981), "Liquefaction of the ground during the 1978 Miyagiken-Oki earthquake," *Soils and Foundations*, Vol. 21, No. 3, pp. 18-34.

Toprak, S. and Holzer, T.L. (2003), "Liquefaction potential index: field assessment," *Journal of Geotechnical and Geoenvironmental Engineering*, ASCE, Vol. 129, No. 4, pp. 315-322.

United States Geological Survey (USGS) (2002a), National Seismic Hazard Maps website, (http://earthquake.usgs.gov/research/hazmaps).

United States Geological Survey (USGS) (2002b), National Seismic Hazard Maps website for de-aggregation, (http://eqint.cr.usgs.gov/eq-men/html/deaggint2002-06.html).

Youd, T.L. and Hoose, S.N. (1977), "Liquefaction susceptibility and geologic setting," *Proceedings of the Sixth World Conference on Earthquake Engineering*, New Delhi, India, Vol. 6, pp. 37-42.

Youd, T.L. and Perkins, D.M. (1987), "Mapping of liquefaction severity index," *Journal of Geotechnical Engineering*, Vol. 113, No. 11, pp. 1374-1392.

Youd, T. L., Idriss, I. M., Andrus, R.D., Arango, I., Castro, G., Christian, J.T., Dobry, R., Liam Finn, W.D., Harder, L.F., Jr., Hynes, M.E., Ishihara, K., Koester, J.P., Liao, S.S.C., Marcuson, W.F., III, Martin, G.R., Mitchell, J.K., Moriwaki, Y., Power, M.S., Robertson, P.K., Seed, R.B., and Stokoe, K.H., II. (2001), "Liquefaction resistance of soils: summary report from the 1996 NCEER and 1998 NCEER/NSF workshops on evaluation of liquefaction resistance of soils," *Journal of Geotechnical and Geoenvironmental Engineering*, Vol. 127, No. 10, pp. 817-833.

Yuan, H., Yang, S.H., Andrus, R.D., and Juang, C.H. (2003), "Liquefaction-induced ground failure: a study of the Chi-Chi earthquake cases," *Engineering Geology*, Vol. 17, pp. 141-155.

Zhang, G., Robertson, P.K., and Brachman, R.W.I. (2002), "Estimating liquefaction-induced ground settlements from CPT for level ground," *Canadian Geotechnical Journal*, Vol. 39 (5), pp. 1168-1180.